MASTERARBEIT | MASTER'S THESIS

Titel | Title

Lipid analysis of erythrocyte membranes by means of mass spectrometry

verfasst von | submitted by

Pavlo Frondzei BSc

angestrebter akademischer Grad | in partial fulfilment of the requirements for the degree of

Master of Science (MSc)

Wien | Vienna, 2025

Studienkennzahl lt. Studienblatt | Degree programme code as it appears on the student record sheet:	UA 066 862
Studienrichtung lt. Studienblatt | Degree programme as it appears on the student record sheet:	Masterstudium Chemie
Betreut von | Supervisor:	Univ.-Prof. Dr. Gunda Köllensperger
Mitbetreut von | Co-Supervisor:	Dott.ssa Dott.ssa.mag. Dr. Fiammetta Di Marco

Acknowledgement

Firstly, I would like to thank Dr. Fiammetta Di Marco for supervising me throughout the practical part and giving me valuable insights and advice. Her experience in the field and technical support have helped me defining this thesis and broadening my understanding of the essence of analytical chemistry.

Secondly, I would like to thank Prof. Gunda Koellensperger for the opportunity of working at her research group and giving me highly valuable knowledge in the field. Especially big thanks to Jana for being a great listener and motivator during the data evaluation and visualization days, I will miss the lunch time together!

Big gratitude goes out to my parents. Thank you for your emotional support when I needed it most. Thanks for moving to Austria and sacrificing your careers for my well-being, thanks to moving to Sweden and letting me become independent.

My biggest thanks go to my girlfriend Selina, who supported me from day one, has been on my side at my lowest and my highest. I would not be the successful person who I am now, without your support.

Abstract

Preterm-born infants rely on red blood cell (RBC) transfusions to have better survival chances. However, the transfusion outcome depends on donor characteristics such as sex and age. Improved survival chances have been reported when preterm infants were transfused with RBCs from specific donor groups. The purposes of this thesis are to investigate differences in RBC membrane lipid composition across different population groups, across fresh and stored blood and therefore possibly explain better transfusion outcomes.

A cohort of 105 samples was analyzed, comparing fresh adult blood, preterm and term RBCs from umbilical cord and four subgroups of donor blood units differing in sex and age. Lipidomic profiling was performed by reversed-phase high-performance liquid chromatography–mass spectrometry for chromatographic separation and species-level quantification and shotgun lipidomics for broad, rapid assessment of membrane lipid composition.

Just a small subset of lipid species differed between adult and neonatal RBCs, while older female donors showed neither differences to other adult groups nor similarities to preterm RBCs. Adult RBCs, fresh or stored, clustered closely together regardless of sex or age. Preterm and term infant RBCs formed distinct separate clusters from adult groups, showing characteristic shifts in saturation, chain length distribution and phospholipid class abundances. Lipid patterns in adult RBCs remained stable across stored and fresh blood, suggesting minimal alteration through routine blood processing.

Neonatal RBCs have unique lipid signatures compared to all adult groups. Factors not investigated in this thesis, such as membrane proteins, glycolipids or small metabolites may explain transfusion-related outcomes in preterm infants. We recommend expanding cohort size, integrating multi-omics layers and incorporating longitudinal sampling to identify donor characteristics that explain transfusion success.

Zusammenfassung

Die Frühgeborenen sind auf Transfusionen roter Blutkörperchen (RBC) angewiesen, um bessere Überlebenschancen zu haben. Das Ergebnis einer Transfusion hängt von Merkmalen des Spenders ab, und zwar von Geschlecht und Alter. Höhere Überlebenschancen bei Frühgeborenen wurden bei Transfusionen der RBC von bestimmten Spendergruppen beobachtet. Die Ziele dieser Masterarbeit sind, die Unterschiede in der Lipidzusammensetzung der Membran der RBC in unterschiedlichen Bevölkerungsgruppen sowie frischen Blutproben und Blutkonserven zu bestimmen und möglicherweise die besseren Transfusionsergebnisse zu erklären.

Eine Stichprobe an 105 Proben wurde analysiert, in welcher Blutproben mit frischem Blut und das Blut von der Nabelschnur der Frühgeburten und rechtzeitig geborenen Kindern verglichen wurden. Zusätzlich wurden 4 Untergruppen an Blutkonserven von Spender:innen unterschiedlichen Alters und Geschlechts analysiert. Die Erstellung des Lipidomprofils erfolgte mithilfe zweier analytischer Methoden: Umkehrphasen-Hochleistungsflüssigkeitschromatographie-Massenspektrometrie, um die Spezies chromatographisch zu trennen und zu quantifizieren, und Shotgun-Lipidomik für umfassende und schnelle Bewertung der Membranlipidzusammensetzung.

Nur eine kleine Anzahl an Lipidspezies war unterschiedlich zwischen den RBC Erwachsener und Säuglingen, während ältere Frauen weder Unterschiede zu anderen Gruppen noch Ähnlichkeiten zu Frühgeburten gezeigt haben. Die RBC Erwachsener aus frischen Proben und Blutkonserven gruppierten nah aneinander, unabhängig von Geschlecht oder Alter. Frühgeborene und rechtzeitig Geborenen gruppierten sich separat von Gruppen Erwachsener, mit typischen Verschiebungen im Sättigungsgrad, Verteilung der Kettenlänge und der Abundanz der Phospholipide. Die Lipidmuster bei Erwachsenen blieb nahezu gleich sowohl in Blutkonserven als auch im frischen Blut, was ein Indiz für minimale Lipidveränderungen durch Blutverarbeitung sein kann.

Verglichen mit anderen Gruppen haben Säuglinge eigene Lipidmuster. Die Faktoren, die in dieser Masterarbeit nicht untersucht wurden, wie Membranproteine, Glykolipide oder kleine Metabolite könnten die Ergebnisse der Bluttransfusionen erklären. Wir empfehlen Erweiterung der Stichprobe, Verwendung von Multi-Omik Ansätzen oder Längsschnittstudien um Merkmale der Spender:innen zu ermitteln, die Transfusionserfolge erklären.

Table of Contents

List of figures

List of tables

List of Abbreviations

ATP	Adenosine triphosphate
DB	Double bond
DDA	Data-dependent acquisition
DHA	Docosahexaenoic acid
DIA	Data independent acquisition
DPG	2,3-Diphosphoglycerate
ESI	Electrospray ionization
ECN	Equivalent carbon number
FWHM	Full width at half maximum
G6PD	Glucose-6-phosphate dehydrogenase
HILIC	Hydrophilic interaction liquid chromatography
HPLC	High-performance liquid chromatography
LC	Liquid chromatography
LPC	Lysophosphatidylcholine
LPE	Lysophosphatidylethanolamine
LPL	Lysophospholipid
MFQL	Molecular Fragmentation Query Language
MS	Mass spectrometry
m/z	Mass-to-charge ratio
NADPH	Nicotinamide adenine dinucleotide phosphate
PBS	Phosphate-buffered saline
PC	Phosphatidylcholine
PCA	Principal component analysis
PE	Phosphatidylethanolamine
PG	Phosphatidylglycerol
PI	Phosphatidylinositol
PL	Phospholipid
PMO	Precursor mass offset
pRBC	Packed red blood cells
PRP	Platelet rich plasma
PS	Phosphatidylserine

PUFAs	Polyunsaturated fatty acids
RBC	Red blood cell
RP	Reversed-phase
RT	Retention time
RP-HPLC	Reversed-phase high-performance liquid chromatography
SD	Standard deviation
SFA	Saturated fatty acid
SFC	Supercritical fluid chromatography
SM	Sphingomyelin
QC	Quality control

1 Introduction

Preterm birth is a critical condition with multiple organ complications. Infants born before 32 weeks or with very low birth weight often develop bronchopulmonary dysplasia, intraventricular haemorrhage, hydrocephalus, periventricular leukomalacia, retinopathy of prematurity, necrotizing enterocolitis, hypoxemia and anemia of prematurity [1]. Despite progress in neonatal intensive care, preterm birth remains a leading cause of death in children under five. Anemia caused by frequent blood sampling and immature erythropoiesis often requires RBC transfusions. Very low birth weight infants frequently receive such transfusions during hospitalization [2]. Transfusion improves oxygen delivery but introduces donor cells into fragile neonatal circulation, raising concerns about donor selection and transfusion practices.

Some studies suggested that donor characteristics such as sex and age can influence transfusion outcomes in premature infants, but the results are controversial [2,3]. Murphy et al. linked transfusion of female donor blood to higher mortality and morbidity in transfused newborns but no effect was found after adjusting for transfusion volume [3]. Another study by Patel et al. explored transfusion effects on preterm infants and, on the opposite of Murphy et al. [3], the results showed that preterm infants receiving only female-donor blood, particularly older female donors, had fewer adverse outcomes than those who received only male-donor-blood [2]. In this study, only about 21% of the female-only blood-transfused group had the composite outcome death, versus the increased 45% in the male-only blood-transfused group [2].

RBCs from female and older donors show less hemolysis, slower loss of flexibility and a lower pro-inflammatory profile during storage [4]. Female donor RBCs shed fewer microparticles and remain more stable than male donor RBCs. Blood from older donors has greater antioxidant capacity and produces fewer oxidative byproducts than blood from younger donors [4]. These features may reduce oxidative and inflammatory stress in recipients. However, lipid-mediated effects are a novel consideration in this context. RBC membrane lipids may influence membrane stability and rigidity and immune and coagulation pathways. The hypothesis of this thesis suggests that variation in RBC membrane lipid composition contributes to different transfusion outcomes in preterm infants.

To explore differences in RBC membrane lipid composition and distribution across human population (different sex and age, stored or fresh blood) and neonatal groups (term and preterm newborns), lipidomics approaches are applied. These approaches allow the profiling of hundreds of molecular species across phospholipids (PLs), sphingolipids and neutral lipids [5]. The goal is to investigate whether different lipid patterns are present in stored blood bags, adults (depending also from their sex and age), term and preterm newborns and if this explains the better outcomes when preterm infants receive blood from older female donors, as observed in a previous study [2]. Two analytical strategies are used for this investigation. Reversed-phase high-performance liquid chromatography mass spectrometry (RP-HPLC-MS) provides

chromatographic separation of lipid classes and high-resolution MS, to identify and quantify lipid species within the RBC membranes. Shotgun lipidomics enable rapid, comprehensive profiling by direct infusion of lipid extract directly into the mass spectrometer.

1.1 Structure of RBC Membrane Lipids in Different Populations

The RBC membrane is made of lipids, proteins and carbohydrates. By weight it is about 49 percent protein, 43 percent lipid and 8 percent carbohydrate [6]. The lipid component forms an asymmetric bilayer that provides the fundamental barrier and flexibility of the cell. Lipids form a bilayer with fatty acid tails pointing inside the membrane layers and polar headgroups exposed to the inner cytoplasmic space and outer cell extracellular surface [6]. The outer leaflet is rich in phosphatidylcholine (PC) and sphingomyelin (SM) and contain cholesterol. The inner leaflet contains phosphatidylethanolamine (PE) phosphatidylserine (PS), phosphatidylinositol (PI) and cholesterol [6], the lipid structures of the lipids are shown in the Figure 1. This asymmetry is important because exposure of PS on the surface signals cell removal [7]. Major lipid classes include PC, PE, PS, PI, SM and cholesterol.

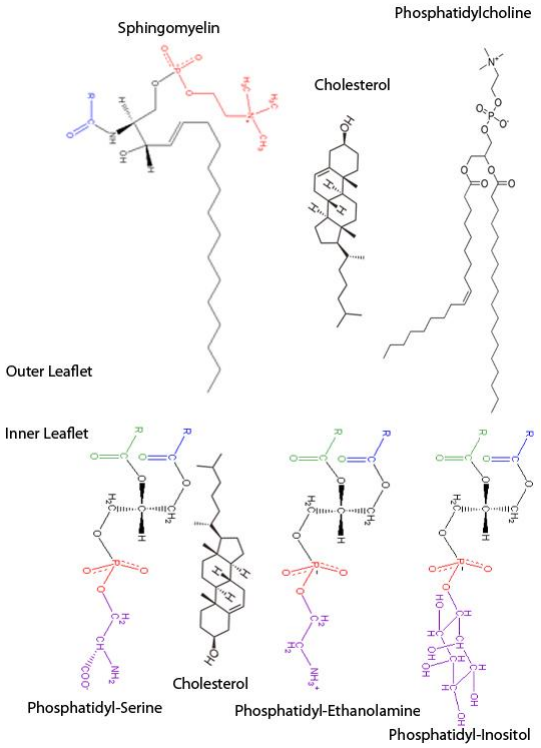

Figure 1: Structural representation of the major lipid classes in the outer and inner leaflets

Minor species such as lysophospholipids (LPLs) and plasmalogens, though present in small amounts, affect membrane function. Together with the transmembrane proteins and the cytoskeleton, these lipids give RBCs strength and flexibility. This composition allows RBCs to deform through capillaries and survive about 120 days in circulation [8].

Cholesterol makes up nearly half of the total lipid mass and intercalates in both leaflets, adding rigidity and reducing permeability. The cholesterol to PL balance maintains fluidity and stability and specific lipid types influence stress responses and cell interactions [9]. The cholesterol to PL molar ratio is about 0.8 to 0.9 and remains tightly regulated [10]. Cholesterol prevents rupture under stress and unsaturated PLs in PC and PE preserve fluidity. It has been shown that if adult RBC membranes are experimentally depleted of cholesterol, their osmotic fragility increases [11,12]. Studies in literature noted that composition of RBC lipids in adults and neonates differ. In particular, PC levels are significantly higher in adult RBCs than in neonatal RBCs, reflecting the maturity of lipid metabolic pathways in adults [13,14]. Thus, the adult RBC's lipid composition, rich in PC and balanced in cholesterol, yields a membrane that is "fluid yet durable."

1.1.1 Difference between neonatal and adult RBC

Neonatal and adult RBCs differ in lipid composition. Neonatal cells are larger and contain more total lipid per cell. Their cholesterol to PL ratio is higher, 1.27 in RBCs from cord compared to about 0.83 in adult female RBCs [15]. Neonatal RBCs show slightly lower resistance to extensional and bending deformations [16]. Neonatal cells also show a lower proportion of PC and slightly higher SM, with similar amounts of PE and PI compared to adults. Another analysis reported a higher SM:PC ratio in neonatal RBCs than in adult RBCs [17]. The higher cholesterol and SM, combined with lower PC, produce stiffer membranes with reduced fluidity. Fluorescence studies confirm that neonatal membranes have lower motional freedom than adult membranes, resembling an adult RBC cooled at 15–22°C [18].

Preterm infant RBCs also differ in lipid subclasses and fatty acids. Ether-linked PLs, or plasmalogens, are key membrane antioxidants [19]. Their levels are lower in both preterm and full-term neonates than in adults, with preterm infants showing the greatest deficit. This may reduce protection against oxidative stress, a common challenge in conditions such as respiratory distress or sepsis [20]. The fatty acid composition of PLs in preterm RBCs shows a higher proportion of ω-6 fatty acids and lower ω-3 fatty acids compared to term infants. Extremely preterm infants accumulate more arachidonic acid (20:4 ω-6) and lose docosahexaenoic acid (22:6 ω-3, DHA) in RBC membranes, relative to term infants and adults [21]. This is largely because the third trimester of pregnancy is when the fetus avidly obtains DHA from the mother; preterm birth interrupts this supply. In the OmegaROP study, low DHA and high arachidonic acid in RBC membranes were linked to higher risk of retinopathy of prematurity. These findings show that preterm infants not only have immature lipid profiles but also develop pro-inflammatory fatty acid patterns shaped by their clinical course [21].

Newborn RBCs, especially in preterm infants, are less deformable, shorter-lived and more vulnerable to oxidative damage than adult RBCs [18]. The membrane rigidity can hinder the RBC's ability to traverse narrow capillaries and release oxygen efficiently. In preterm infants, the stiff membranes still pose a challenge to optimal oxygen delivery to tissues [8]. Markers of lipid peroxidation are higher in neonatal than adult RBCs, showing ongoing oxidative damage. Combined with immature antioxidant defences, this shortens neonatal

RBC lifespan to about 60–80 days compared to 120 days in adults. These lipid traits mark neonatal RBCs as fundamentally different from adult cells in function [8].

While these leaflet asymmetries and class proportions are broadly conserved, inter-donor differences in membrane robustness become evident under stress such as cold storage, where genetic and demographic factors modulate hemolysis and deformability [22,23].

1.1.2 Sex and age differences in RBCs upon storage

Adult male and female RBCs share the same basic membrane components, but storage studies show clear sex-based differences. Large donor cohorts found that male RBCs are more prone to hemolysis than female RBCs [24]. One factor is SM content, which is higher in female RBCs [23]. More SM and a higher SM:PC ratio correlate with stronger membranes and lower hemolysis [25]. Male RBCs, with slightly less SM and more unsaturated lipids, are more vulnerable to peroxidation and vesiculation. During refrigerated storage, male RBCs lose membrane lipids faster. Szczesny-Malysiak et al. showed that male units had more cholesterol and triglyceride release, more microvesicle shedding, faster loss of deformability and higher hemolysis [23]. Female RBCs maintain stability longer and shed fewer vesicles which may delay clearance after transfusion [26].

Functionally, female RBCs withstand storage stress better. They reach recipients with fewer microparticles, less PS exposure and more intact membranes. These features may explain why transfusions from female donors, particularly older women, are linked to better outcomes in preterm infants [26]. These systematic differences between RBCs highlight developmental and sex-related variation in RBC biology. They also support the hypothesis that RBCs from older female donors may be more compatible with the neonatal circulation, helping explain outcome differences in transfused preterm infants.

1.2 Blood Bags and Lipid Changes During Storage

When RBCs are stored under blood bank conditions, they develop progressive biochemical and structural changes called the storage lesion. In most settings, units can be stored for up to 42 days at 4 °C. During this time pH falls, nutrients are depleted, waste products accumulate and oxidative and membrane damage occurs [27].

The major lipid classes of RBC membranes remain stable during refrigerated storage. Shotgun lipidomics shows that even after 42 days, the proportions of PC, PE, PS, PI and SM are largely unchanged [28]. Microvesicles shed during storage carry a lipid composition like the parent membrane, suggesting that vesiculation removes a representative portion rather than selectively depleting certain lipids. Cholesterol per cell is also preserved, though some shifts into vesicles. As a result, the overall cholesterol-to-PL ratio in the unit stays constant. Laurén et al. confirmed that total cholesterol to PL ratio in stored blood does not change

significantly, since vesicles retain the cholesterol that leaves the RBCs. Thus, the bulk lipid composition of RBCs is maintained throughout storage [28].

Although the bulk lipid classes remain stable, storage drives qualitative and biochemical changes. LPLs and free fatty acids accumulate over time. A fraction of PC is degraded by phospholipases or mild oxidation into lysophosphatidylcholine (LPC) and a free fatty acid, leading to measurable LPC buildup in both the membrane and supernatant [29]. LPC is pro-inflammatory and has been linked to transfusion-related lung injury and other complications [30]. Lysophosphatidylethanolamine (LPE) also arises from PE breakdown but is less abundant. Plasmalogens decline during storage, as their vinyl-ether bonds are vulnerable to oxidative cleavage, generating LPLs and reactive aldehydes. This removes a key antioxidant lipid from the membrane [31]. In parallel, free fatty acids accumulate in the storage solution, reflecting the PL cleavage. Some of fatty acids may reinsert into membranes or circulate after transfusion, with effects on the recipient that remain uncertain [29].

During storage, the fatty acyl composition of RBC membranes shifts, because RBCs cannot remodel their lipids, oxidative damage accumulates [32]. Polyunsaturated fatty acids (PUFAs) such as linoleic acid (18:2) and arachidonic acid (20:4) are preferentially lost through peroxidation, leaving membranes enriched in saturated chains. This makes the PLs pack more tightly, increasing membrane order. At the same time, PS becomes externalized on some cells. Normally kept on the inner leaflet, PS flips outward during storage and PS-bearing microvesicles accumulate [23]. Surface PS is pro-coagulant and pro-phagocytic, promoting clearance. The total PS content does not change, but its redistribution contributes to storage lesion severity [33].

From the recipient's view, transfusing older blood introduces bioactive lipids and vesicles that build up during storage. Although increases are smaller than in platelet units, the LPC in aged RBCs can still drive inflammation [34]. It has been linked to transfusion-related acute lung injury by priming neutrophils and activating endothelium in the lungs, causing capillary leak and respiratory distress [30]. In preterm infants, repeated transfusions amplify these risks. Each blood unit adds more LPC and microvesicles, compounding oxidative and inflammatory stress. Clinical data show that the number of transfusions in extremely preterm infants correlates with higher chance of necrotizing enterocolitis [35].

In summary, storage time and conditions lead to lipid alterations in RBC units. Major PL classes remain, but membranes accumulate oxidative damage, lose unsaturated fatty acids, gain lysolipids and become more rigid. These changes can reduce transfusion efficacy and pose risks by delivering pro-inflammatory lipids and vesicles to patients. Donor characteristics modulate these effects: female sex and older age tend to confer more lipid stability, resulting in less degradation. This convergence of evidence supports the rationale that choosing blood from donors with favourable profiles and/or limiting storage duration could improve outcomes, particularly for sensitive recipients like preterm infants. Understanding the lipidomic profile of

stored blood may help develop interventions to better preserve RBC membrane integrity and ensure safer transfusions.

1.3 Lipidomics analyses

Lipidomics is a branch of omics disciplines enabling the study of lipids in complex biological samples and mainly rely on the technological advances in MS. The field focuses on identifying and quantifying lipid species, as well as studying their roles and interactions with proteins and metabolites. While related to metabolomics, lipidomics is distinct because lipids have unique structures and functions. Modern lipidomics typically uses four main analytical platforms: Hydrophilic interaction liquid chromatography (HILIC) [36], supercritical fluid chromatography (SFC) [37], RP-HPLC–MS [38] and shotgun lipidomics by direct infusion [39] . Studying RBC lipids in adults, term infants and preterm infants is particularly challenging due to wide dynamic ranges and the presence of many isomeric species. In this work, RP-HPLC-MS and shotgun lipidomics are used for the lipidomics analyses.

1.4 RP-HPLC–MS Lipidomics of RBCs

RP-LC separates lipids primarily by hydrophobic interactions, meaning lipids elute in order of increasing fatty acyl chain length and decreasing unsaturation. RP-HPLC–MS separates lipid extracts on a nonpolar column, most often C18 or C8, prior to MS detection [38]. In RBC lipidomics, RP-HPLC can resolve isomeric species, such as PC 18:1/18:1 versus PC 18:0/18:2, which share the same total carbons and double bonds (DB) but differ in acyl composition [40,41]. Chromatographic separation spreads the ESI ionization of analytes in a span of time, lowering ion suppression and exposing low-abundance lipids that would be hidden in direct infusion [42]. Different lipid classes elute at characteristic ranges: very polar LPLs elute early, diacyl PLs and sphingolipids elute mid-to-late and highly nonpolar neutral lipids (e.g. triacylglycerols) elute last, following their relative hydrophobicity [43].

Electrospray ionization (ESI) is the standard ionization method for LC-MS lipidomics and analyses are typically performed in both positive-ion and negative-ion modes to capture all major lipid classes [44]. No single polarity can ionize all lipids effectively, since different lipid classes have varying affinities for positive or negative ESI. Positive ESI favours choline-containing species (PC, LPC, SM), which form protonated or adduct ions [45], while negative ESI is optimal for anionic lipids (PE, LPE, PS, PI), producing deprotonated ions and class-characteristic fragments [46]. In positive mode, lipids with basic or quaternary ammonium headgroups ionize readily: for instance, choline-containing PLs like PC and SM yield abundant [M+H]^+ ions or sodium adducts [43]. In contrast, acidic or anionic lipids (e.g., PE, PS, PI and their lyso- forms) respond better in negative mode by deprotonation, giving [M–H]^− ions along with class-specific fragment ions (such as the headgroup-specific fragments for PS or PI) [46].

Reversed-phase (RP) retention of lipids is often characterized by the Equivalent Carbon Number (ECN) model, which quantifies the combined effect of chain length and unsaturation on hydrophobicity. In essence, RT

increases with the total number of carbons in the fatty acyl chains and decreases with the number of double bonds [40,47]. Each added DB typically offsets the retention increase of about two methylene groups. This relationship is expressed in the ECN model, defined as: RT Lipid X:Y = RT Lipid (X+2CH2):(Y+1DB). In other words, a lipid with X carbons and Y DBs will elute at a similar RT to a lipid with two more carbons and one more DB. The ECN model provides a simple framework to predict and compare RTs across species with varying chain lengths and degrees of unsaturation. This principle was first described in the 1980s for PLs such as PC and for triacylglycerols [48]. Since then, it has been validated in many studies and is now routinely applied in lipidomics to support annotation, resolve isomeric overlaps and detect misassigned peaks.

The ECN model predicts RT of lipids with the same headgroup in RP separation. It accounts for acyl chain length and degree of saturation. One study shows a strong correlation in retention across lipids with different headgroups but the same fatty acid motif. This inter-class relationship expands the use of RT models in lipidomics [47]. The model helpes assign lipids to peaks where isomeric overlap was present. It improves confidence in distinguishing lipids that share similar masses but differ in structure. This reduces ambiguity in peak identification and strengthenes lipid annotation.

Even though many lipids coelute, they can still be distinguished by their exact mass, isotopic patterns and elution behaviour compared to the other lipids of the same class. A molecule can be identified by the matching of the experimental and the theoretical isotopic pattern in the mass spectrum. There are more than 90,000 lipid species, which makes analysis difficult since many are structurally similar and hard to resolve in complex mixtures [49]. Small structural differences can cause overlap during lipidomics analyses, complicating peak assignment. The Lipidomics Standards Initiative gives examples of good laboratory practice emphasizing the need for correction [50]. In lipidomics, isomericity is an analytical challenge, since lipids share the elemental composition and mass, resulting in producing identical m/z values. An MS-based identification is not enough to identify the lipids, while chromatographic separation can indeed resolve some isomers. If isomers are not resolved, quantification reflects combined signals rather than individual molecules. This can bias interpretation of lipid class composition and pathway activity [51].

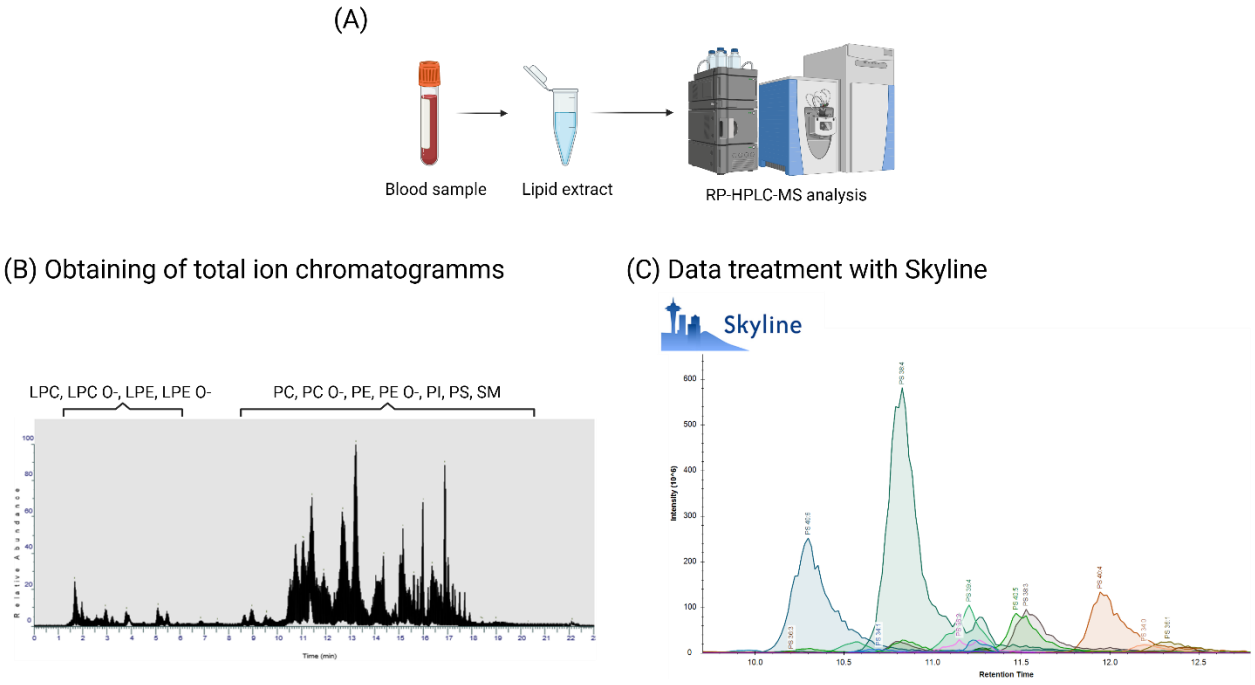

Figure 2: Experimental setup of RP-HPLC-MS

(A) Summary of sample preparation, RP-HPLC-MS analysis. (B) Total ion chromatogram obtained during measurement run with lipid elution order. (C) Data treatment with Skyline software showing detected lipid species of one lipid class.

Created in https://BioRender.com

An RP-HPLC–MS system typically includes a high-resolution mass spectrometer such as a ToF or Orbitrap. In this work, high-resolution detection was performed on an Orbitrap platform (Figure 2). The instrument provides the mass accuracy and resolving power needed for confident lipid identification. The Orbitrap is a high-resolution Fourier-transform mass analyser. It traps ions in an electrostatic field and measures their mass-to-charge ratio (m/z) from oscillation frequencies. Its core design uses a spindle-shaped central electrode and a surrounding barrel electrode that form a stable potential well. Ions injected into this field orbit the spindle and oscillate harmonically along the trap axis, with frequency determined only by their m/z and the field strength. Detection is non-destructive: the oscillating ions induce an image current on split detector electrodes, even if at a point ions decay for collisions. The resulting transient signal, containing multiple frequencies, is digitized and Fourier-transformed to produce a mass spectrum, where frequency corresponds to m/z and amplitude to abundance [52].

Orbitrap achieves very high mass resolution: up to 480,000 full width at half maximum (FWHM) at m/z 200 and in optimized modes reaching ~1,000,000 FWHM. Such resolution enables separation of closely spaced ion species across a wide mass range, including low molecular weight analytes. Mass accuracy is typically 1–5 ppm and with proper calibration can fall below 1 ppm. This accuracy results from stable frequency measurement and the fact that the axial oscillation frequency is independent of space-charge effects to first order, giving the Orbitrap a higher dynamic range and more consistent accuracy than conventional ion traps with m/z-dependent voltages [53].

Orbitrap mass spectrometers have become central to many analytical chemistry and bioanalytical applications. Often configured in hybrid instruments (e.g. quadrupole-Orbitrap or linear ion trap-Orbitrap systems), they combine a fast front-end for ion selection with the Orbitrap as the high-resolution detector [54]. In metabolomics and lipidomics, Orbitrap instruments allow detection of small molecules with high selectivity, resolving isobaric metabolites and providing molecular formula information from accurate masses.

Choice of acquisition strategy shapes what the Orbitrap records and how results are interpreted. Two strategies are common for data acquisition: data independent acquisition (DIA) and data dependent acquisition (DDA). In DIA, the mass range is divided into fixed windows and each window is fragmented in sequence. This records fragments for all precursors in that window and allows later reanalysis. Using more windows also lengthens the cycle time and can reduce sampling across chromatographic peaks.

DDA, or auto-MS/MS, begins with a survey scan to detect peaks above an intensity threshold. The instrument then triggers MS/MS on those peaks which are most intense, often as parallel reaction monitoring events. Analysts can use inclusion lists to prioritize m/z values. This enables full-scan MS and targeted MS/MS for abundant or selected compounds. The drawback is that low-abundance analytes may be missed if they never pass the threshold and fast elution can cause missed apex sampling. In RBC lipid profiling shotgun lipidomics, this means species like PC and PE are readily fragmented, while low-level PS or PI may be overlooked. Dynamic or iterative exclusion lists can improve coverage but often require multiple injections [55].

Limitations of RP-HPLC-MS include slower analysis and potential bias in quantification. Typical runs last 15–30 minutes, which lowers throughput compared to direct infusion that takes only minutes. This is a concern for large studies, though UHPLC and SFC improve speed [37]. RP cannot resolve all isomers. Sn-positional isomers co-elute on C18 and DB positional isomers also overlap. Specialized methods such as ozone-induced dissociation or silver-ion chromatography are needed. Using one internal standard per class can cause matrix-dependent errors, so careful validation is required. Neutral lipids like cholesterol are poorly detected under standard RP-LC-ESI conditions and may need method adjustments [56].

1.5 Previous findings on RBCs via RP-HPLC-MS based lipidomics

Timperio et al. developed one of the first comprehensive RP-HPLC–ESI–qTOF lipidomics workflows specifically for RBCs [57]. Their work focuses on profiling the intact lipidome of human RBC membranes and tracking how it changes during blood bank storage, but their method itself provides a clear baseline of RBC lipid composition under healthy conditions. When comparing fresh and stored RBCs, they observe progressive lipid remodelling during storage. Notably, there is an accumulation of ceramides and other sphingolipid derivatives and subtle shifts in glycerophospholipid species that are considered part of the storage lesion. These findings indicate that even though bulk lipid classes remain relatively stable, qualitative changes occur over weeks of cold storage. RP-HPLC–MS reduces spectral congestion compared to direct

infusion and reveal low-abundance species such as minor LPLs (LPC, LPE) and ether-linked forms, which are often underrepresented in older datasets. The study provides a detailed lipidomic baseline of RBC membranes under healthy and stored conditions, establishing RP-HPLC–MS as a robust platform for RBC lipidomics [57].

Vasku et al. performed a comprehensive lipidomic analysis of RBC membranes (alongside plasma and ocular tissues) using complementary HILIC and RP-LC-HRMS [58]. In their workflow, RBC lipids are extracted and analysed in two runs: one by HILIC and one by RP-UHPLC, both coupled to high-resolution MS. This enables detection of ~500 lipid species in each sample. RP chromatography proves especially effective for separating nonpolar lipid classes (e.g. diacylglycerols, triacylglycerols, cholesterol esters), which do not elute in HILIC. However, there is a disadvantage: polar PLs tend to coelute more in RPC, making their resolution more challenging in that mode. The study reports relative intensity distributions of lipid classes in RBCs as compared to plasma and tissues, thus establishing how RBC membranes compare in lipid composition among tissues. Their data confirm that RPC is more sensitive in detecting hydrophobic lipid species [58].

1.6 Shotgun Lipidomics of RBCs

Shotgun lipidomics is a direct infusion method where total lipid extracts are introduced into a mass spectrometer without chromatography (Figure 3). Lipid ions can be detected within a single spectrum when using full-scan acquisition, although not all experiments necessarily employ this mode. In practice, targeted methods such as selected ion monitoring (SIM) or multiple reaction monitoring (MRM), as well as MS/MS experiments, may also be used to detect specific lipid ions [59]. The approach depends on high mass resolution and accurate mass acquisition to separate overlapping species, combined with class-specific fragmentation for identification [60].

To infuse lipid into a mass spectrometer in an automated fashion, the Advion TriVersa NanoMate is often used. This is an automated autosampler and nanoESI ionization source that serves as a front-end interface for mass spectrometers. At its core is the ESI Chip®, a silicon microfluidic device with many nozzles, each acting as an electrospray emitter. A robotic arm handles disposable conductive pipette tips, aspirates small sample volumes and delivers them to the chip [61]. High voltage applied to the liquid forms a Taylor cone at the nozzle, producing a fine spray of charged droplets into the mass spectrometer [62]. At nanolitre-per-minute flow rates, solvent evaporates rapidly, leading to efficient ion desolvation and ionization, even for large biomolecules. The multi-nozzle chip design allows each sample to use a fresh emitter, reducing clogging and contamination. Disposable pipette tips keep samples isolated until infusion, minimizing carryover. The system thus combines autosampling with highly stable nanoESI performance, offering reproducible ionization and high sensitivity across many samples. This makes it especially useful for lipidomics and proteomics workflows where sample volumes are limited and cross-contamination must be avoided [61].

Shotgun lipidomics requires samples to be clean and well-prepared. A limitation is the reliance on consumable chips and pipette tips, which increases operating cost. Despite this, the TriVersa NanoMate has become an important tool in applications such as high-throughput screening, shotgun analyses of complex mixtures and native MS of fragile biomolecular complexes, where its automation, reproducibility and gentle ionization provide clear advantages [63].

In direct infusion, classic DDA is not effective because the most intense ions (e.g., abundant PC 16:0/18:1 in RBC) would dominate and be repeatedly chosen for MS/MS, while low-abundance species would never get fragmented. Instead, shotgun lipidomics uses targeted or DIA-like acquisition to obtain MS/MS information. Shotgun DIA fragments all ions, giving an unbiased view of the lipid extract. In RBC analysis this allows detection of low-abundance species such as PI that DDA might miss. The method is reproducible since fragmentation is deterministic, which supports quantitative comparisons across groups. The drawback is the complexity of the data, as assigning fragments to their correct precursors requires advanced software or prior information [55].

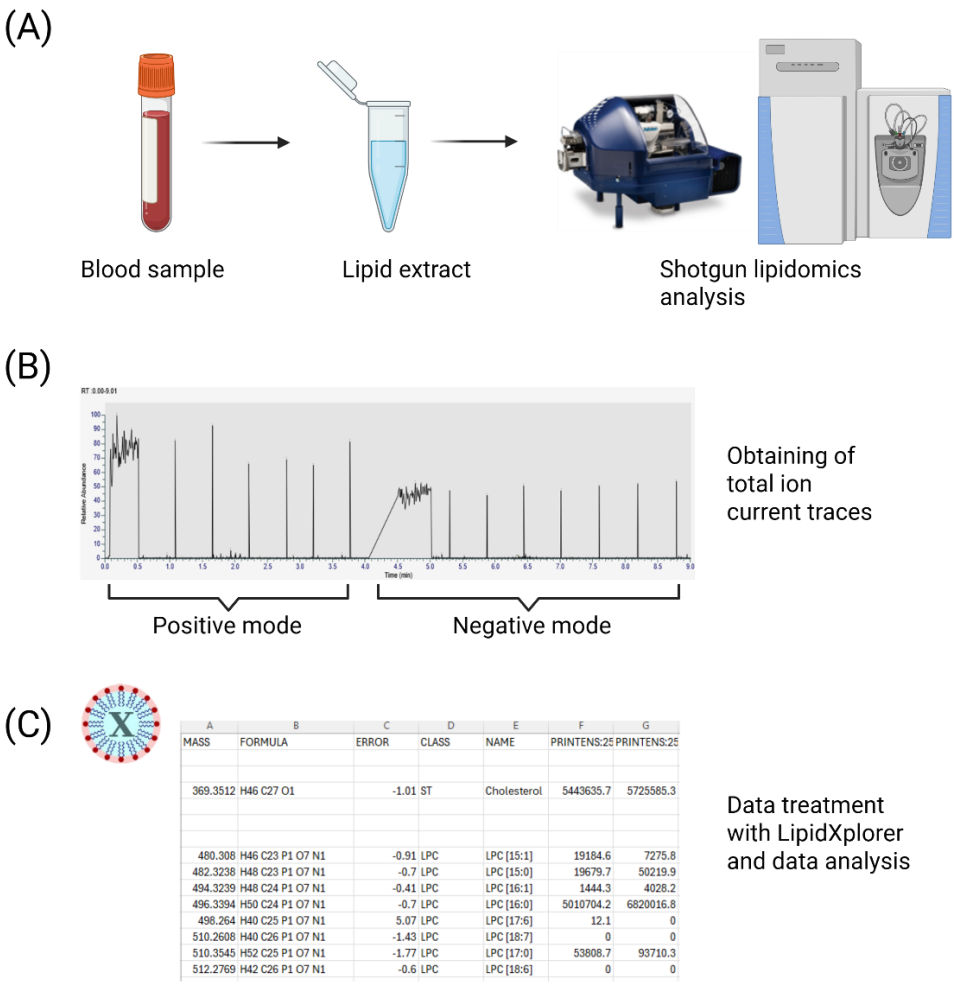

MASS	FORMULA	ERROR	CLASS	NAME	PRINTENS:25	PRINTENS:25
369.3512	H46 C27 O1	-1.01	ST	Cholesterol	5443635.7	5725585.3
480.308	H46 C23 P1 O7 N1	-0.91	LPC	LPC [15:1]	19184.6	7275.8
482.3238	H48 C23 P1 O7 N1	-0.7	LPC	LPC [15:0]	19679.7	50219.9
494.3239	H48 C24 P1 O7 N1	-0.41	LPC	LPC [16:1]	1444.3	4028.2
496.3394	H50 C24 P1 O7 N1	-0.7	LPC	LPC [16:0]	5010704.2	6820016.8
498.264	H40 C25 P1 O7 N1	5.07	LPC	LPC [17:6]	12.1	0
510.2608	H40 C26 P1 O7 N1	-1.43	LPC	LPC [18:7]	0	0
510.3545	H52 C25 P1 O7 N1	-1.77	LPC	LPC [17:0]	53808.7	93710.3
512.2769	H42 C26 P1 O7 N1	-0.6	LPC	LPC [18:6]	0	0

Figure 3: Experimental setup of shotgun lipidomics technique

(A) Summary of sample preparation, shotgun analysis. (B) Total ion current traces obtained during direct infusion, showing a polarity switch in one run. (C) Data treatment with LipidXplorer software and further statistical data analysis. Created in https://BioRender.com

Shotgun lipidomics offers high throughput and direct quantitation. Each sample can be analysed within minutes since no LC step is required. All analytes and internal standards enter the ion source at the same time, thus high-abundance lipids can dominate ionization and suppress signals from minor species [64]. As a result, low-abundance lipids often have higher detection limits than in LC-MS, where separation reduces competition [42]. A benefit is that ions are ionized in the same matrix condition, thus matrix effect is reduced compared to RP-HPLC-MS analysis in gradient mode. This makes the signal ratio of analyte to internal standard closely reflect concentration. Using a full set of isotopically labelled synthetic standards allows robust and comprehensive quantification.

1.7 LipidXplorer

LipidXplorer is an open-source software for identifying and quantifying lipids in shotgun MS data. A key feature is the MasterScan, a unified data structure that consolidates and denoises spectra into a resolution-corrected peak list [65]. Identfication of lipid using LipidXplorer is based on the Molecular Fragmentation Query Language (MFQL). MFQL is a scripting language that allows users to define lipid identification rules based on lipid structure characteristics and fragmentation patterns, a part of the script is shown in Figure 4. The query defines precursor ions (prPC in the Figure) within the PC elemental range and fragment ions (headPC in the Figure) corresponding to the diagnostic phosphocholine head group ($C_5H_{15}O_4PN^+$, m/z 184.0733). Identification requires a match of prPC in MS^1 with confirmation of the head group in MS^2. A filter condition ensures even carbon numbers in fatty acyl chains. The report outputs precursor mass, assigned PC species name, elemental composition, mass error, precursor intensity and fragment ion intensity, enabling automated annotation of PC species from high-resolution tandem MS data.

```
QUERYNAME = Phosphatidylcholine;
DEFINE prPC = 'C[20..48] H[30..200] N[1] O[8] P[1]' WITH DBR = (1.5, 7.5), CHG = 1;
DEFINE headPC = 'C5 H15 O4 P1 N1' WITH CHG = 1;

IDENTIFY
      prPC IN MS1+ AND
      headPC IN MS2+

SUCHTHAT
      isEven(prPC.chemsc[C])

REPORT
      MASS = prPC.mass;
      NAME = "PC [%d:%d]" % "((prPC.chemsc - headPC.chemsc)[C] - 3, prPC.chemsc[db] - 1.5";
      CHEMSC = prPC.chemsc;
      ERROR = "%dppm" % "(prPC.errppm)";
      INTENS = prPC.intensity;
      FRAGINTENS = headPC.intensity;;
```

Figure 4: MFQL script for identifying PC species

This avoids reliance on static spectral libraries and enables detection of uncommon or novel lipid species. LipidXplorer supports reliable lipid identification and quantification, which is critical for studying membrane biology, metabolism, inflammation and neurodegeneration [65]. This makes it well suited for exploratory

studies and biomarker discovery. LipidXplorer output categorizes lipids into headgroup intensity ('Head'), fatty acyl chain intensity ('FA1', 'FA2') and 'PRINTENS' states for precursor intensity. This reflects the modular architecture of lipid molecules, where the polar headgroup defines the lipid class, the fatty acyl chains specify the molecular species and the intensity provides the basis for quantitation.

1.8 Previous findings on RBCs via Shotgun lipidomics

Brügger et al. pioneered a nano-ESI shotgun lipidomics method to quantify RBC membrane lipids with picomole sensitivity [45]. They demonstrate direct infusion MS/MS can profile all major PL classes in human RBC extracts, including PC, PE, PS, PI SM, minor classes (Phosphatidylglycerol (PG), PA) and their plasmalogen analogues. This study establishes that RBC membranes can be rapidly analysed without chromatography, enabling detection of plasmalogen species and very low-abundance lipids. It provides a foundational reference for the RBC lipid composition, confirming the presence of the key classes above in healthy RBC [45].

Leidl et al. performed comprehensive shotgun lipid profiling of circulating blood cells (monocytes, lymphocytes, granulocytes, platelets and RBCs) using direct-infusion ESI-MS/MS [66]. They report that PC and free cholesterol are the dominant lipid components of the RBC membrane, with an unusually low PC/cholesterol molar ratio. RBCs are found to have a unique PL species pattern, including a high content of saturated and monounsaturated fatty acyl chains compared to other blood cells. Notably, RBCs contain significant amounts of PE largely confined to the inner membrane leaflet along with PS and SM, with smaller proportions of PI. Overall, this study provides a quantitative baseline for RBC lipid class composition [66].

Vahedi et al. used direct-infusion triple quadrupole MS to quantify human RBC membrane lipids, with a novel focus on bilayer leaflet asymmetry [67]. They extract and analyse only the outer leaflet lipids using a cyclodextrin exchange method, then profile the lipids by shotgun MS. The data confirmes that PC and SM are the most abundant outer-leaflet PLs in healthy RBCs. PC 34:1 (commonly 16:0/18:1) and SM 34:1 (often 16:0 with an 18:1 sphingosine base) are among the most dominant species in the RBC membrane outer leaflet. This shows that monounsaturated lipids with one DB make up a large share of the RBC lipidome, often the largest unsaturation group. By contrast, PS and PE are essentially absent from the outer leaflet. This study's key finding is a quantitative confirmation of RBC membrane asymmetry and composition: the outer leaflet is dominated by choline lipids (PC, SM) while inner leaflet amino PLs (PE, PS) are hidden from the extracellular side [67].

1.9 Findings on RBCs by alternative methods

Neonatal RBC membranes are known to be less fluid and more rigid in their hydrophobic core than adult membranes [8,18]. To investigate the rigidity and fluidity of the membranes, researchers introduced an SM to PC ratio, that reflects the balance of these lipids. SM-rich erythrocyte membrane tends to organize SM and cholesterol into tightly packed, liquid-ordered domains and this ordering correlates with decreased

membrane fluidity and cell deformability [68]. This suggests that the higher SM content in neonatal RBCs plays a direct role in their stiffer membranes. In stored blood, shifts in this ratio can track membrane remodelling and storage lesions. One study reported an SM:PC ratio of 0.89 in neonatal RBCs compared with 0.81 in adult RBCs [17], while another report found an SM/PC ratio of about 1.03 in cord blood erythrocytes vs 0.81 in adult cells [69]. These findings indicate that neonatal RBC membranes are relatively enriched in SM, or relatively depleted in PC, compared with adult membranes.

Speaking about separate lipid classes, LPC and other LPLs are present at very low levels in fresh, healthy RBCs. Neerhout reported that LPC made up about 1.0% of neonatal RBC PLs and 1.2% in adults [13]. This suggests neonates do not have more LPC than adults, with a slightly lower fraction in newborns. Modern MS detects lyso-species with high sensitivity and handling or storage can generate LPC. Vlaar et al. found that significant amounts of LPC appear in blood components over storage time, especially when plasma is present. They showed that partial hydrolysis of PC by PLA_2 is responsible and that RBCs stored in saline/glucose additive did not accumulate LPC, whereas those stored in plasma did [70].

Comparative studies of infants, including preterm, versus adults generally do not show higher levels of very-long-chain lysolipids in infants. In fact, some species appear lower. Across the lifespan, RBC fatty acyl profiles show gradual changes. One blood-spot study demonstrated that very-long-chain LPCs decrease from neonates to adults. Concentrations of C22:0-, C24:0- and C26:0-LPC fall with age, while C20:0-LPC rises [71]. At the same time, neonates did not show higher C20:0 LPC than adults. Instead, they had lower C20:0 and higher C22–C24 fractions. Another neonatal study found that the major LPC species measured (16:0, 18:0, 18:1, 18:2, 20:4) were all significantly lower in cord blood at birth than in adult blood and very-low-birth-weight infants showed prolonged suppression of LPC after birth [72].

Lower plasmalogen levels in neonates are well documented and are linked to increased vulnerability to oxidative stress, since plasmalogens act as protective lipids against oxidation. Studies show that neonates have significantly reduced RBC plasmalogen content, both choline and ethanolamine types, compared with adults, due to developmental immaturity [20].

Hypoxia, reoxygenation at birth or complications like retinopathy of prematurity, are examples of oxidative stress and can drive accumulation of RBC membrane oxidation products [8]. It is likely that a greater fraction of PE O- is converted to LPE O- in these cells, since plasmalogens protect membranes by sacrificing their vinyl-ether bond. When oxidized, this bond breaks, producing a lysoplasmalogen and a reactive aldehyde [20]. Thus, elevated LPE O- in neonates may reflect ongoing plasmalogen turnover.

Gercken et al. analysed the fatty acid composition of erythrocyte PLs in adults, normal newborns and neonates with Rh erythroblastosis. Within the major PL classes, PC shows clear developmental differences: newborn RBCs contain relatively more SFAs and arachidonic acid (20:4) in PC compared with adults, while levels of linoleic acid (18:2) are reduced. LPC, though present only as a minor fraction, is consistently detected

in both adult and neonatal erythrocytes. The authors observed that neonatal LPC species tend to reflect the same enrichment in saturated and arachidonate species found in PC, supporting the idea that LPC largely arises from partial hydrolysis of PC. These findings establish early evidence that both PC and LPC in neonatal RBCs differ systematically from adults, reflecting developmental regulation of fatty acid incorporation into membrane choline-containing PLs [73].

Castillo Salinas et al. investigated RBC fatty acid composition in preterm (<32 weeks gestation) versus term infants, both at birth and after one month of life [74]. Using GC the authors demonstrate that preterms are born with a distinct RBC lipid profile, described by significantly higher levels of SFAs such as stearic acid (18:0) and lignoceric acid (24:0), a deficit in linoleic acid (18:2 n-6) and an enrichment in arachidonic acid (20:4 n-6). These findings show that preterm infants lack the final phase of fat accretion, leaving them deficient in 2-double-bond lipids and enriched in 4-double-bond species. The fatty acid balance has implications for membrane rigidity, oxidative stress and developmental outcomes, highlighting the need for adapted nutritional strategies, including DHA and PUFA supplementation, to compensate for the disrupted perinatal lipid supply [74].

The study by Wendel examined fatty acid composition in erythrocyte membranes of patients with disorders of propionate metabolism and highlighted the abnormal accumulation of odd-numbered long-chain fatty acids in this pathological context [75]. Under normal physiological conditions, almost all fatty acids in adult humans are even-numbered, so adult RBC lipid species predominantly show even total carbon counts. Odd totals arise only from trace odd-chain fatty acids such as C15:0 or C17:0, which are derived from diet or endogenous metabolism and account for only a very small fraction of RBC membrane lipids. This explains why the overall fatty acid distribution in healthy adult RBCs is strongly centred on even numbers and deviations toward odd-chain enrichment serve as a metabolic hallmark in certain inherited disorders [75].

Aparicio et al. examined longitudinal changes in maternal plasma fatty acid composition during pregnancy, focusing on SFAs, n-6 and n-3 PUFAs [76]. They find significant increases in n-3 PUFAs, especially DHA (22:6), during late gestation, reflecting the placenta's active transfer of long-chain PUFAs to the fetus. Their results on DHA support the interpretation that the six-double-bond fraction rises in newborn samples as a consequence of maternal supply [76].

1.10 Hypothesis

Clinical data show that extremely preterm infants transfused with blood from older women have improved survival and lower morbidity compared to those receiving blood from younger or male donors [2]. Differences in RBC membrane lipids may explain why transfusions from older female donors are linked to better survival and outcomes in preterm infants. The distinct lipid profile of older female RBCs could make them more compatible with the neonatal circulation, reducing post-transfusion complications.

The aim of this thesis is to examine how RBC membrane lipid composition differs across human populations, with a focus on donors of different sex and age compared to neonatal RBCs from term and preterm infants. Identifying such differences is significant because it links biochemical profiles to clinical outcomes and could inform transfusion practice in future.

2 Materials and Methods

2.1 Solvents and standards

All solvents for the extraction as well as for the LC were LC-MS grade. Chloroform ($CHCl_3$), acetonitrile (ACN), methanol (MeOH), isopropanol (IPA) were LC-MS grade (Thermo Fisher Scientific, Vienna, Austria). Formic acid was ordered from VWR, while ammonium formate and ammonium hydrogen carbonate were purchased from Thermo Fisher Scientific (Vienna, Austria).

SPLASH™ Lipidomix™ Mass Spec Standard (330707-1EA-015) has been used both for shotgun and RPLC-MS lipidomics analyses, purchased from Avanti Polar Lipids. This mix contains following lipid species: PC 15:0-18:1 (d7), PE 15:0-18:1 (d7), PS 15:0-18:1 (d7), PG 15:0-18:1 (d7), PI 15:0-18:1 (d7), Phosphatic Acid (PA) 15:0-18:1 (d7), LPC 18:1 (d7), LPE 18:1 (d7), Cholesteryl ester (CE) 18:1 (d7), Monoacylglycerol (MG) 18:1 (d7), Diacylglycerol (DG) 15:0-18:1 (d7), Triacylglycerol (TG) 15:0-18:1 (d7)-15:0, SM d18:1-18:1 (d9) as well as Cholesterol (d7).

2.2 Sample collection and storage

The blood samples used in this study can be classified into three groups according to the method of collection: RBC transfusions from packed red blood cell-bags (pRBC), cord blood RBCs and adult RBCs.

(A) RBC Transfusions (pRBC-bags)

pRBC transfusion bags used in this study were a donation from Dr. Christof Jungbauer and Mag. Robert Geretschläger (Austrian Red Cross). Small volumes (6-10 mL) of pharmaceutical-grade pRBC-units derived from the blood of 60 female or male donors younger than 30 years of age or older than 55 years of age, were aliquoted into smaller PVC-DINCH bags, stored for a maximum of 7 days at 4 °C and irradiated with 30 Gy within 24 h ahead of retrieval. The usage of small volumes of industry-grade pRBC units for scientific purposes was covered under the ethics approval EK20210506_01 approved by the ethics committee of the Austrian Red Cross.

(B) Cord blood RBCs

Blood was drawn aseptically into 9 mL Heparin tubes (Greiner Bio-One) from the umbilical cord vein of 22 term-born (> 36 weeks of gestation) and 9 prematurely born (< 36 weeks of gestation) infants directly after caesarean section. Infants whose mothers suffered from severe autoimmunity, acquire immunodeficiencies, hereditary monogenic diseases, transmissible infectious diseases (e.g.: Human immunodeficiency virus, Hepatitis), severe anaemia or infants with signs of chromosomal defects, congenital malformations or inborn errors of metabolism were excluded from the study. Informed consent was obtained from mothers prior to sampling. Procedures were approved by the ethics committee of the Medical University of Vienna (ref. 1704/2023 & 2040/2022).

(C) Adult RBCs

Blood was drawn from the antecubital vein of healthy, 14 adult volunteers between 20 and 30 years of age into 9 mL Heparin tubes (Greiner Bio-One). Informed consent was obtained prior to blood sampling. Procedures were approved by the ethics committee of the Medical University of Vienna (ref. 1704/2023 & 2040/2022).

2.3 Sample cohort

Samples were organized into eight predefined groups, for a total of 105. These included fresh blood samples (Paragraph 2.2.C), 7 female adults and 7 male adults; 9 preterm infants born before 36 weeks of gestation and 22 term infants born after 36 weeks. Four additional groups were defined from stored donor blood units (Paragraph 2.2.A). These represented different age and sex: 15 young men under 30 years, 15 young women under 30 years, 15 older men above 55 years and 15 older women above 55 years. This structure ensured coverage of both biological variation (age and sex) and clinical relevance (adult donors vs neonatal RBCs). Together, these comparisons provided a framework to assess how membrane lipid profiles differ and whether these differences may influence transfusion outcomes in preterm infants. A graphical representation of the cohort clustering and the corresponding label for each group is shown in Figure 5.

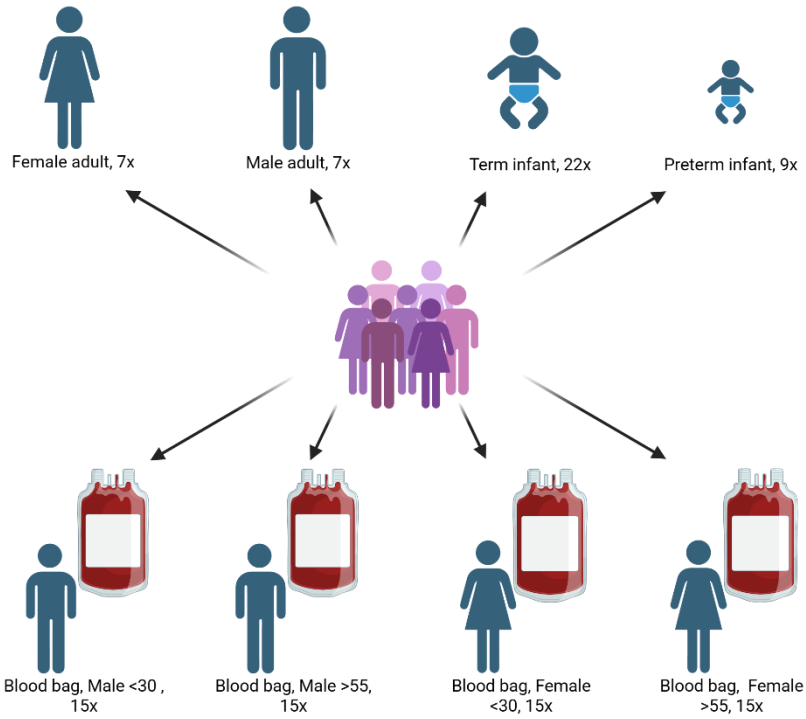

Figure 5: Study cohort with corresponding label and number of samples from each group

Created in https://BioRender.com

2.4 Isolation/preparation of RBCs

Blood was pooled in a 15 mL conical-bottom Falcon tube (Corning) and centrifuged at 280 x g for 8 min at 4 °C (Allegra X-12R, Beckman Coulter) to retrieve platelet rich plasma (PRP). PRP was subsequently discarded,

the remaining cells were resuspended in an equal amount of phosphate buffered saline (Thermo Fisher Scientific) and the procedure was repeated. Finally, the cell pellet was resuspended in Phosphate-buffered saline (PBS), re-aliquoted into 2mL round-bottom Eppendorf tubes and centrifuged at 10.000 x g for 2 min at room temperature (Pico 17 microcentrifuge, Thermo Fisher Scientific). Plasma and buffy coat were manually discarded; the cells resuspended to a final volume of 12 mL in PBS and filtered once (adult cells) or twice (cord blood-derived cells) through an Acrodisc® WBC (white blood cell) Syringe Filter (Cytiva) to deplete residual leukocytes. Erythrocytes from leukocyte-filtered, irradiated blood bags were retrieved using an 18-gauge blunt fill needle (BD-Biosciences) and carefully transferred into a 50 mL conical-bottom Falcon tube (Corning). Cells were then resuspended to a total volume of 50 mL in PBS to dilute residual storage medium. Filtered cells and diluted blood-bag-derived erythrocytes were centrifuged at 3200 x g for 15 min at 4 °C (Allegra X-12R, Beckmann Coulter) without breaks and the resulting supernatant was discarded using a vacuum suction unit. Afterwards, pRBCs were carefully resuspended and homogenized using a 1000 µL pipette tip to avoid differences in cell concentrations due to residual PBS contamination.

2.4.1 Isolation of erythrocyte membranes

The isolation method of erythrocyte membranes has been performed adapted to already established methods [77,78]. Packed RBCs were diluted 1:10 in ice-cold 5mM sodium-phosphate Buffer (pH = 6.5, Sigma Aldrich) supplemented with Halt™ Proteinase-Phosphatase Inhibitor Cocktail (Thermo Fisher Scientific). After homogenization using a 1000 µL pipette tip, the suspension was centrifuged at 20.000 x g for 10 min at 4 °C (Mikro 220R, Hettich). The resulting hemolysate was discarded and the membrane fraction completely resuspended with 1 mL ice-cold 5 mM Na-Phosphate Buffer. The procedure was repeated a total of seven times, until the resulting membrane pellet appeared cloudy-white to yellowish. After the last centrifugation the supernatant was discarded completely and 15 µL of pure membranes were retrieved from the center of the cloudy pellet, transferred into a round-bottom 2 mL Eppendorf tube and immediately snap-frozen in liquid nitrogen. Samples were stored at -80 °C until further analysis.

2.5 Sample preparation and calibration

RBC membrane lipids were extracted by a liquid/liquid biphasic extraction as following (Figure 6). RBC membrane samples were thawed on ice and homogenized by pipetting four times with a 100 µL pipette (Figure 6 (1)). Subsequently, they were centrifuged at 10,000 × g for 5 min at 4 °C (Figure 6 (2)). To each sample, 490 µL of methanol were added, followed by 10 µL of SPLASH® Lipidomix (1:100 diluted in methanol), added as an internal one-point calibration isotopically labelled standard (Figure 6 (3)). The tubes were vortexed for 20 s and supplemented with 1 mL chloroform (Figure 6 (3)), then incubated for lipid extraction at 4 °C under agitation (1000 rpm) for 1.5 h (Figure 6 (4)).

Phase separation was induced by adding 300 µL water containing 250 mM ammonium bicarbonate (Figure 6 (5)), followed by vortexing for 20 s and centrifugation at 10,000 × g for 5 min at 4 °C (Figure 6 (6)). A volume of 900 µL of the lower organic phase was collected and transferred into fresh Eppendorf tubes (Figure 6 (7)).

Samples were dried in a vacuum centrifuge for 1 h (Figure 6 (8)) and subsequently reconstituted in 50 µL of a shotgun solvent mixture (isopropanol/methanol/chloroform, 4:2:1, v/v/v) containing 7.5 mM ammonium formate (Figure 6 (9)). After vortexing for 20 s, the reconstituted extracts were transferred into HPLC vials for chromatographic separation and MS analysis (Figure 6 (10)). Aliquots not subjected to immediate analysis were resuspended in the shotgun solvent mixture and stored at −80 °C.

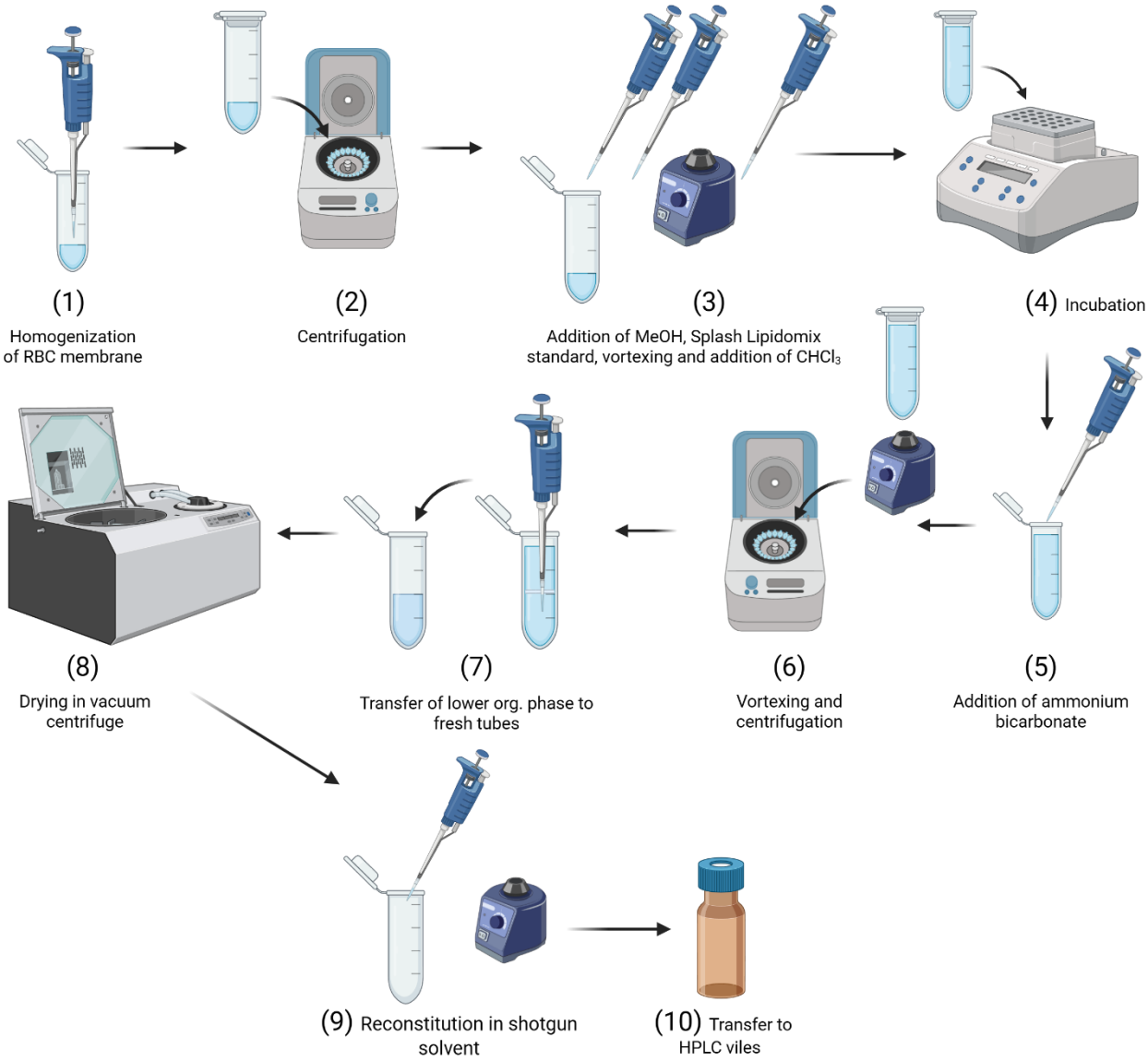

Figure 6: Lipid extraction in RBC membrane samples

Created in https://BioRender.com

2.6 Data acquisition

2.6.1 Shotgun lipidomics

Shotgun lipidomics analyses were performed using an TriVersa NanoMate (Advion Interchim Scientific®, Ithaca, NY, USA) system coupled to a high-resolution Q Exactive HF™ quadrupole-Orbitrap mass spectrometer (Thermo Fisher Scientific, Bremen, Germany). A volume of 15 µL of each sample was transferred into a 96-well plate (Eppendorf twin.tec® PCR Plate 96, skirted, 150 µL, PCR clean, colorless) and

sealed with aluminum foil (Corning 6570, Corning® 96-well Microplate Aluminum Sealing Tape, non-sterile). Following chip alignment and spray verification, the instrument was operated with the following settings: sample volume 10 µL; return of unused sample to the well enabled; aspiration of 2 µL air after sample; temperature 20 °C; delivery time 9 min; gas pressure 0.9 psi; spray voltage 1.1 kV. An inclusion list was created to drive broad MS/MS coverage across the lipid mass range. For positive mode, targets spanned m/z 260.16100 to 1199.00990 in 1.00100 m/z increments. For negative mode, targets spanned m/z 300.20100 to 1599.49900 in 1.00100 m/z increments. The combined list contained 2238 masses. Full MS scans were acquired at a resolution of 240,000, while DIA scans were acquired at a resolution of 60,000. The automatic gain control target was set to 1×10^6.

For LPC, PC, PC O-, PS and SM, quantification was based on precursor ion intensity. For PE, PE O- and PI, the intensity of the lipid head fragment was used instead.

Shotgun lipidomics analysis results in a total ion current trace, a graph of current intensity vs time point of infusion. The full method lasts 9 minutes. At the start, between 0 and 0.5 minutes, a spray voltage of 1.1 kV is applied and full MS1 acquisition in positive mode begins. Between the large peaks of full MS1 in positive mode, DIA scans are acquired. For example, from 0.5 to 1.08 minutes, DIA and MS2 events are recorded. This cycle is repeated six times in total until minute 4. At this point, the polarity switches from positive to negative and full MS1 acquisition in negative mode starts. Each high peak after minute 5 corresponds to a full MS1 in negative mode. In between these peaks, DIA scans in negative mode are performed. This alternating acquisition strategy allows alternated acquisition of both MS1 and MS2 data across polarities within a single run, improving coverage of lipid species present in the sample.

2.6.2 RP-HPLC-MS

RP separation was performed using an Acquity HSS (High-strength silica) T3 C18 column (150 × 2.1 mm, 1.8 µm) equipped with an Acquity VanGuard pre-column (5 × 2.1 mm, 100 Å, 1.8 µm; Waters). The column oven was maintained at 40 °C, with a flow rate of 0.25 mL/min. Mobile phase A consisted of acetonitrile/water (60:40, v/v) and mobile phase B of isopropanol/acetonitrile (90:10, v/v), both supplemented with 10 mM ammonium formate and 0.1% formic acid. The gradient of the mobile phase during the measurement, starting at 45% of mobile phase A and 55% of mobile phase B and further course is shown in Figure 7.

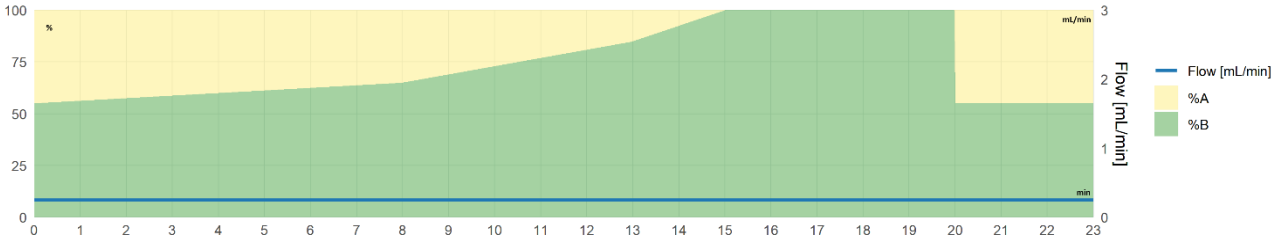

Figure 7: Visual representation of the RP gradient for RP-HPLC-MS

Data acquisition was carried out on a high-resolution Q Exactive HF™ quadrupole-Orbitrap mass spectrometer (Thermo Fisher Scientific, Bremen, Germany) equipped with an ESI source. The MS parameters were configured as follows: sheath gas flow rate 30, auxiliary gas flow rate 25, sweep gas flow rate 2, spray voltage 3.1 kV (in both positive and negative ionization modes), capillary temperature 200 °C and S-Lens RF level 30. The automatic gain control target was set to 1×10^6. Full MS scans were acquired in polarity switching mode (positive and negative) at a resolution of 60,000. The m/z range for both positive and negative mode spanned from 250 to 1200 m/z.

2.6.3 Quality control and randomization

Samples were analysed in randomized order to minimize sequence effects and potential batch bias. Three solvent blank injections were included at both the beginning and the end of the run to monitor carryover and background signal. In addition, blank samples and diluted SPLASH® Lipidomix standards were injected between groups to control for carry-over and assess system stability. This design ensured that observed differences between groups reflected true biological variation rather than analytical artifacts.

2.7 Data processing

2.7.1 Shotgun lipidomics

The raw data (.raw) files were converted into .mzML format using MSConvert 3.0 (ProteoWizard). Conversion parameters included 32-bit binary encoding precision, write index, zlib compression and Trans-Proteomic Pipeline (TPP) compatibility. A peak picking filter with a vendor-defined MS level of 1 was applied.

For LipidXplorer processing, the resolution gradient, a critical parameter, was determined in advance. To this end, averaged full MS spectra (positive and negative) and two representative MS/MS spectra (positive and negative) with ions distributed across the entire m/z range and signal intensities above 10^6 were selected. The top ion tables were exported from Xcalibur and plotted in Excel. Linear interpolation of the peak data was used to determine the resolution gradient, where the slope of the resulting equation represents the gradient value. LipidXplorer settings were configured separately for positive and negative ionization modes.

- **Positive mode (MS1):** selection window 0.5 Da; time range 30–240 s; m/z range 260–1200; resolution 230,000; mass tolerance 5 ppm; absolute threshold 0 ppm; resolution gradient −145; minimum occupation 0; frequency filter 0; MS1 offset 0 Da.

- **Positive mode (MS/MS):** m/z range 80–1200; resolution 110,000; tolerance 0.02 Da; absolute threshold 0 ppm; resolution gradient −67; minimum occupation 0; frequency filter 0; precursor mass offset (PMO) 0 Da.

- **Negative mode (MS1):** selection window 0.5 Da; time range 300–540 s; m/z range 300–1600; resolution 220,000; mass tolerance 5 ppm; absolute threshold 0 ppm; resolution gradient −142; minimum occupation 0; frequency filter 0; MS1 offset 0 Da.

- **Negative mode (MS/MS):** m/z range 80–1600; resolution 60,000; tolerance 0.02 Da; absolute threshold 0 ppm; resolution gradient -55; minimum occupation 0; frequency filter 0; PMO 0 Da.

Prior to data analysis, MFQL files corresponding to lipid classes in the respective ionization mode were imported into LipidXplorer. The software was then executed and the resulting .csv-output files were further processed in Excel, where the data has been cleaned up from mismatches and lipids with unusually high DB number.

2.7.2 RP-HPLC-MS

The .raw files were imported into Skyline 22.2 (MacCoss Lab) with a predefined lipid transition list for manual peak integration based on untargeted results obtained from shotgun lipidomics analysis. The integrated peak areas were then exported as a CSV file and further processed using Microsoft Excel and RStudio (version 2025.05.0+496). A total of 105 samples were analysed using RP-HPLC-MS. The following samples were measured in technical duplicates: Adult #4, #6, #7, #8, #9, as well as Term #2, #3, #4, #5, #6, #8, #9 and Blood bag #7.

After manual peak integration was completed and results were exported from Skyline, the fractional abundance of each lipid was calculated via RStudio. Those values were normalized to 100% for each sample to allow comparison between the total lipid class distribution between sample groups.

For the PS+PI fraction, the fractional abundance of each identified lipid species was first calculated and normalized to 100% within each sample. The summed values of all lipid species belonging to PS and PI were then used to determine the total PS+PI fraction.

For lipid species distribution within lipid class, the fractional abundance was calculated for each identified lipid and normalized to 100% within its lipid class. This approach allows direct comparison of species distribution patterns across groups.

For the unsaturation degree, fractional abundance of all lipid species in investigated lipid classes was normalized to 100% for each sample and then divided into groups according to the number of double bonds. This calculation provides insight into distribution of lipid species with different unsaturation between the cohort groups.

Distribution of fatty acyl chain length was examined to highlight possible difference between the different cohort groups. The shortest lipid detected was LPC 14:0, while the longest was SM species with 44 carbons in various DB states. To analyse this systematically, the dataset was divided into two ranges. For single-chain lipids (LPC, LPE, LPC O-, LPE O-), the longest detected was LPC 24:0. For double-chain lipids, the shortest detected was PC 26:0. Fractional abundances were calculated and normalized to 100 within each sample for the range 14–24 carbons and separately for the range 26–44 carbons. This allowed comparison of chain length distributions across groups without mixing single- and double-chain classes.

For the SM to PC ratio, the fractional abundance was calculated for each identified lipid and those values were normalized to 100% for each sample. Then, a sum of all fractional abundances for lipid species within PC and SM and finally a SM/PC ratio have been calculated.

Subsequent statistical analyses were performed using MetaboAnalyst 6.0. During preprocessing, no filters were applied in the data filtering step, meaning that all measured lipids were retained for analysis. There has been no additional sample normalization carried out. In addition, no data transformation or scaling procedures were applied. This approach ensured that the dataset was evaluated in its original form, without adjustments that could introduce bias or obscure true biological differences.

3 Results and Discussion

This thesis aims in investigating differences in RBC membrane lipid composition across different groups. It compares older (> 55-year-old) male and female donors as well as donor blood from blood bags with neonatal RBCs from term and preterm infants. The objective is to test whether lipid differences explain the improved outcomes observed when preterm infants receive blood from older female donors [2]. To address this, two complementary strategies were used. Untargeted shotgun lipidomics with the Advion TriVersa NanoMate provided a broad overview of the lipid composition. Semi-untargeted lipidomics with RP-HPLC-MS then focused on specific classes, including LPC, LPC O-, LPE, LPE O-, PC, PC O-, PE, PE O-, PI, PS and SM.

3.1 Untargeted shotgun lipidomics analysis

In order to gain insights into lipid composition in RBC membrane, an untargeted shotgun lipidomics workflow was performed in test RBC samples of adults and term infants. Measurements resulted in obtaining total ion current traces as shown in Figure 8.

These data provided an initial overview of lipid distribution across groups using an untargeted method. After lipid identification and quantitation performed with LipidXplorer across the two different groups of adult and term infants, lipids were plotted according to the different classes found (Figure 10-11). In accordance with literature [6], RBC membrane resulted composed mainly of PLs (PC, PE etc), LPLs and SM. Interestingly, the two groups (adult and term) showed difference in lipid pattern.

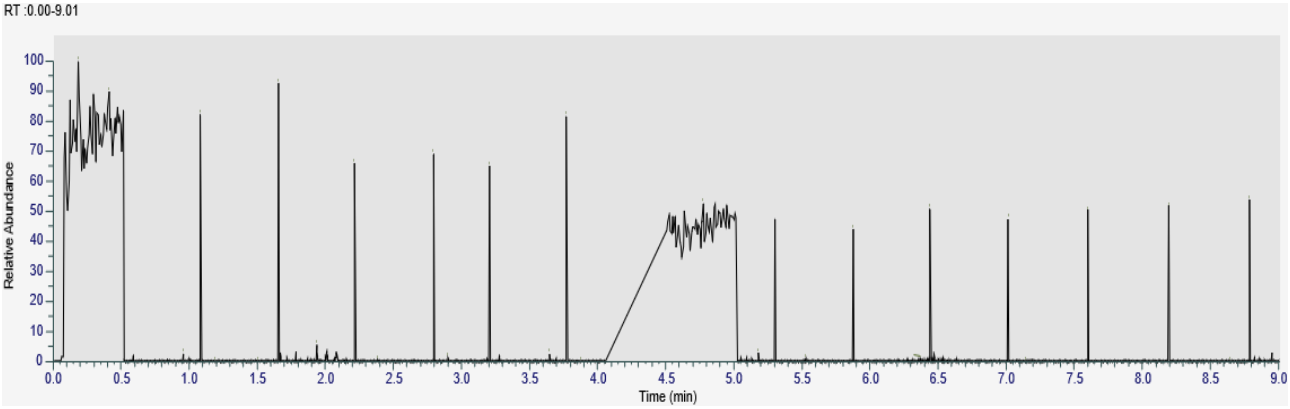

Figure 8: Total ion current trace of RBC sample of Adult #14 obtained in shotgun run

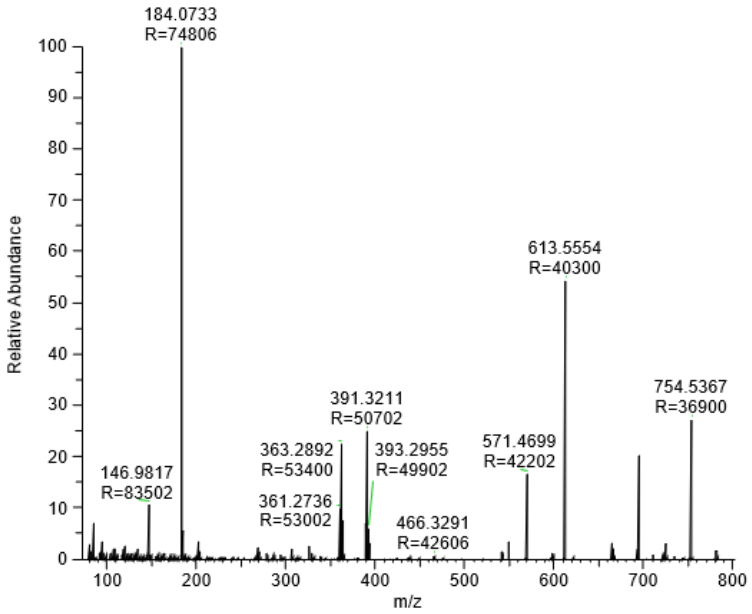

Figure 9: An excerpt from total ion current trace of Adult #14 obtained in shotgun run at RT 1.92, showing a typical lipid class selective fragment of LPC, PC, PC O- and SM classes at m/z 184.0733

A representative positive-ion spectrum from the shotgun analysis of Adult #14 is dominated by the phosphocholine head-group fragment at m/z 184.0733, the class-selective ion that marks choline-containing lipids as LPC, PC, ether-PC (PC O-) and SM (Figure 9). The high resolving power (R values annotated at each peak) and sub-ppm mass accuracy confirm confident head-group assignment and reliable deconvolution from neighbouring background ions. The most abundant species were PC 34:1 and PC 34:2, consistent with published findings [67]. Term infant RBCs contained more PC 34:1 and less PC 34:2 compared with adults. Additional PCs enriched in term infant RBCs included PC 32:0, PC 32:1, PC 36:4, PC 38:4 and PC 38:6. In contrast, PC 36:1 and PC 36:2 were more abundant in adult RBCs. The remaining species within the top 15 showed no significant differences between groups.

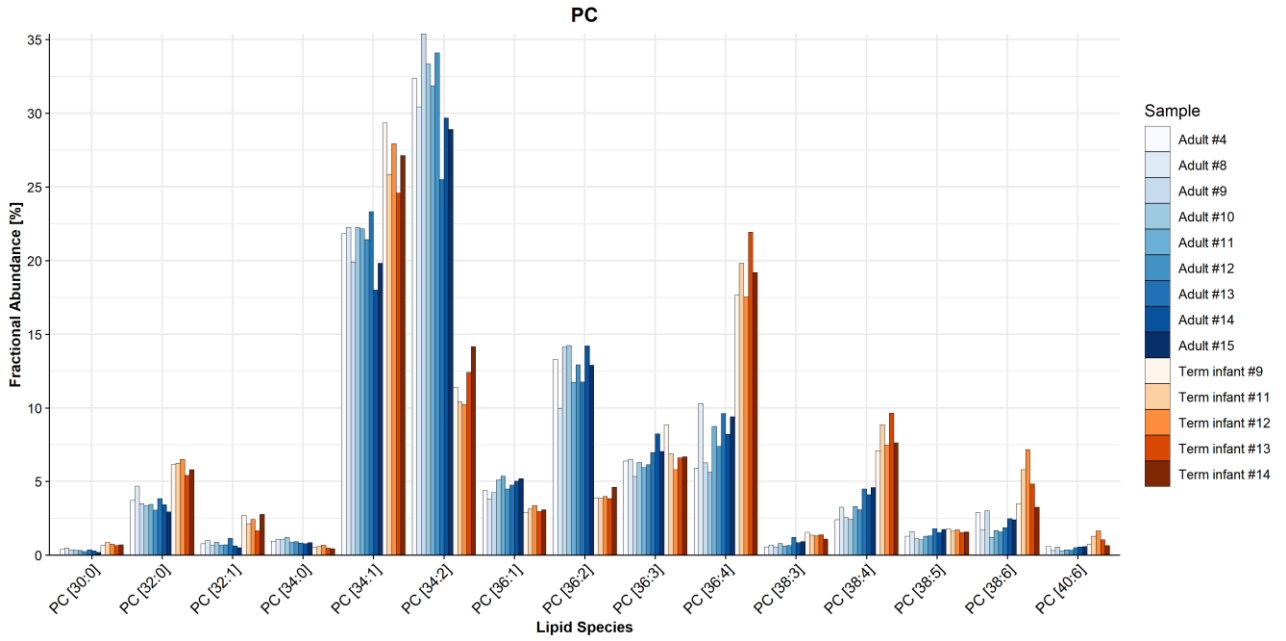

Figure 10: Top 15 PC species by fractional abundance and their distribution in fresh blood samples from adults and term infants

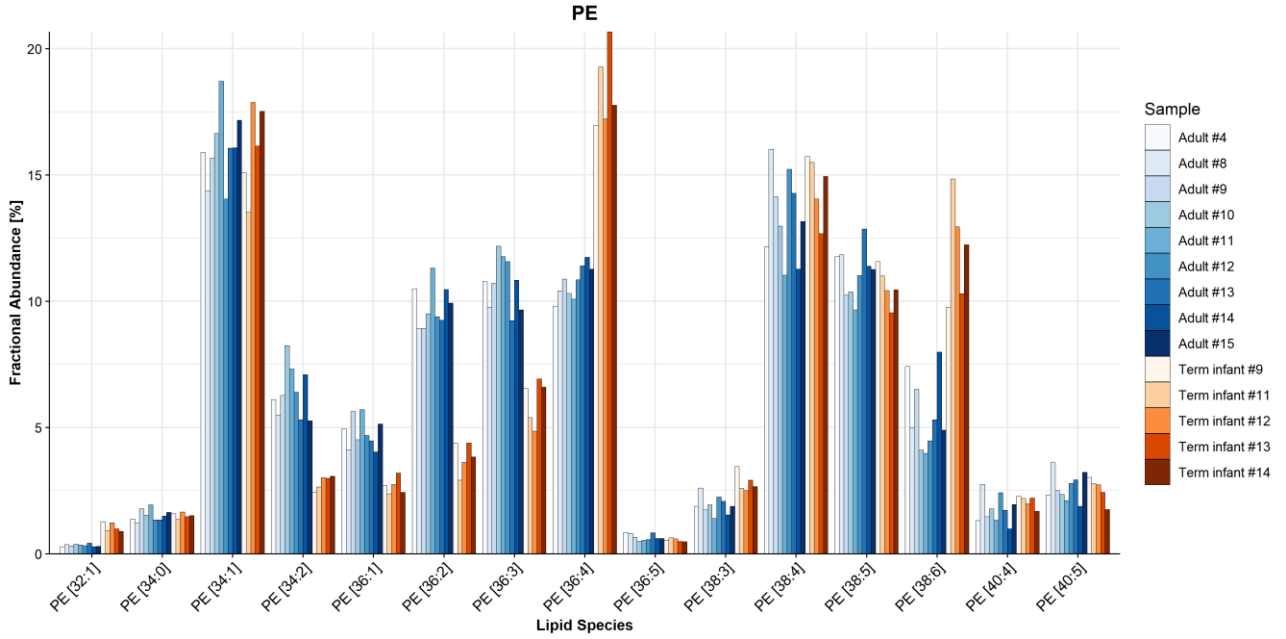

Figure 11: Top 15 PE species by fractional abundance and their distribution in fresh blood samples from adults and term infants

Regarding the distribution of PE species (Figure 11), clear group-specific patterns emerge. PE 32:1, 36:4 and 38:6 are more abundant in RBCs of term infants, indicating an enrichment of unsaturated PE species. Several mid-chain PEs, including 34:0, 34:1, 36:5, 38:3, 38:4, 38:5, 40:4 and 40:5, show no significant differences between infants and adults, suggesting these species are maintained at stable levels. These findings show that infant RBC membranes are characterized by an enrichment in certain unsaturated PE species, while adults show a more diverse distribution trending toward other PEs. Such compositional differences may contribute to the known disparities in membrane fluidity, deformability and oxidative resilience between infant and adult RBCs [8]. The lipid species distribution for other lipid classes can be found in attachment

(Figures A1-A6). In conclusion, untargeted shotgun lipidomics analysis provided us with an exploration of lipid classes present in RBC membranes and gave us a first glance of differences in lipid distribution in adults and term newborns.

3.2 Signal stability in RP-HPLC-MS analysis

RP-HPLC-MS analysis were conducted on the entire cohort (Paragraph 2.3) to assess differences in lipid composition between the different groups (fresh blood samples, preterm and term infants and stored blood units). To ensure reliability of the fractional abundance data of the found lipid species in terms of signal stability, a solution of SPLASH® Lipidomix diluted 1:555 in MeOH was injected multiple times during the chromatographic sequence and used as a quality control (QC) for signal stability. The measurement was carried out in three days; thus, a QC solution was necessary to exclude batch-to-batch variability. Blank samples and diluted SPLASH® Lipidomix standards were injected between sample groups in the chromatographic sequence to monitor carry-over, confirm system stability and provide anchors for normalization.

Areas of deuterated standard peaks were plotted and confirmed intra- and inter-day signal stability (Figure 12). Since RBC membrane showed to be composed by LPLs and SM (see Paragraph 3.1), the relevant deuterated lipids selected were LPC 18:1 (d7), LPE 18:1 (d7), PC 33:1 (d7), PE 33:1 (d7), PI 33:1 (d7), PS 33:1 (d7) and SM 36:1;2 (d9). The bar chart demonstrates that variation in the signal area of deuterated lipids between SPLASH injections was minimal. The overall signal remained stable across the full measurement sequence on all three days.

Comparing the results of the injections on different days, the inter-day signal stability can be considered excellent. Day-to-day variation in QC injections was minimal and trends remained flat across batches. Intra-day variation was slightly higher, which is typical for ESI-MS and has been reported earlier [79]. Signal drift and minor spray fluctuations were observed but stayed within acceptable limits. RTS were stable and the internal standards tracked well.

The signal stability check of the third measurement showed the same trend as the first (Figure 12 (3 and 6)), with no significant deviations. The species signal area remained relatively constant. Despite the decrease in lipid QC intensities observed during the second measurement, MS stability is considered maintained since lipid signals stayed stable and chromatographic stability for lipids was confirmed by assessing RTs. These results indicate that the method and generated data are reliable and suitable for further evaluation.

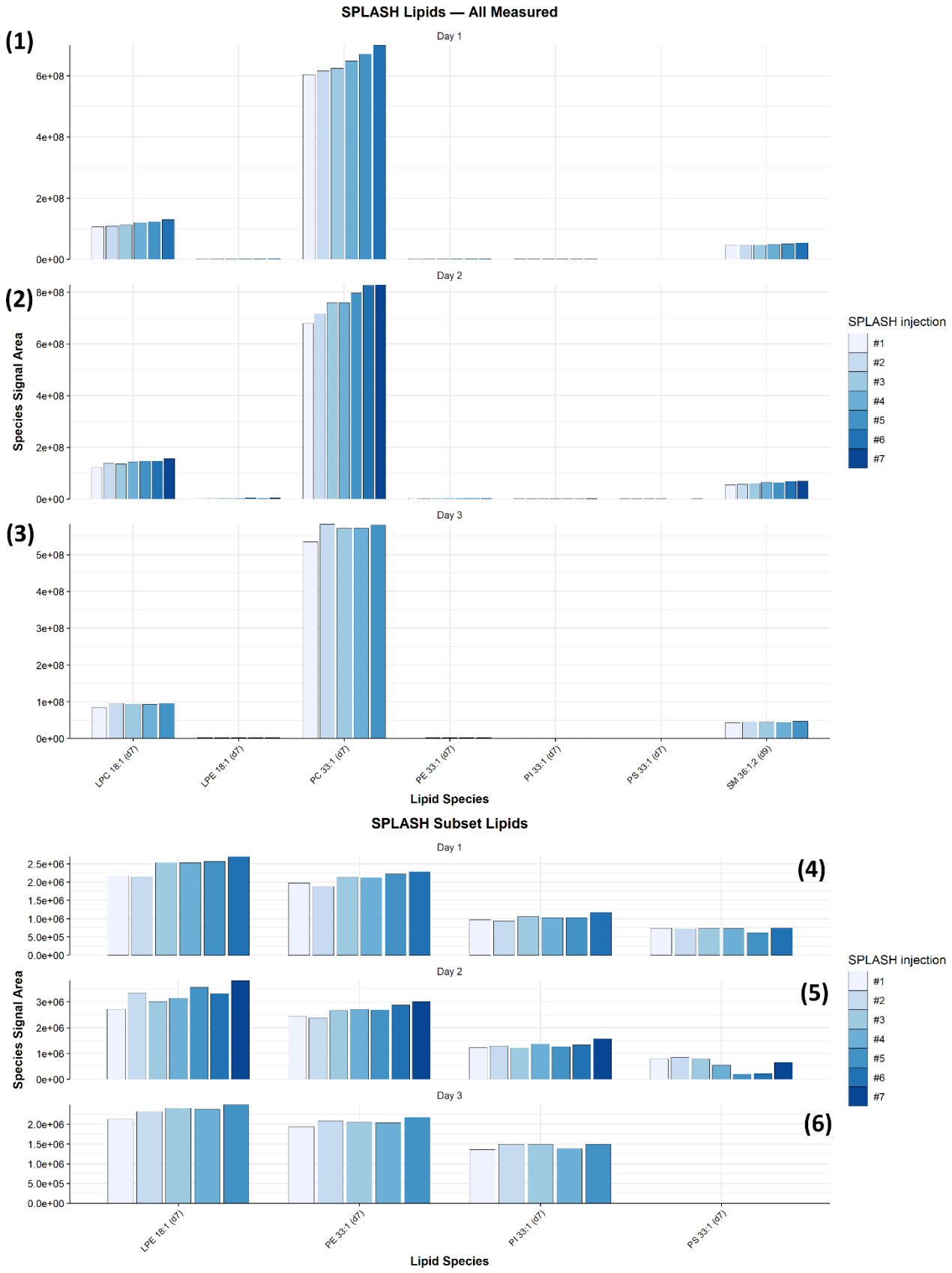

Figure 12: Peak areas for deuterated lipids in the SPLASH Lipidomix standard during the measurement days.

(1) corresponding to the measurement of day 1, while (4) provides a zoom-in onto the deuterated lipids with lesser signal area. (2) and (5) correspond to measurement of day 2, (3) and (6) to day 3, respectively

3.3 Semi-untargeted RP-HPLC-MS lipidomics

The chromatogram of the 23-minute method for sample Term #2 allows observation of distinct regions of lipid elution (Figure 13), which reflect differences in hydrophobicity of the lipid classes. Early in the run, more polar lipid classes such as LPC, LPC O-, LPE and LPE O- elute. These are followed by less polar classes including PC, PC O-, PE, PE O-, PI, PS and SM, which elute and appear later in the gradient. Lipid species from those classes overlap and elute at the same time, as shown on the extracted ion chromatogram (Figure 14). The separation allows partial resolution of lipid classes, yet many lipids from different classes coelute, contributing to spectral complexity. RT patterns nevertheless provide an additional identification parameter, as lipids of the same classes elute depending on the fatty acid chain length and number of unsaturation following the ECN rule [48,47]. This helps to validate peak assignments and to improve confidence in distinguishing isobaric or isomeric species.

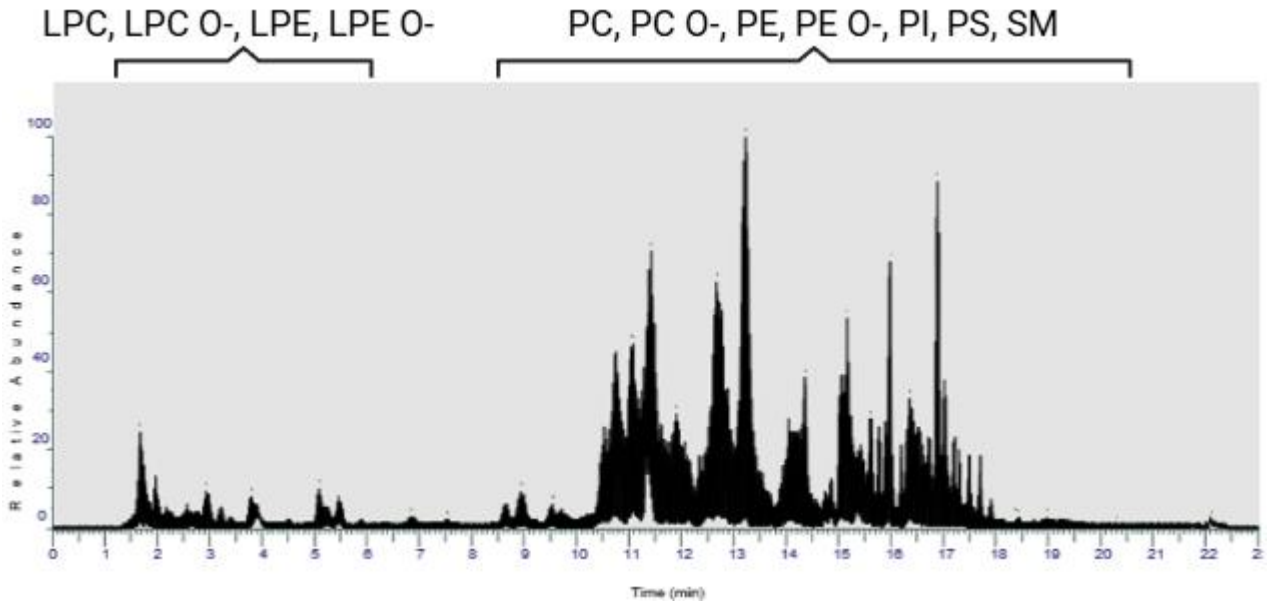

Figure 13: Chromatogram of RBC sample of Term #2 obtained in RP-HPLC-MS run

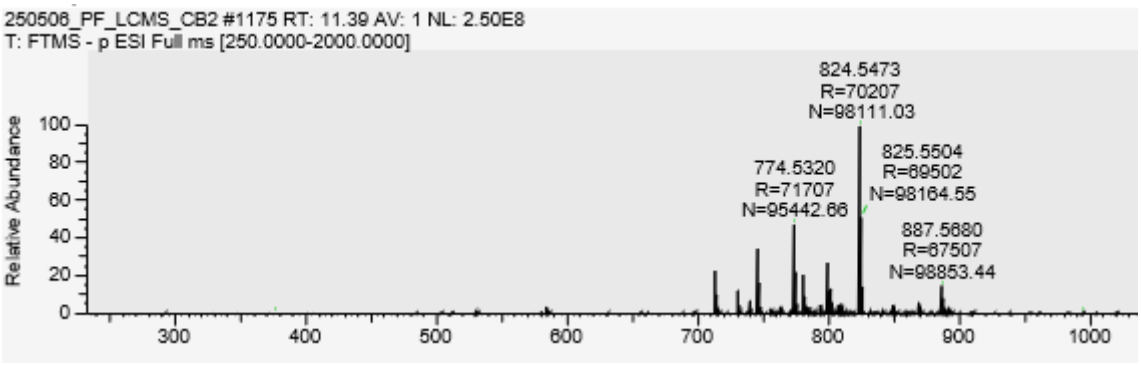

Figure 14: Extracted ion chromatogram of Term #2 obtained in RP-HPLC-MS run at RT 11.39

3.3.1 Isotopic pattern

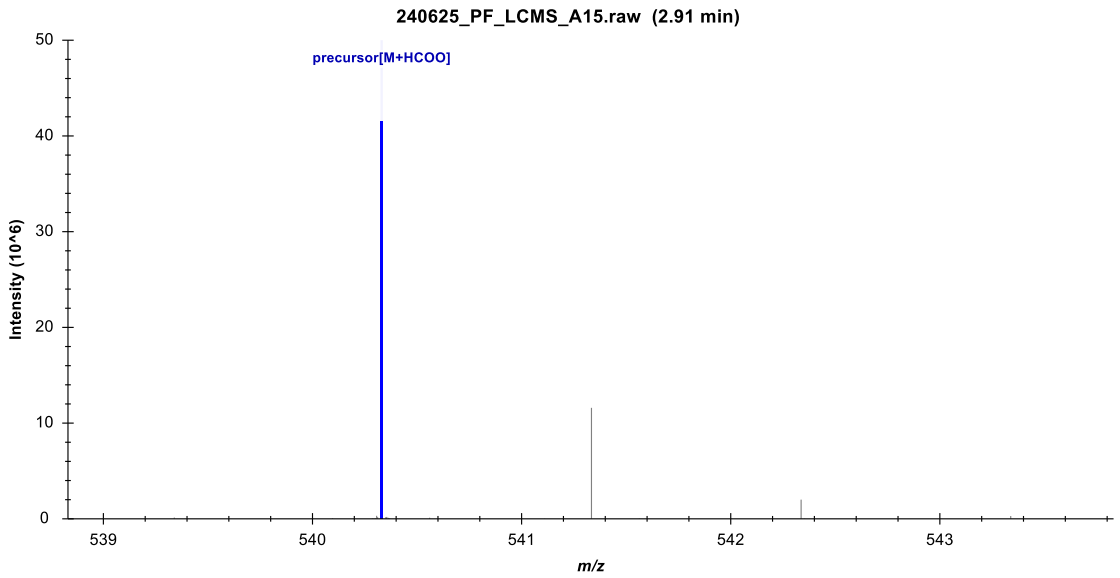

Figure 15: Isotopic pattern of LPC 16:0 in Adult sample #15

The isotopic pattern confirms LPC 16:0 because the monoisotopic peak appears exactly at the expected m/z value for the $[M+HCOO]^-$ adduct, the M+1 isotope peak shows the correct relative intensity for the carbon count of a C_{16} LPC, the M+2 peak matches the predicted lower abundance and no abnormal A+2 signal is present. Together, the exact mass and isotopic distribution identify the lipid as LPC 16:0, as shown in Figure 15.

The observation of the isotopic pattern in the mass spectrum is a reliable way to confirm lipid identity. A case where Skyline software produced a false identification is seen in the Figure 16. The peak highlighted in blue was assigned as PC 37:4 by the software, but closer inspection reveals inconsistencies. The isotopic pattern is too narrow for a PC 37 carbons. The M+1 and M+2 peaks are weak, while a true PC 37:4 would exhibit a higher M+1 intensity and a more extended isotopic tail. Furthermore, the measured monoisotopic m/z for the $[M+HCOO]^-$ adduct deviates from the theoretical m/z expected for PC 37:4. These two aspects, isotopic pattern match and distribution and exact mass comparison, clearly indicate that the peak is misassigned since the m/z value is rather the M+1 isotope of another species. This example highlights the importance of manual verification of automated peak assignments.

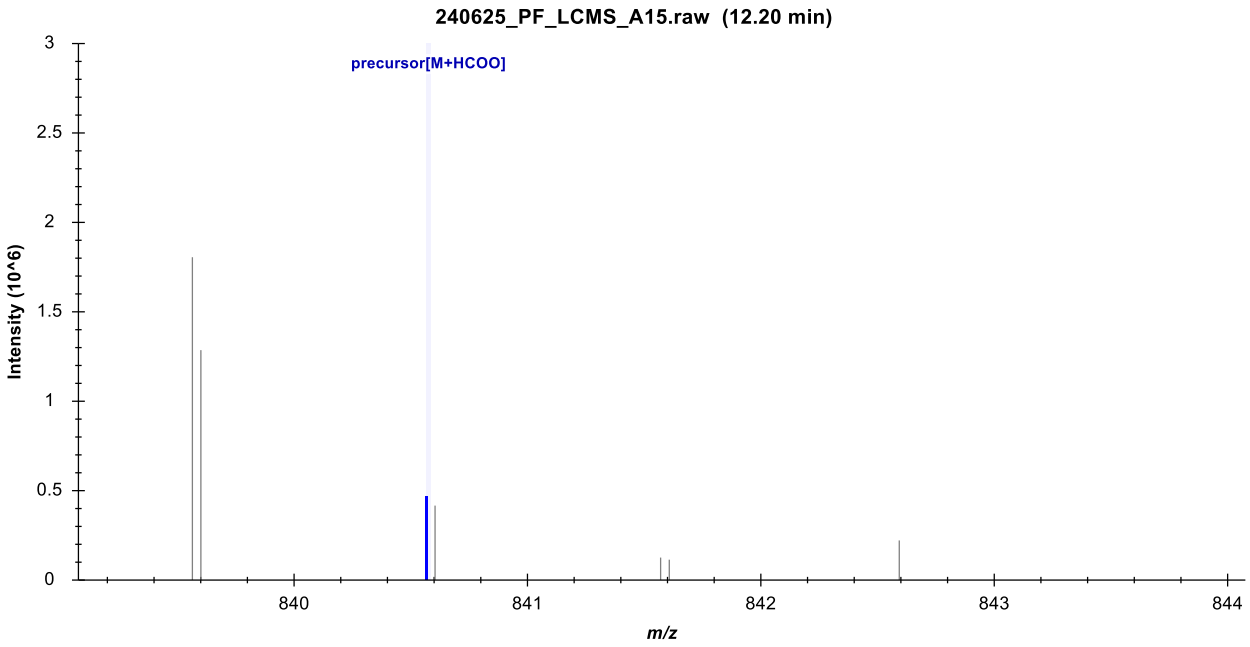

Figure 16: Isotopic pattern of falsely annotated PC 37:4 Adult male sample #15

3.3.2 Equivalent carbon number

The ECN model is particularly useful when multiple lipid classes are analysed together, as it allows researchers to anticipate where lipids of a given composition should elute, adding an additional layer of confidence to mass-based identifications.

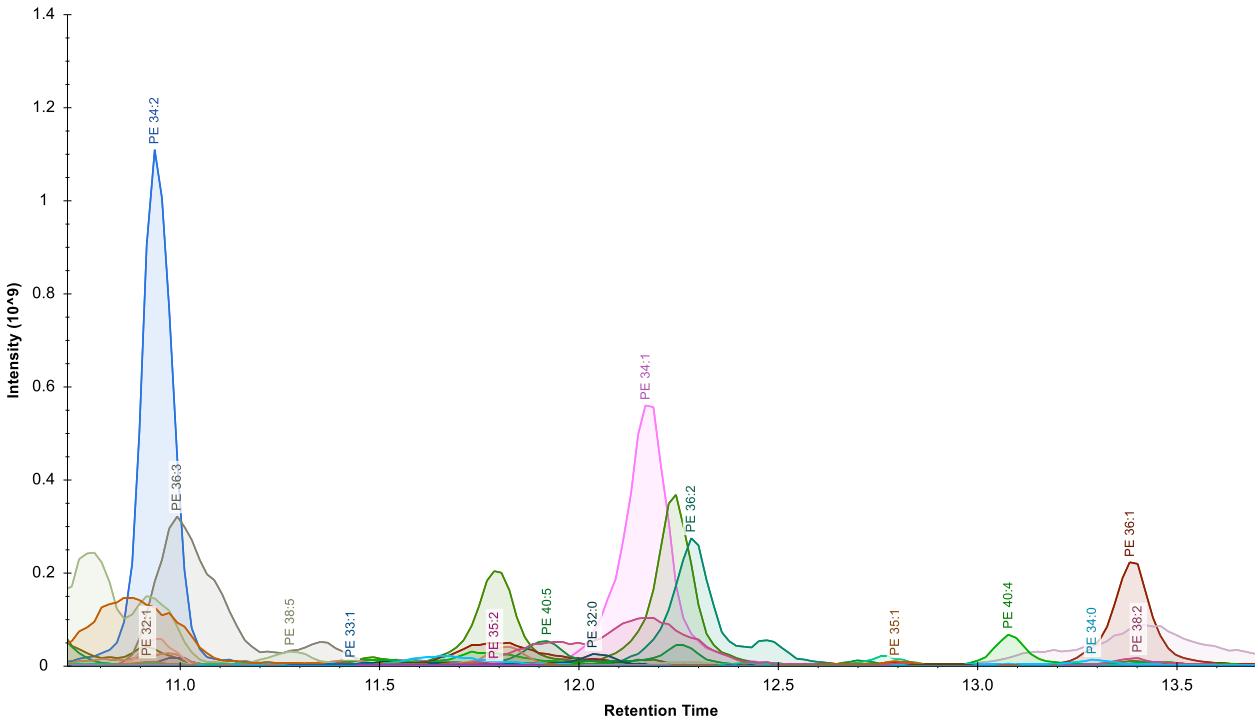

Figure 17: Representation of overlapping RTs of PE species according to ECN rule in Adult #15

A zoomed-in region of the chromatogram showing PE species of fresh blood sample Adult 15 is seen in Figure 17. PE 32:1, 34:2 and 36:3 elute at about 11 minutes. PE 32:0, 34:1 and 36:2 elute between 12 and 12.3

minutes. PE 34:0, 36:1 and 38:2 elute later at around 13.4 minutes. The ECN relationship is visible in this pattern, although it applies most clearly to the more abundant lipids in the class, that is aligning with the literature.

Using our RP-HPLC-MS method, we were able to separate isomeric species such as PC and PE. PC 31:0 and PE 34:0, which follow nearly the same elution curve except for a peak at 12.5 minutes, reflecting that isomeric species with the same mass produce identical extracted traces in positive ion mode, as seen in Figure 18. The way to differentiate these two lipids is observing the adjacent lipid species, so PE 34:0 must elute after PE 33:0 and PC 31:0 must elute after 30:0 respectively, following the ECN rule [48]. Table 1 shows the isomeric overlaps that were relevant for data treatment of this thesis.

Table 1: Relevant isomeric overlap rules used for lipid identification

Lipid classes	Type of overlap	Example
PC-PE	PC = PE + $3CH_2$	$[PC\ 32:0+H]^+ = [PE\ 35:0+H]^+ = [PC\ 32:0+Na]^+ = [PE\ 35:0+Na]^+$
PC-PS	$[PC+HCOO]^- = [PS+3CH_2\text{-}DB\text{-}H]^-$	$[PC\ 33:1+HCOO]^- = [PS\ 36:0-H]^-$

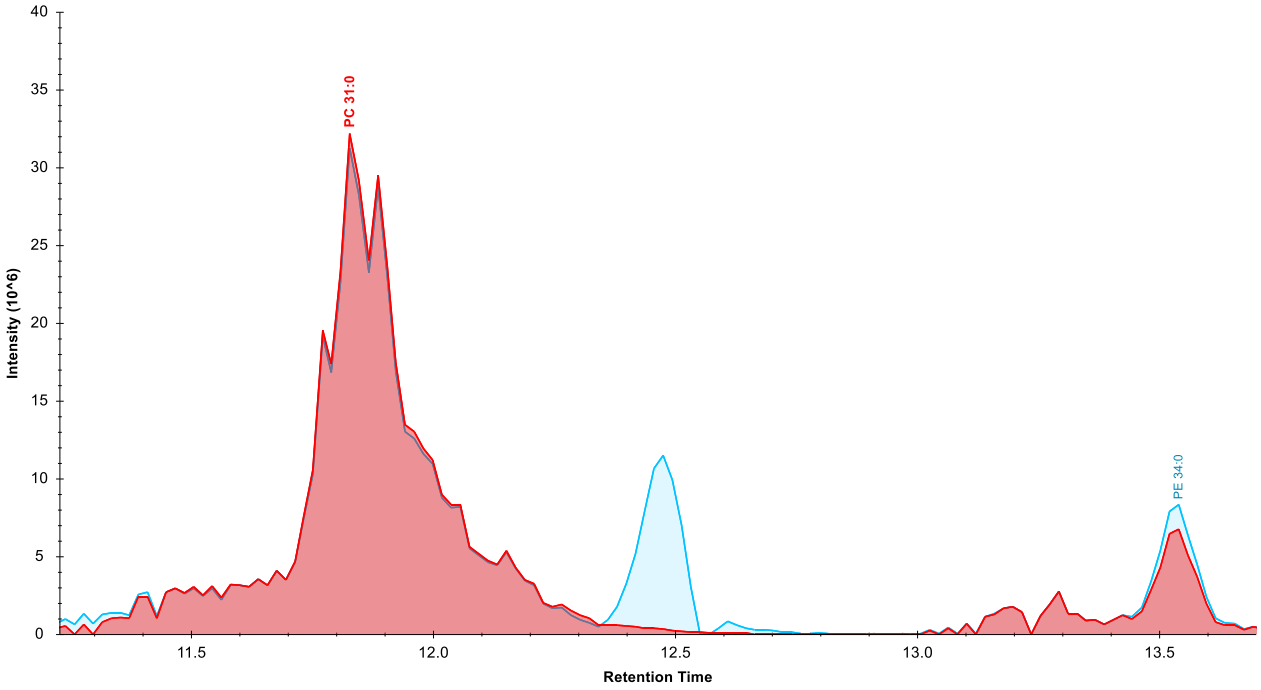

Figure 18: An example of lipid overlaps between PC 31:0 and PE 34:0 in positive mode

3.3.3 Correlation of RT

The relationship between acyl chain length and RT for PC and SM is presented in Figures 19 and 20 respectively. Both classes follow a clear linear trend, where longer acyl chains correspond to longer RTs when the number of DBs kept constant. This trend is useful for predicting the RTs of longer or less abundant lipids that may not be easily identified otherwise, what is in alignment with the literature [47]. The graphs also serve

as a validation tool for lipid assignment, since deviations from the expected trend may indicate misannotation. Within the same chain length, lipids with more DBs elute earlier, consistent with reduced hydrophobicity from unsaturation. For SM, the presence of the hydroxyl group in the sphingoid base increases polarity, resulting in shorter RTs compared to PC species of similar acyl chain length. This systematic behaviour strengthens confidence in both identification and RT prediction across datasets.

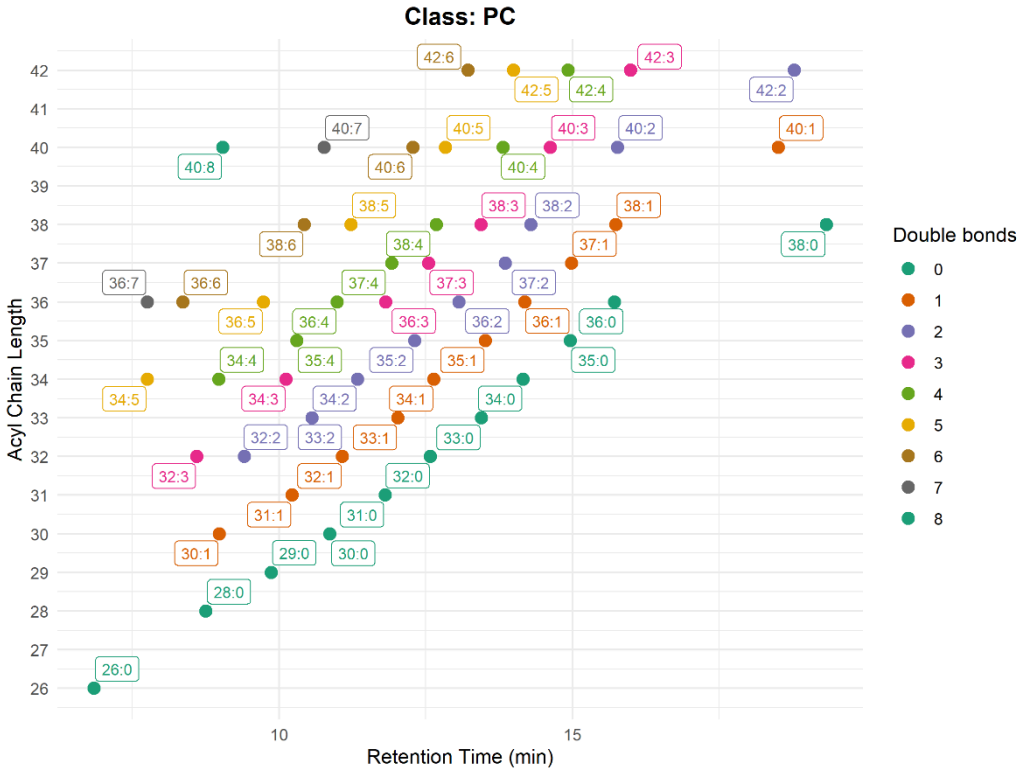

Figure 19: Acyl chain length and unsaturation plotted against RT for PC species

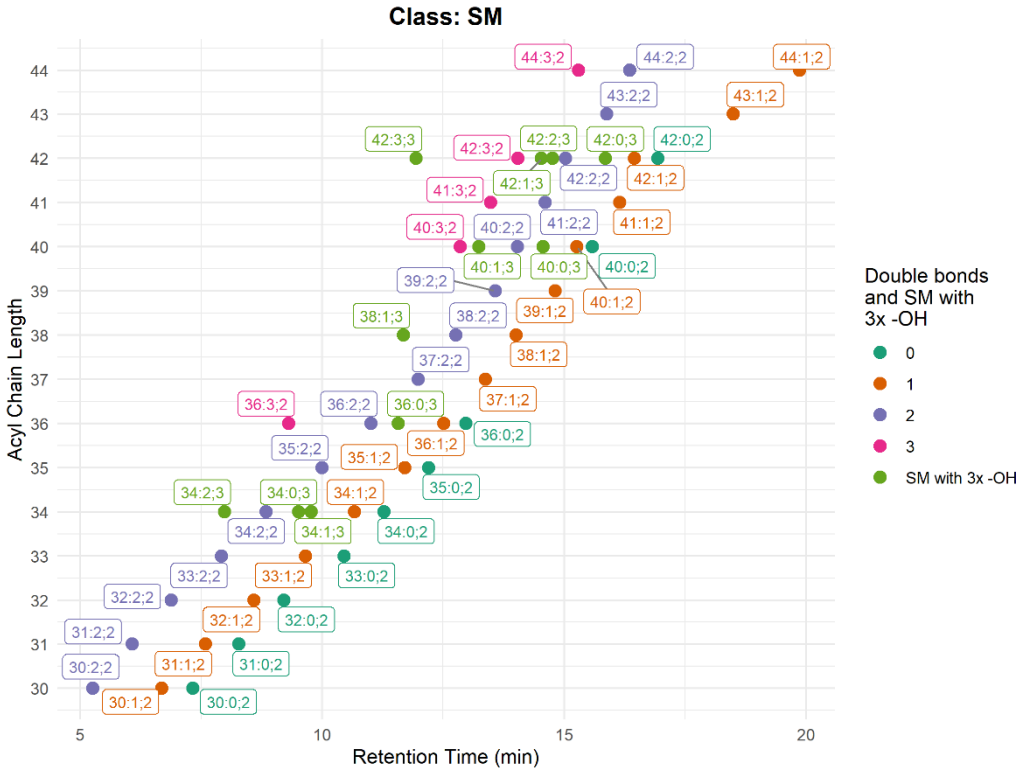

Figure 20: Acyl chain length and unsaturation plotted against RT for SM species

3.3.4 Lipid distribution

The first step focused on identifying differences between lipid classes across the sample groups and highlighting "lipids of interest," defined as species showing significant variation in their class and sample groups. The mean fractional abundance of all investigated lipid classes across the different groups is shown in Figure 21, with zoomed-in views to show each class clearly, including those present at low abundance (Figure 21, (2) and (3)).

As seen from the data (Figure 21 (1)), PC and SM are the most abundant lipid classes across all sample groups. Neonatal RBC membranes show no significant differences in PL composition compared with fresh blood samples and donor blood bags. The means and standard deviations (SDs) for fresh blood, stored blood units, term and preterm infant samples all overlap, indicating that fractional abundances of PC and SM remain stable across adult and neonatal groups.

For LPC, children's samples and fresh adult samples show slightly lower levels compared with donor groups, while the donor groups themselves show similar values. In PE, adult samples are not significantly but elevated compared with both neonatal groups. For PC O-, PE O- and PS, the values remain consistent across all sample groups, with no notable differences observed.

Lipid classes Cholesterol, LPC O-, LPE and PI show no significant changes between each other as seen on Figure 21 (2). For LPC O-, fresh adult blood sample groups show slightly lower levels, while children's samples and donor groups show similar fractional abundances around ~0.025%. LPE shows no meaningful variation

across groups, with all samples clustering around ~0.025%, indicating a stable distribution. PI, however, presents a different pattern. Although SDs are relatively high, some trending can be observed. The term infant group shows the highest fractional abundance at 0.34%, followed by the preterm group at 0.31%. In contrast, adult and donor groups both average around 0.2%. These results suggest that PI may be more abundant in neonatal RBC membranes.

A detailed view of the LPE O- class with highest levels found in term and preterm infant samples, followed by the donor elder women group is shown in Figure 21 (3). The remaining donor groups show similar values without noticeable differences. The lowest level is observed in fresh blood samples from adult women.

It is possible that with an expanded cohort PI levels could turn out to be higher in newborns compared to other groups. However, based on the current dataset this cannot be concluded with certainty. The variability observed within the groups is substantial and limits the strength of the interpretation. Some neonatal samples suggest a tendency toward elevated PI, but the overlap with adult values prevents drawing solid conclusions. To properly address this question, further replication would be required, requiring a larger sample size and balanced representation of all groups. Only a broader cohort could confirm whether the apparent differences in PI reflect a true biological signal or simply result from inter-individual variation.

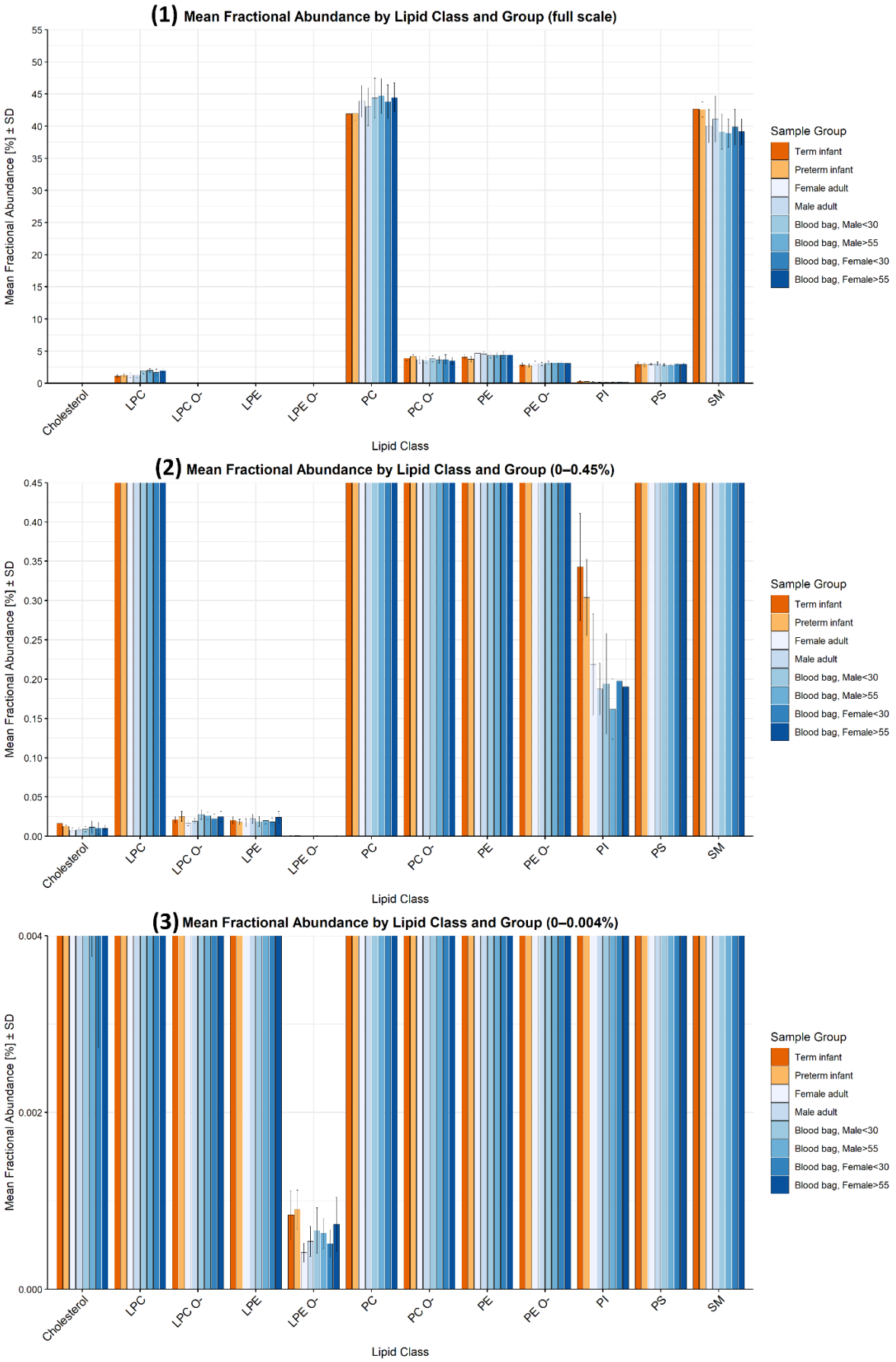

Figure 21: Distribution of mean fractional abundance by lipid classes in the investigated cohort groups

(1) corresponds to full scale distribution, (2) and (3) provide a zoomed in overview of lower abundant lipid classes

In full-term infants, SM constitutes about 26% of RBC membrane PLs, while PC accounts for approximately 28%. In adults, the composition shifts slightly, with SM at around 24% and PC at 30% [13]. In the found data, the children's groups (term and preterm) show markedly higher values, with SM at 42.5% and PC at 41.5%. However, the percentages reported in this work cannot be compared directly with absolute values from the literature. The approach used here did not involve absolute quantification, but rather relative profiling of lipid classes and species. As a result, the calculated ratios are inherently biased by the ionization efficiency of each lipid class under the applied ESI conditions. Different lipid classes ionize with varying efficiencies in positive or negative mode, meaning that some classes are systematically overrepresented while others appear lower than they truly are.

Neonatal RBC membranes have been reported to contain about 15.2% combined PS and PI, compared with 13.1% in adults [13]. The absolute percentages differ substantially from the literature and cannot be compared directly, since the results refer to fractional abundance and not to quantitated lipid amount. For PS and PI, the calculated combined values shown in Figure 22 show no meaningful difference between sample groups, since found fractions in all investigated cohort groups are slightly above 3%. Term, preterm and adult samples all fall within a similar range and the SDs overlap.

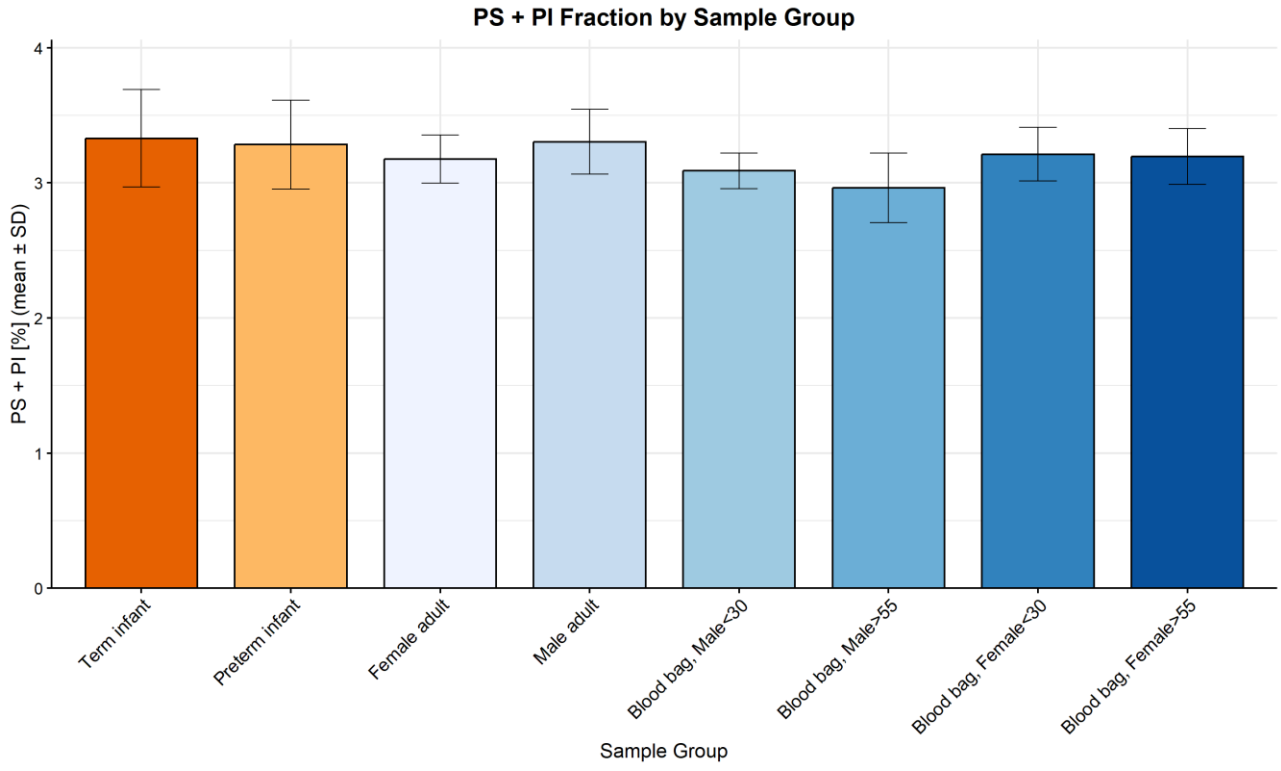

Figure 22: PS and PI fractional abundance fractions in the investigated cohort groups

The PE and PS fractions appear to remain stable across developmental stages and adult cohorts. Neerhout reported only a slight decrease in PE in neonates, while most studies, including those on adults of different ages, found no major age-dependent change in either PE or PS levels in RBC membranes [13].

Reports consistently indicate that neonatal PC O- and PE O- are lower than adult values and gradually increase during infancy until adult levels are reached [20]. The data obtained here does not align with this pattern, as no reduction in fractional abundance of PC O- and PE O- was observed in neonatal groups. This discrepancy may reflect methodological differences, sample variability, or limitations in the lipid classes analysed.

The levels of LPE O- also reflect the variability of the samples throughout the cohort, however, elevated levels could be explained by the protecting mechanisms that transform PE O- to LPE O- during the oxidative stress [8,20].

Fresh adult RBCs have minimal LPC, consistent with the observation that fresh adult samples in this dataset showed very low levels. During storage, LPC can accumulate as part of the storage lesion, but this increase is largely plasma-derived and temperature-dependent, with limited accumulation under standard RBC storage conditions at 4 °C [70].

3.4.1.1 Investigation of lipid species distribution within lipid classes

After evaluating lipid class distributions across the study cohort, the analysis was extended to the level of individual lipid species. The goal was to identify whether differences observed at the class level were also reflected within specific molecular species. For this purpose, the fractional abundance was calculated for each identified lipid and normalized to 100% within its lipid class. This approach allows direct comparison of species distribution patterns across groups. These were selected based on the largest differences in mean fractional abundance between preterm infant samples and the other cohort groups. By concentrating on the most variable lipids, it becomes easier to highlight biologically meaningful differences while retaining readability. For presentation, only the graphs for PC and SM are shown here, since these were identified as the most abundant classes in the dataset and exhibited notable group-dependent variation. The results for the remaining lipid classes are included in the appendix.

LPC levels show clear shifts between neonatal and adult groups in some lipid species (Figure 23). In term and preterm infants, LPC species 20:3, 20:4 are elevated compared to fresh blood samples and stored blood bag units. Several other LPC species remain unchanged across groups. In contrast, LPC 17:0, 18:0 and 18:2 are consistently lower in neonates. This distribution highlights that neonatal RBC membranes are not globally enriched in LPC (Figure 19 (1)) but show specific increases in certain species.

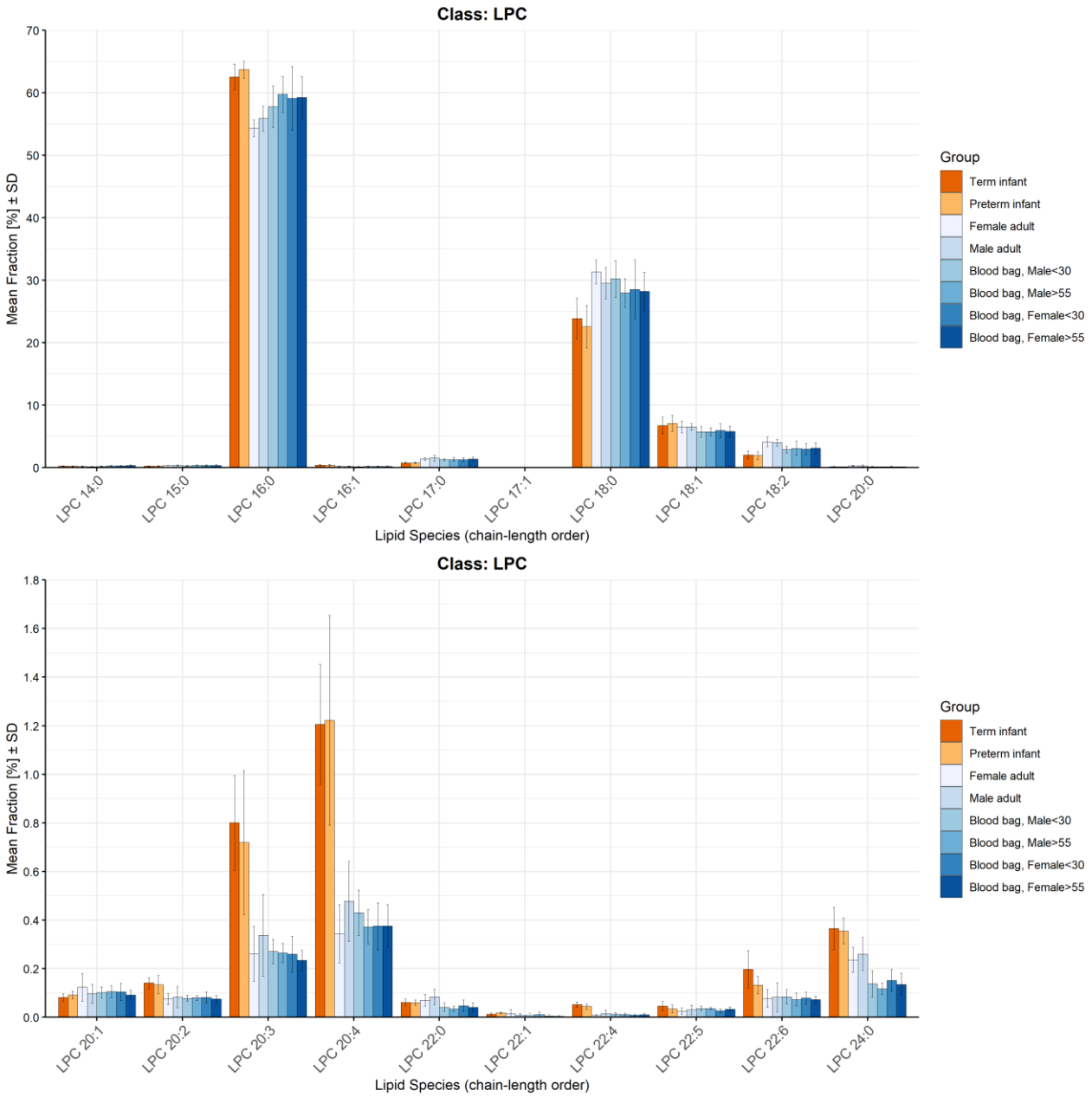

Figure 23: Detected LPC species, their fractional abundance and distribution in the cohort groups

LPC O- species show selective differences between groups (Figure 24). Term infants show not significantly different but elevated levels of LPC O-16:0, while other groups remain lower. For LPC O-16:1, LPC O-18:0 and LPC O-18:1, no differences are observed. These species show comparable values across all groups, indicating that only LPC O-16:0 demonstrates a specific enrichment in term infants, while the rest of the ether-linked LPC remain stable. Studies on individual ether-linked LPCs in RBC membranes are limited. The data observed in our findings suggests that there is considerable variability in adult RBC membrane lipid composition.

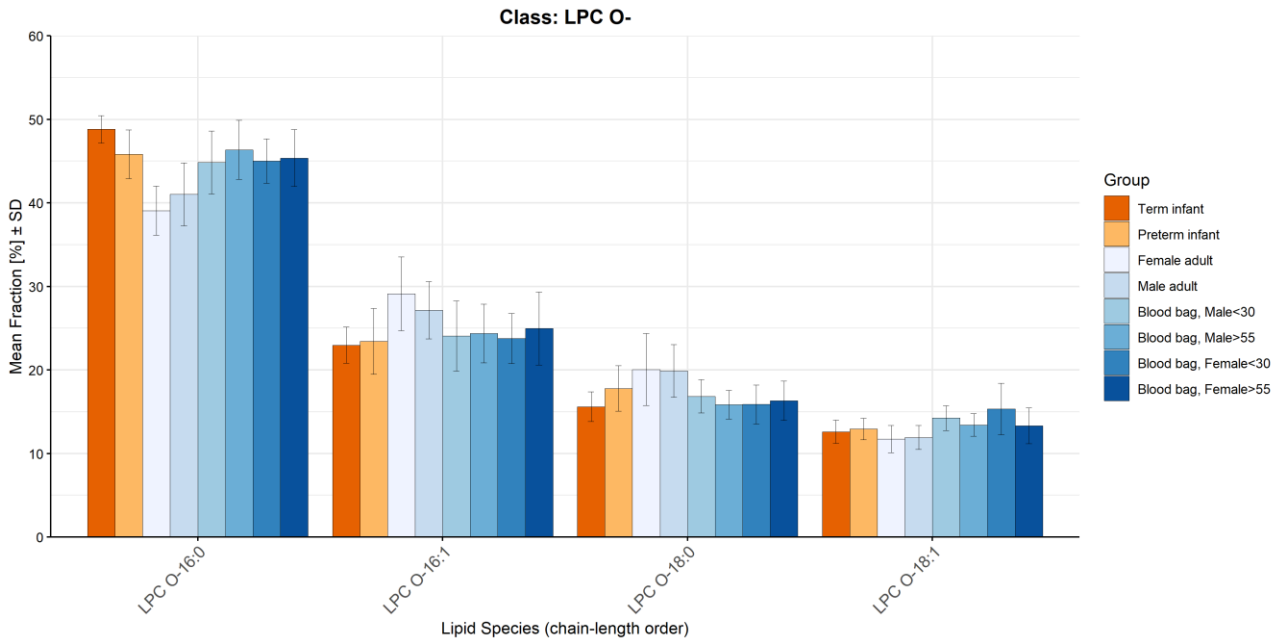

Figure 24: Detected LPC O- species, their fractional abundance and distribution in the cohort groups

LPE profiles show scattered differences between children and other groups (Figure 25). Both neonatal groups have higher LPE 16:0, with the strongest elevation in preterm infants. LPE species carrying polyunsaturates such as 20:3 and 22:6 are also slightly increased in neonates, reflecting their enrichment in arachidonic acid precursors and DHA. In contrast, several common species are reduced. Neonates show lower levels of LPE 18:0, 18:1, 18:2 and 22:5. Some species remain unchanged, including 17:0, 20:4 and 22:4, which appear stable across groups.

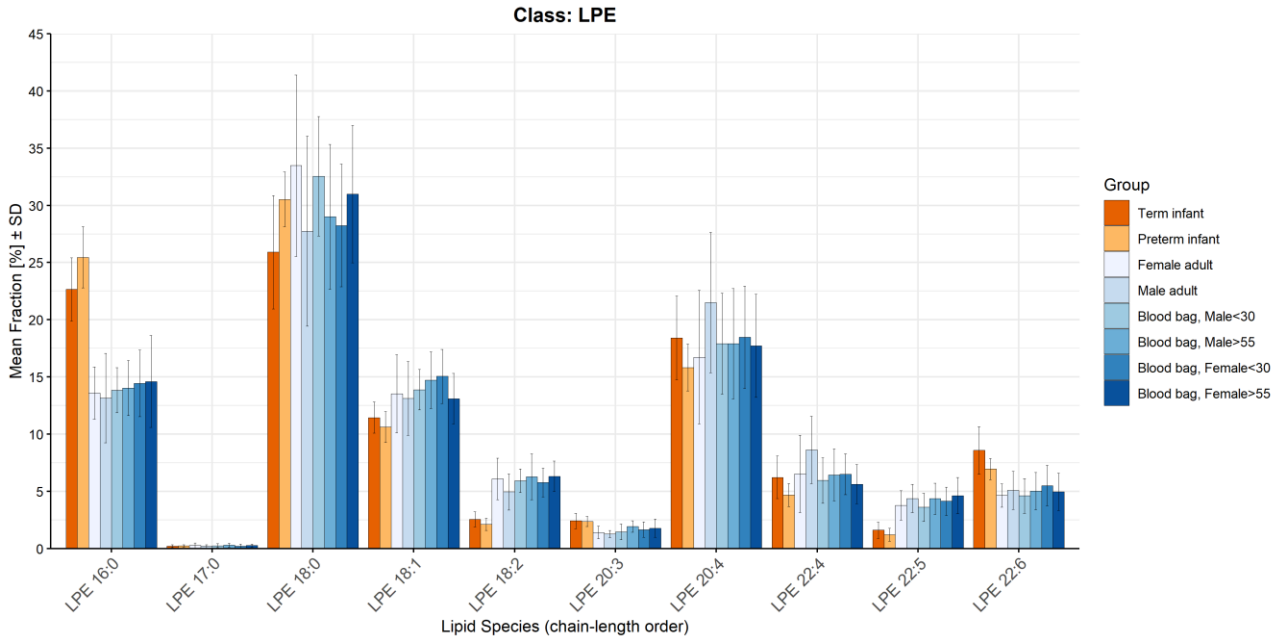

Figure 25: Detected LPE species, their fractional abundance and distribution in the cohort groups

LPE O- levels are similar across all sample groups (Figure 26).

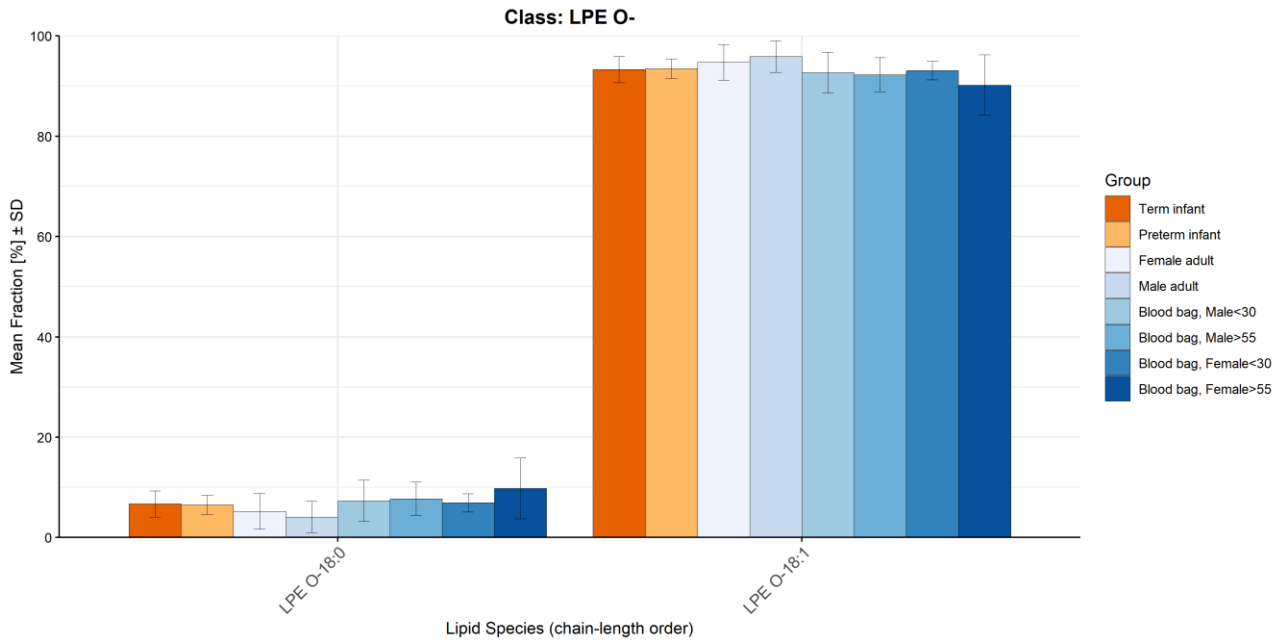

Figure 26: Detected LPE O- species, their fractional abundance and distribution in the cohort groups

In fresh blood and blood bag groups, the values of PC species are consistent and SDs overlap, indicating no clear trend within these groups as shown in Figure 27. In contrast, neonatal samples show distinct differences. Species PC 32:0, 32:1, 34:1, 36:4, 38:4 and 38:6 are higher in neonates compared to others. PC 38:3 and 40:6 are elevated only in term infants. Conversely, lower levels are observed in neonatal samples for PC 34:2, 34:3, 36:1, 36:2 and 36:5.

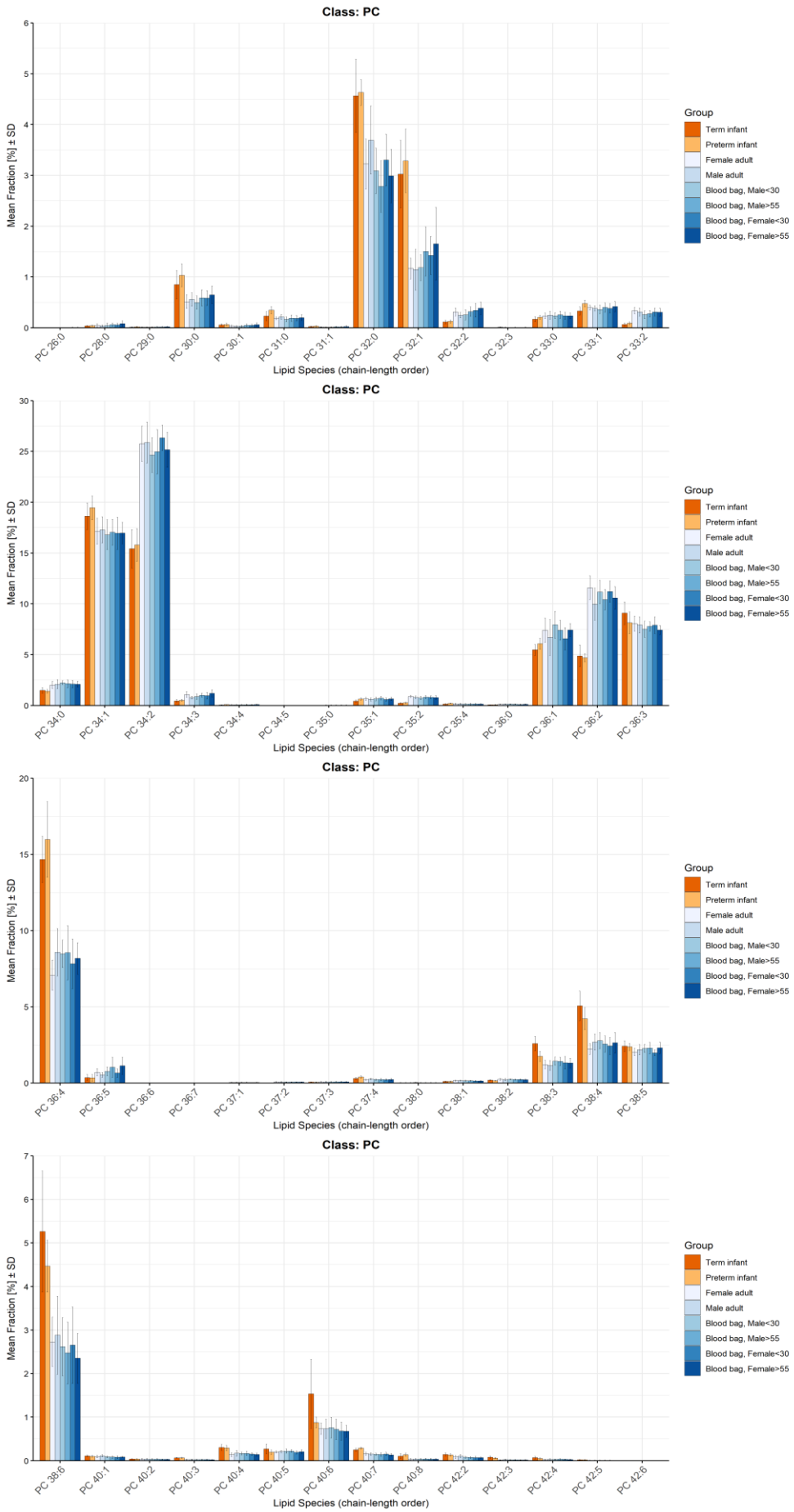

Figure 27: Detected PC species, their fractional abundance and distribution in the cohort groups

PC O- species show distinct patterns between term and preterm infants (Figure 28). Term infants have higher levels of PC O-32:0 and PC O-36:4, while preterm infants remain at the same level as other groups. On the other hand, preterm infants show elevated PC O-36:1, PC O-36:2 and PC O-38:5, while term infants align with adults and stored blood units for these species. Both neonatal groups are increased in PC O-32:1, PC O-34:1 and PC O-38:4, suggesting an enrichment in selected ether-linked PCs. At the same time, neonatal samples are reduced in PC O-34:0, PC O-34:2, PC O-34:3, PC O-36:0, PC O-36:3 and PC O-38:1 compared to adults and blood bags. These results reveal developmental shifts in ether-linked PC composition that differ between preterm and term infants, with some overlaps but also unique changes in specific species.

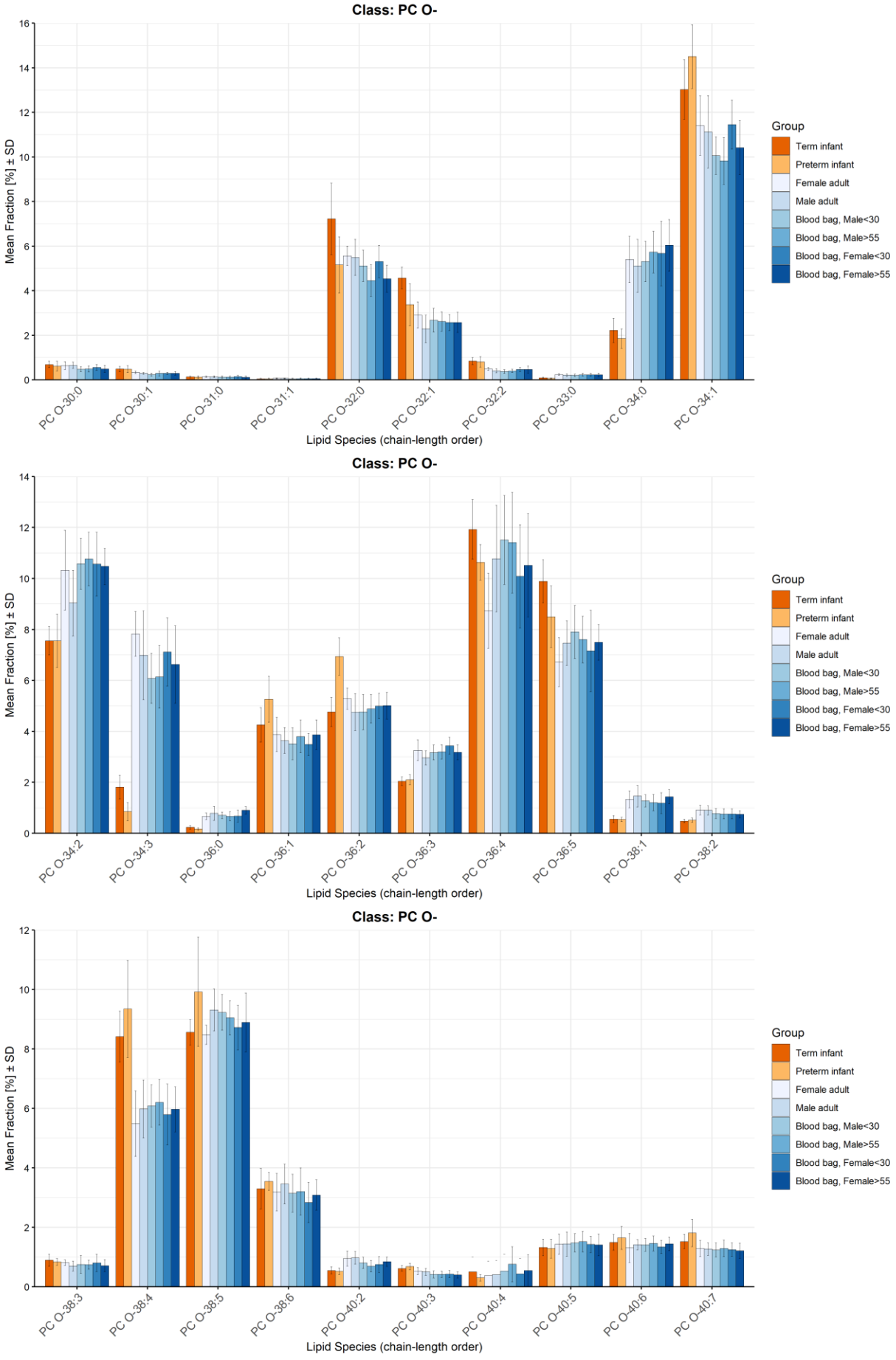

Figure 28: Detected PC O- species, their fractional abundance and distribution in the cohort groups

PE species show several neonatal-specific shifts compared to adult and donor samples (Figure 29). Both term and preterm infants show higher levels of PE 32:1, PE 36:4, PE 38:3, PE 38:4, PE 38:6, PE 40:6 and PE 40:7, showing an enrichment of polyunsaturated ethanolamine PLs in neonatal RBCs. At the same time, several lipid species are reduced in neonates. These include PE 34:2, PE 36:1, PE 36:2, PE 36:3 and PE 40:5. A mixed pattern is observed for PE 38:5: preterm infants show levels like adults, while term infants show a marked reduction. Other species such as PE 34:1 and PE 36:5 remain unchanged across all groups, suggesting that not all ethanolamine PLs are subject to developmental shifts. Overall, the results indicate that neonates favour PE species with multiple DBs, while certain mid-chain or less unsaturated species are reduced, with some species-specific differences between term and preterm infants.

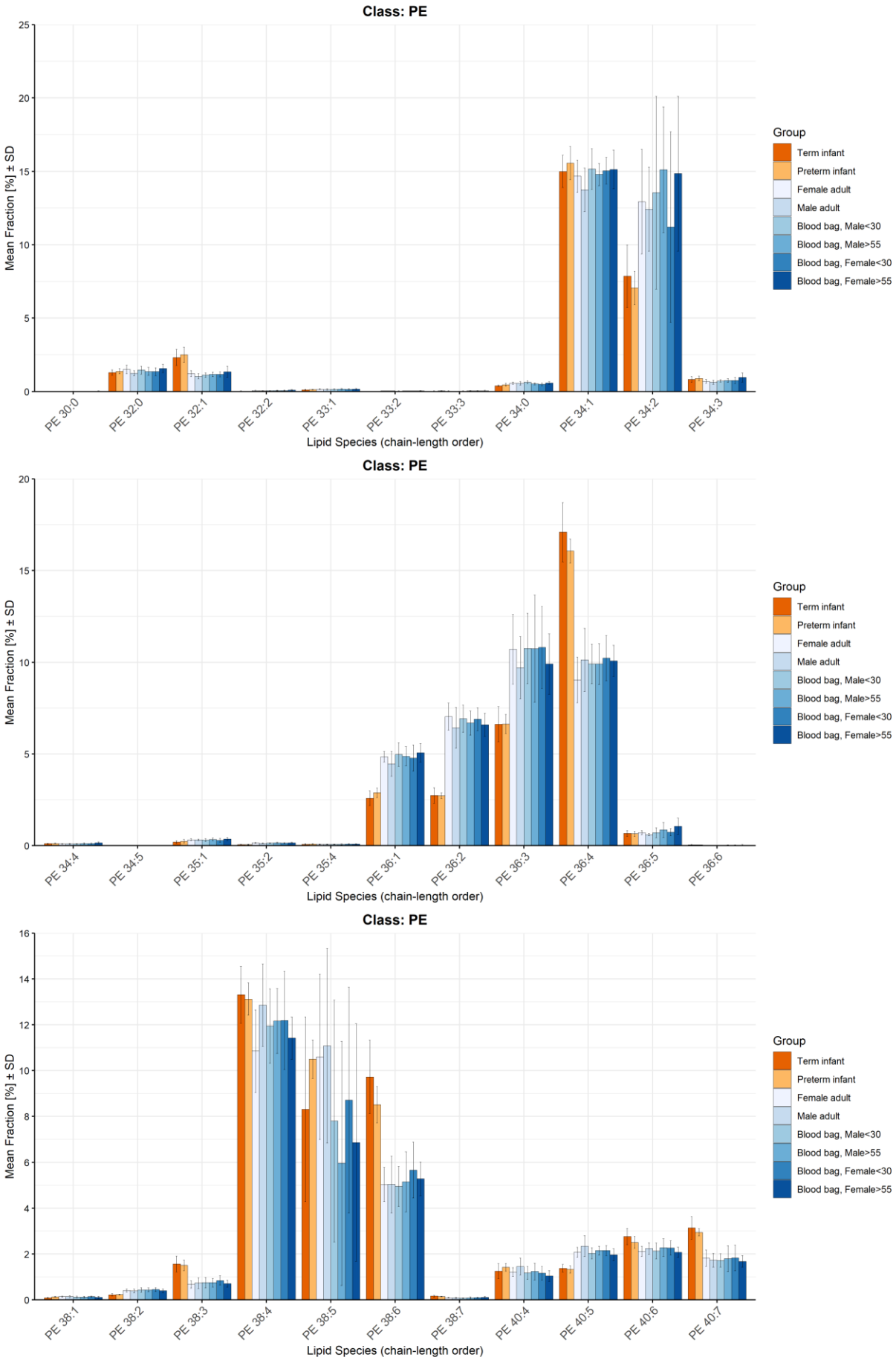

Figure 29: Detected PE species, their fractional abundance and distribution in the cohort groups

PE O- species show distinct differences between neonatal and adult RBCs (Figure 30). Both term and preterm infants show higher levels of PE O−36:2, PE O−38:4, PE O−38:7, PE O−40:7 and PE O−40:8. These species are enriched in neonates, suggesting increased representation of ether-linked ethanolamine PLs carrying long-chain PUFAs. In contrast, several ether-linked PE species are consistently lower in neonates than in adults. These include PE O−34:3, PE O−36:4, PE O−36:6, PE O−38:6 and PE O−40:6. The pattern indicates that neonates do not uniformly increase all ether-PE species but rather show selective enrichment of highly unsaturated species while being depleted in others. This selective profile may reflect developmental constraints in plasmalogen metabolism and remodelling, where certain double-bond configurations are favoured in early life, while others remain underrepresented compared to adult RBC membranes.

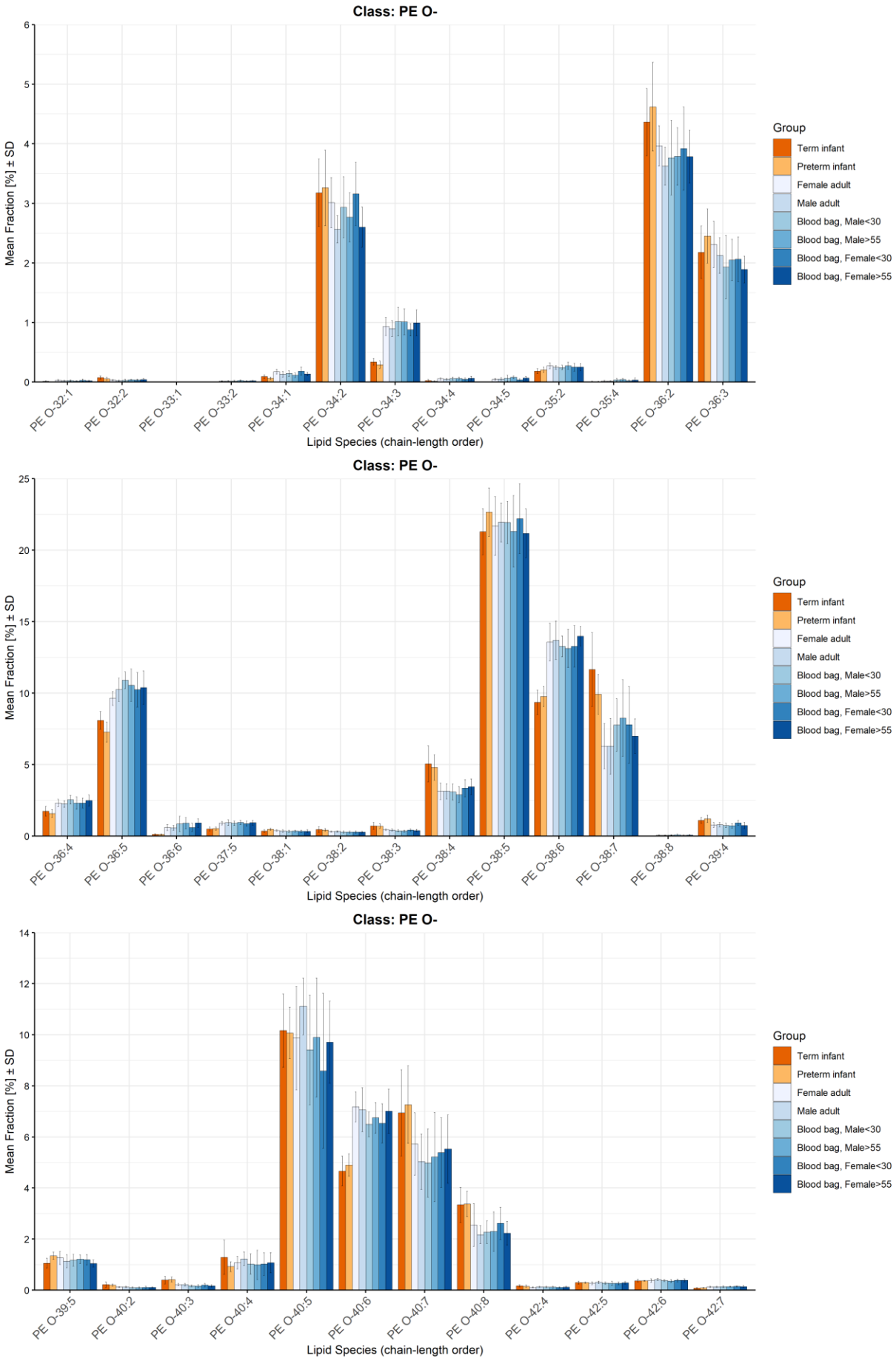

Figure 30: Detected PE O- species, their fractional abundance and distribution in the cohort groups

PI species also show clear group-specific differences (Figure 31). Term infants show a distinct elevation in PI 36:4, while both term and preterm infants have higher levels of PI 38:3, PI 40:4 and PI 40:6 compared to adults and blood bags. At the same time, several PI species are consistently reduced in children's samples. These include PI 34:2, PI 36:0, PI 36:1, PI 36:2, PI 36:3, PI 38:4 and PI 40:5. The distribution highlights that not all polyunsaturated PI species are equally enriched in neonates. Notably, PI 38:4 remains the dominant PI in RBCs across all groups, confirming its role as the major PI molecular species in the membrane. The selective shifts observed in other PI species suggest developmental regulation of fatty acid incorporation into PI, with neonates favouring certain highly unsaturated forms while showing deficits in others.

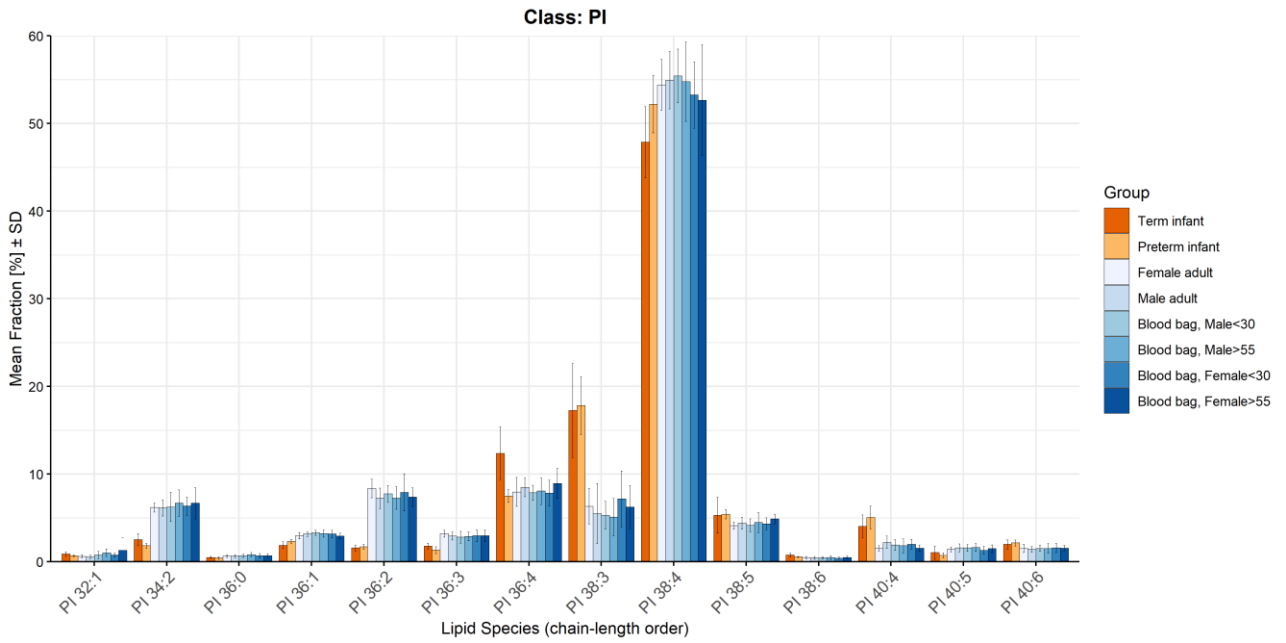

Figure 31: Detected PI species, their fractional abundance and distribution in the cohort groups

PS shows several consistent differences between neonatal and adult groups (Figure 32). Both term and preterm infants have elevated levels of PS 34:1, PS 36:4, PS 38:3, PS 39:6 and PS 40:6. Term infants also show a specific increase in PS 39:4, which is not seen in preterm group. In contrast, both neonatal groups show reduced levels of PS 36:1, PS 36:2, PS 38:4, PS 38:5 and PS 40:5 compared to adults and blood bags. This pattern indicates that neonatal RBC membranes are enriched in specific mono- and polyunsaturated PS species while lacking others, pointing to selective remodelling of PS in early development.

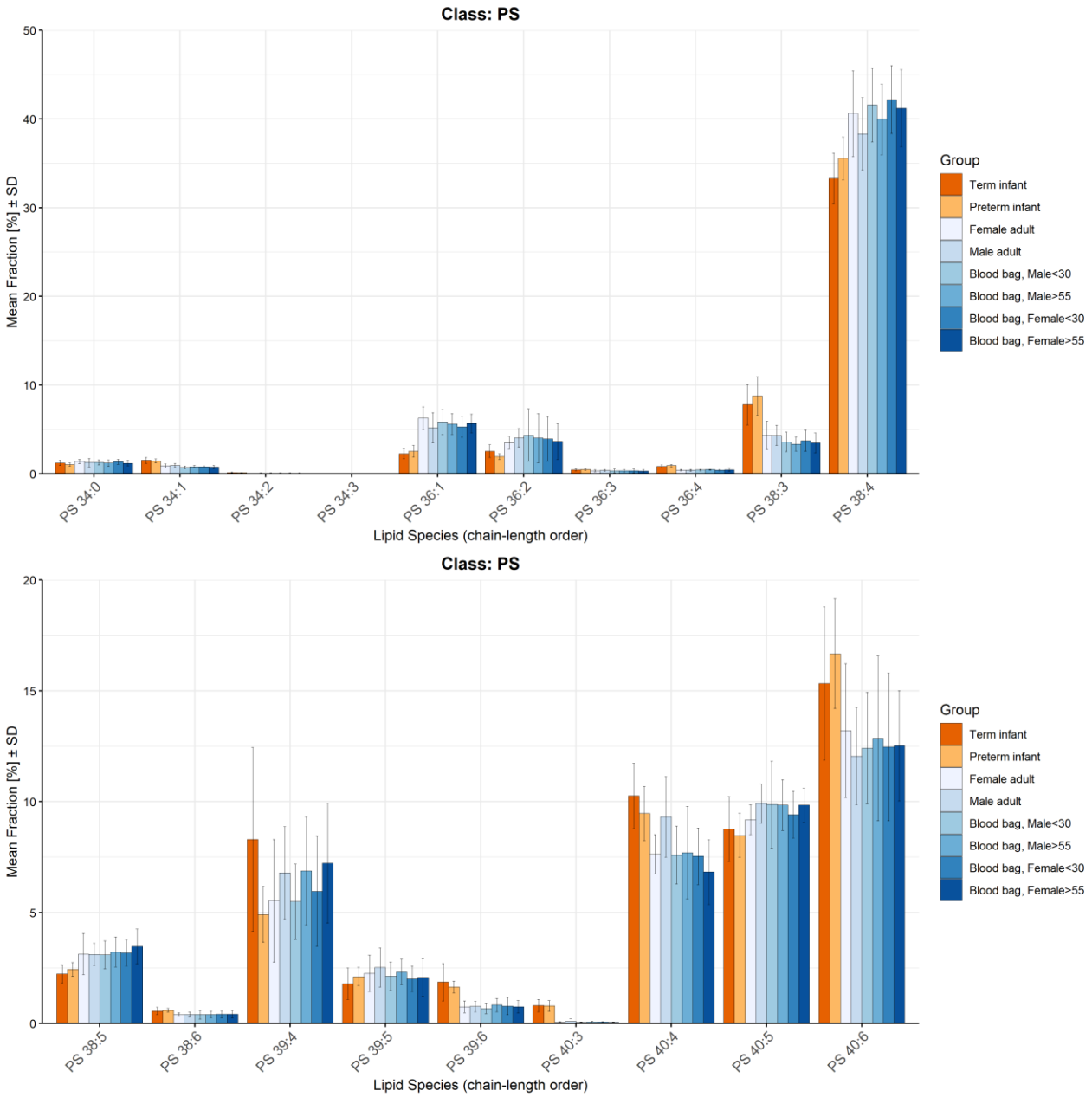

Figure 32: Detected PS species, their fractional abundance and distribution in the cohort groups

Donor groups and adult samples remain at similar levels with no clear differences between them, as seen in the distribution of lipids in the SM class (Figure 33). In contrast, neonatal groups show distinct shifts. Elevated levels are seen for SM 34:0;2, SM 36:1;2, SM 36:2;2, SM 42:0;2, SM 44:1;2 and SM 44:2;2, while depressed levels are observed for SM 40:1;2, SM 40:2;2, SM 41:1;2, SM 41:2;2, SM 42:2;2 and SM 43:1;2.

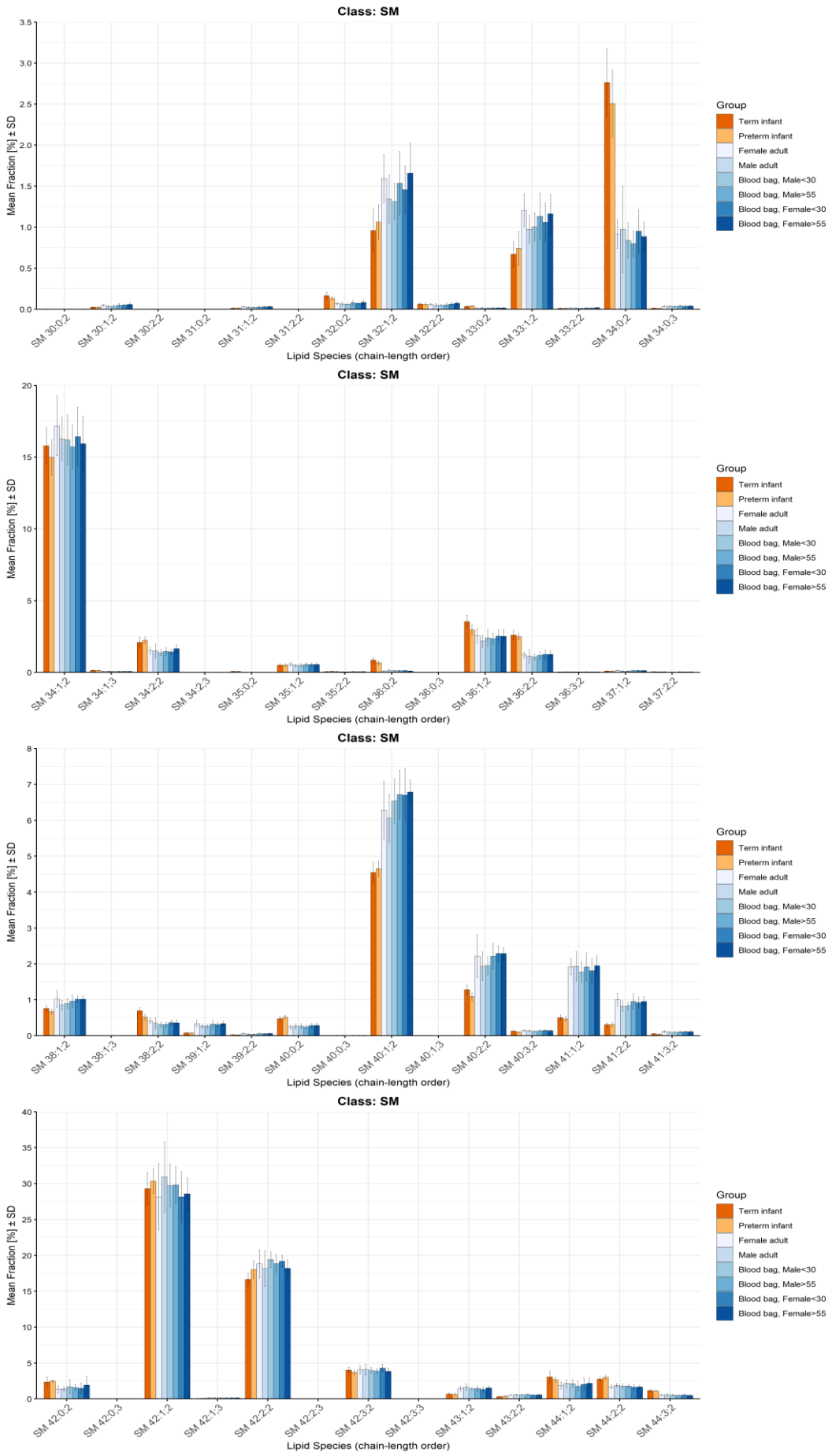

Figure 33: Detected SM species, their fractional abundance and distribution in the cohort groups

3.4.1.2 Statistical analysis

3.4.1.2.1 Neonatal vs adult lipid distribution

For clustering analysis, Principal Component Analysis (PCA) was performed in MetaboAnalyst. Heatmaps were generated to highlight lipid species that differ significantly between groups, serving as a visual tool to identify patterns of separation.

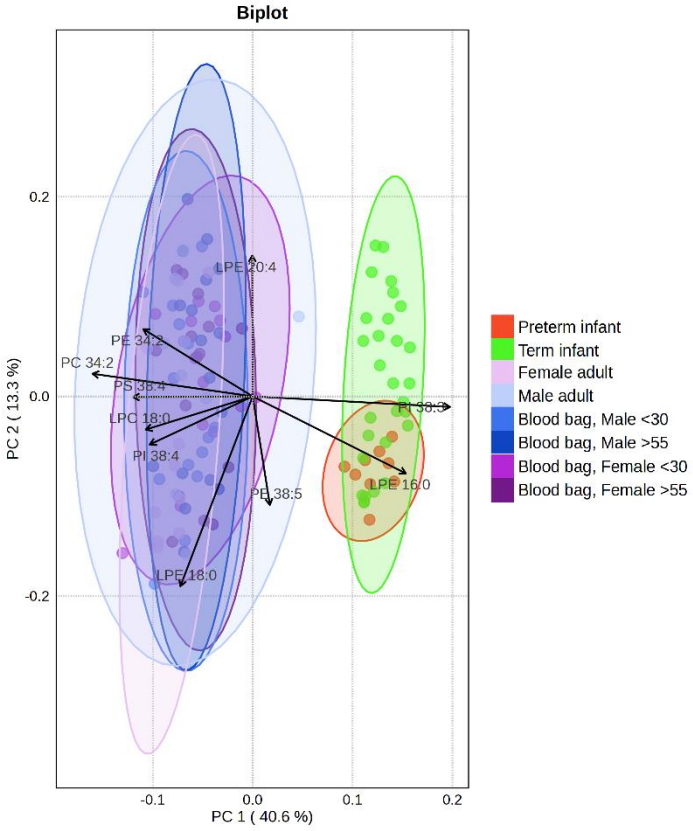

Figure 34: Biplot of fractional abundances of lipid species for investigated sample groups

The PCA analysis reveals a clear clustering of neonatal samples, with both term and preterm infants forming distinct and separate groups as shown in Figure 34. These neonatal clusters are clearly separated from the adult and donor samples, highlighting systematic differences in RBC lipid composition between newborns and adults. The adult and donor groups, however, overlap almost completely, showing no separation by sex or age. This tight clustering of adults indicates that, within the adult population, there is considerable variability in adult RBC membrane lipid composition. This variability does not appear to be systematically influenced by donor sex or age; it reflects inter-individual differences. Those likely shaped by a combination of genetic factors, long-term dietary patterns, metabolic state and possibly subtle environmental influences. The contrast with neonates emphasizes the developmental shift in RBC membrane composition and suggests that additional approaches beyond PCA may be needed to further explore variations among adult donors. It is also important to clarify that the source of blood differs. For infants, samples have been obtained as cord blood collected immediately after delivery, reflecting the in-utero environment at the time of birth. By contrast, adult samples have been obtained as drawn venous blood, representing circulating erythrocytes after months in the adult circulation. This distinction is relevant because cord blood captures the neonatal

state at a single time point, whereas adult blood reflects fully mature and long-lived RBCs. The difference in sampling origin should therefore be considered when interpreting compositional differences between neonatal and adult RBCs.

A heatmap was created to visualize the top 25 lipid species that differed most strongly between the sample groups (Figure 35). Lipids located in the upper half of the heatmap, ranging from PE O- 38:6 to SM 41:2;2, are generally more abundant in adult and donor groups. These species likely reflect the mature RBC lipid composition that is maintained consistently across age and sex in adults. In contrast, the lower half of the heatmap, beginning with PC 42:5 to SM 36:2;2, shows higher abundance in neonatal groups, both term and preterm. This shift reflects the developmental differences in membrane lipid profiles, where neonates exhibit distinct enrichment in certain lipid species.

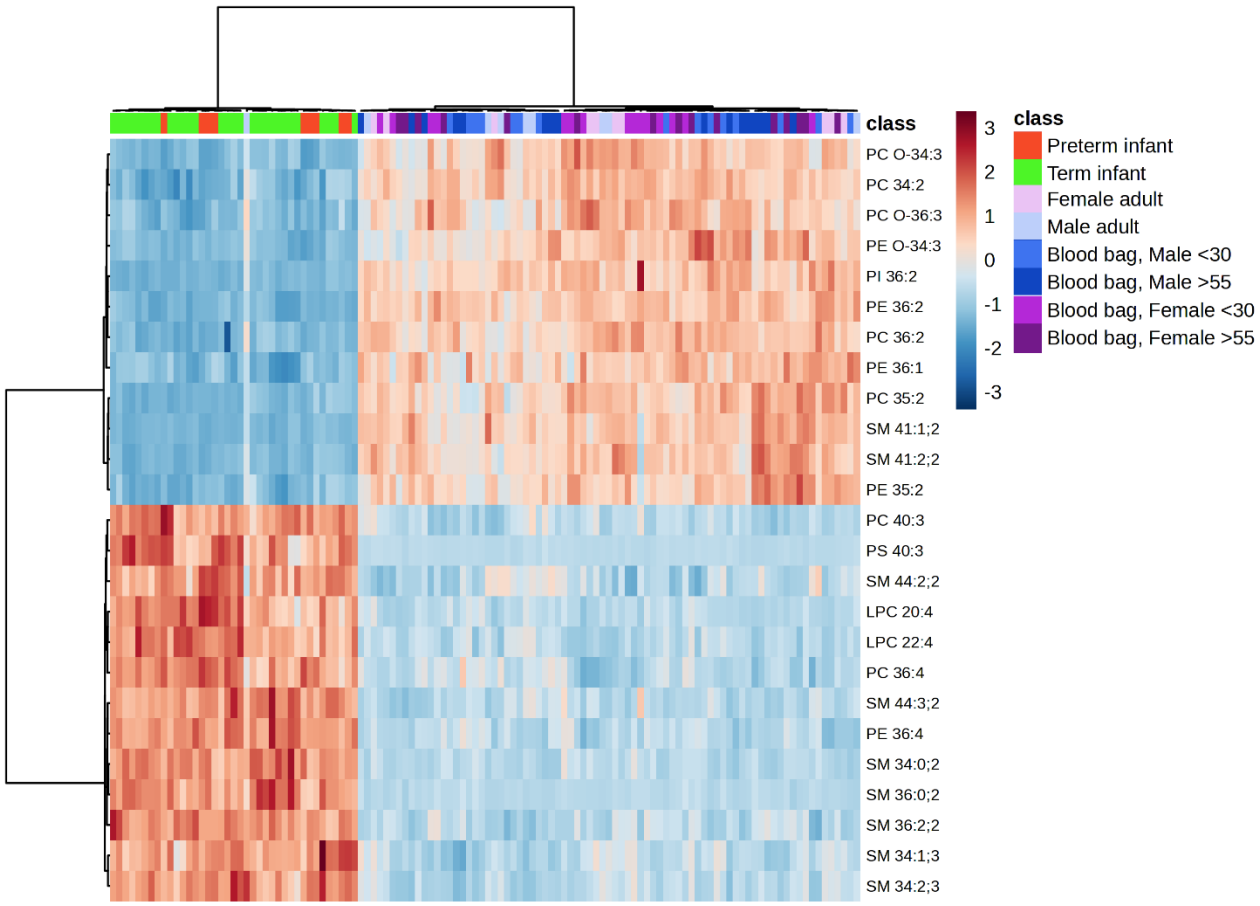

Figure 35: Heatmap showing top 25 lipid species with biggest fractional abundance differences and their up-/downregulation in the RBC samples in investigated groups

The bar charts, biplot and heatmap highlight a set of lipid species that drive the clear separation of neonatal groups from adult and donor samples. These differences are not restricted to a single class and occur across nearly all the lipid classes examined. Certain lipids show consistent enrichment in neonates, while others are depleted compared to adults. Together, these shifts create the clustering patterns observed in PCA and heatmap analyses. Some of lipids that have been either present in the top 25 of most different lipids withing cohort groups or picked manually according to ANOVA results are presented in the Figure 36.

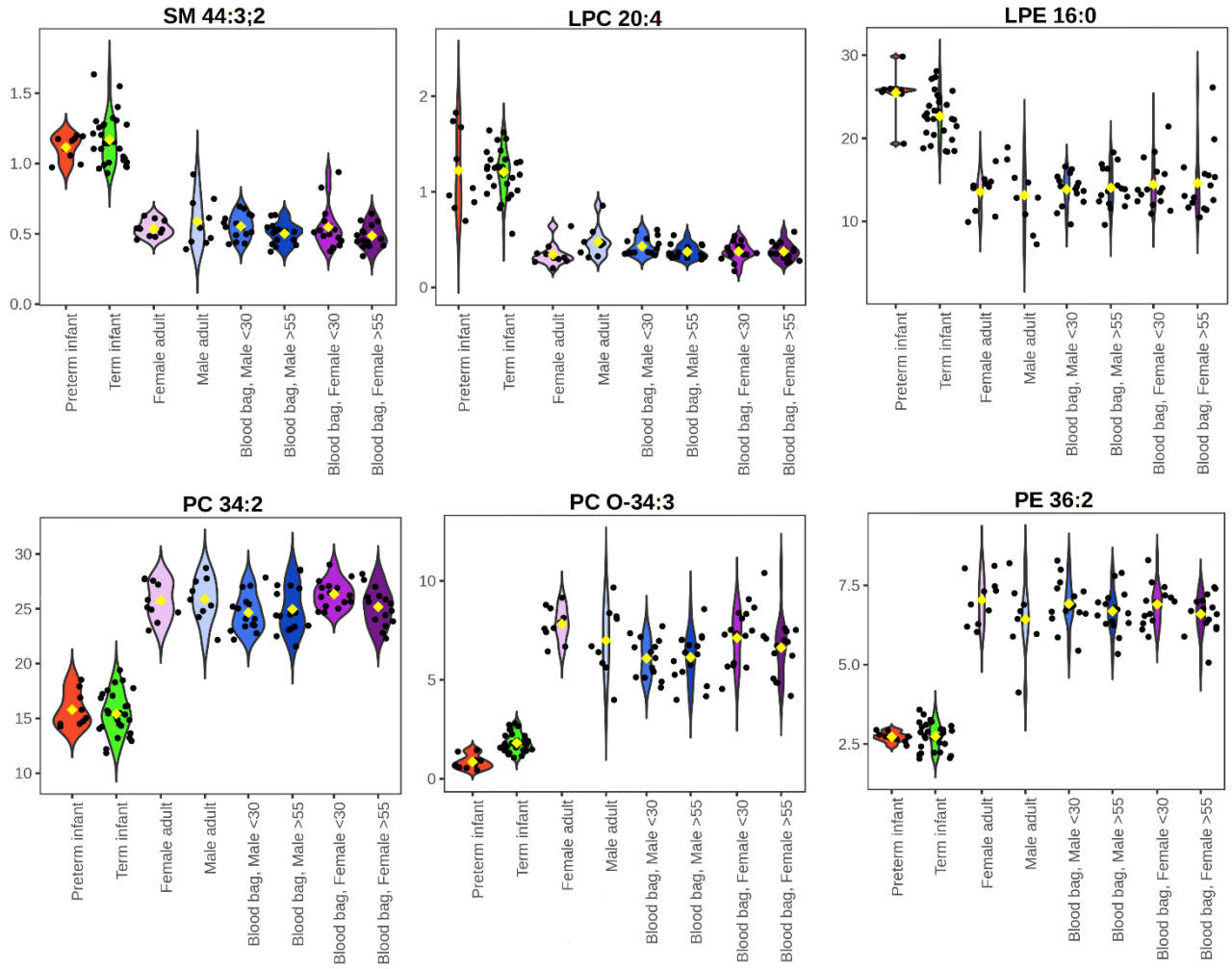

Figure 36: Lipids showing the biggest difference in fractional abundance between RBCs of infants, fresh blood and blood bags

Literature evidence partially supports the elevations of LPC (Figure 23), since data shows that neonatal RBCs are enriched in palmitate (16:0) and several long-chain polyunsaturates such as 20:3 and 20:4. However, oleic (18:1) and linoleic acid (18:2) are lower in the observed data, which is not in alignment with the literature [13].

The species that remain unchanged are minor fatty acids present only in trace amounts in RBC membranes, such as 14:0, 15:0, 17:1, 20:1 and 20:2. Their low abundance remains consistent across life stages [13,73]. A decrease in concentration of C22:0-, C24:0- and C26:0 with age, while C20:0 rises, was not observed [71]. Findings regarding lower LPC 16:0, 18:0, 18:1, 18:2, 20:4 in cord blood of neonates [72] only partially support observed data, since only 18:0 and 18:2 are slightly lower than in the fresh/blood bag samples.

Neonatal RBCs elevated LPE 16:0 is consistent with their higher palmitate content [13]. Literature suggests cord RBCs are enriched in stearate (18:0) and arachidonic acid (20:4), which should lead to higher LPE 18:0 and LPE 20:4 [13], yet the data here show lower 18:0 and unchanged 20:4. This discrepancy indicates that while some neonatal LPE species follow expected fatty acid enrichment, others diverge from reported trends.

PC 34:2 (16:0/18:2) is a defining feature of adult RBC membranes, reflecting the higher linoleic acid intake in adults. In neonates, linoleic acid (18:2) is markedly lower, what is also consistent with literature [73]. Adult

RBCs contain PC 36:2 as one of their major components [67], showing higher linoleic acid content in adult membranes. Newborns have much less linoleate available for PL synthesis, so PC 36:2 is reduced. During the third trimester, the fetus receives an enriched supply of arachidonic acid and DHA from the mother, while limiting transfer of linoleic acid [8]. This explains why neonatal RBCs contain more PC 36:4, 38:4, 38:6 but fewer linoleate PCs.

3.4.1.2.2 Term vs Preterm lipid distribution

As seen from the distribution of the top 15 lipids and from the initial MetaboAnalyst results (Figure 34), preterm and term groups generally follow the same trend and show similar fractional abundances. Both neonatal groups cluster together and separate clearly from adults and blood bags. To investigate this clustering in more detail and find possible differences between these two groups, biplot and heatmap were generated. A complete overlap of term and preterm infant groups is shown in Figure 37.

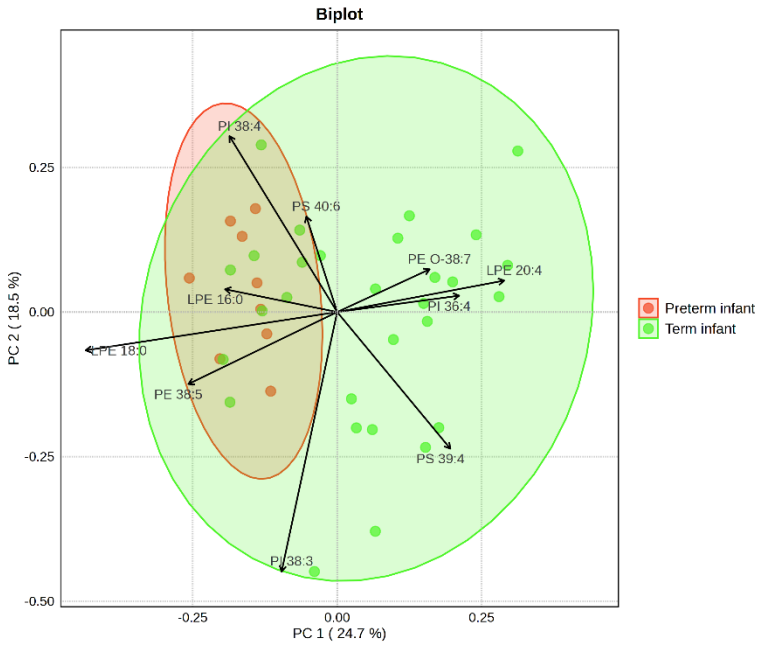

Figure 37: Biplot of fractional abundances of lipid species for term and preterm infant RBCs

Heatmap shows top 25 of most abundant and different lipids between preterm and term groups (Figure 38). Interestingly, one term sample, Term infant #10, clusters with the preterm group. Metadata shows that this child was born in the 36th week, which classifies it as late preterm and could explain its similarity to the preterm cluster. However, another child, Term infant #14, was also born in the 36th week, however, it does not cluster with the preterm and instead groups with the term samples. A closer look at the metadata shows that Term infant #10 had the lowest birth weight of all term infants, only 2420 g. This value is just 79 g higher than the two heaviest preterm infants (#2 and #3). This observation proposes that gestational age alone does not determine clustering in the lipidomic data. Birth weight might play an important role, potentially

reflecting differences in developmental maturity or nutritional status at birth. The fact that two infants born in the same week cluster differently underscores that the lipid composition of neonatal RBC membranes may be shaped by multiple factors, including gestational age, intrauterine growth and overall birth weight. This highlights the complexity of neonatal lipid metabolism and suggests that both gestational age and size at birth need to be considered when interpreting group-specific lipidomic signatures.

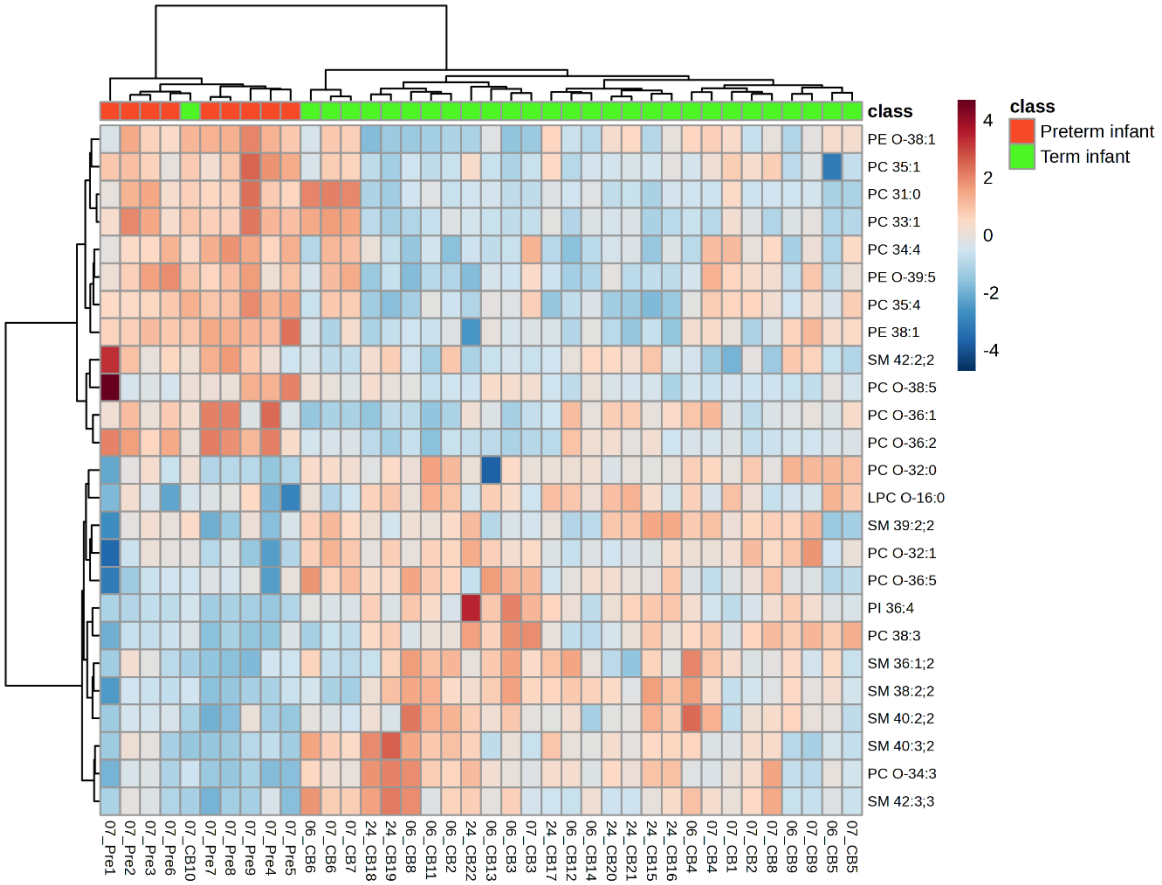

Figure 38: Heatmap showing top 25 lipid species and their up-/downregulation in the RBC samples between children RBCs

3.4.1.2.3 Blood bags vs fresh blood

In the third approach, fresh blood and donor blood bag samples were generalized into two supergroups without considering age or sex. Comparison of fresh and donor sample groups was carried out as well. PCA results (Figure 39) showed a trending towards separation between fresh blood and donor blood bags. The analysis confirms that age and sex of adult donors might influence the lipid distribution in RBC membranes.

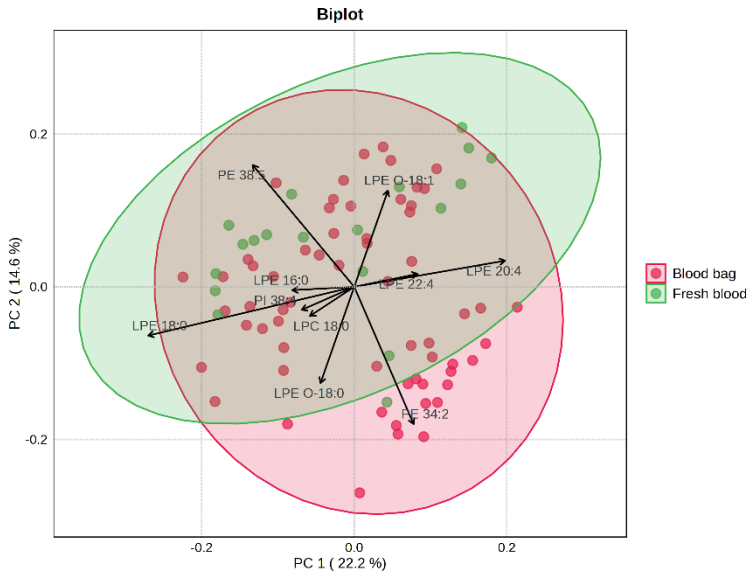

Figure 39: Biplot of fractional abundances of lipid species for fresh and stored blood bag RBCs

3.3.5 Distribution of lipids according to unsaturation

Degree of unsaturation was calculated for every identified lipid species across all eight groups. This allows direct comparison of double-bond content between adults, term and preterm infants and donor subgroups by sex and age (Figure 40). Results are summarized as class-level and species-level DB counts. Group means and SDs were computed to assess variance. These metrics enable detection of shifts in saturation that may drive the observed PCA separation of neonatal samples from adults.

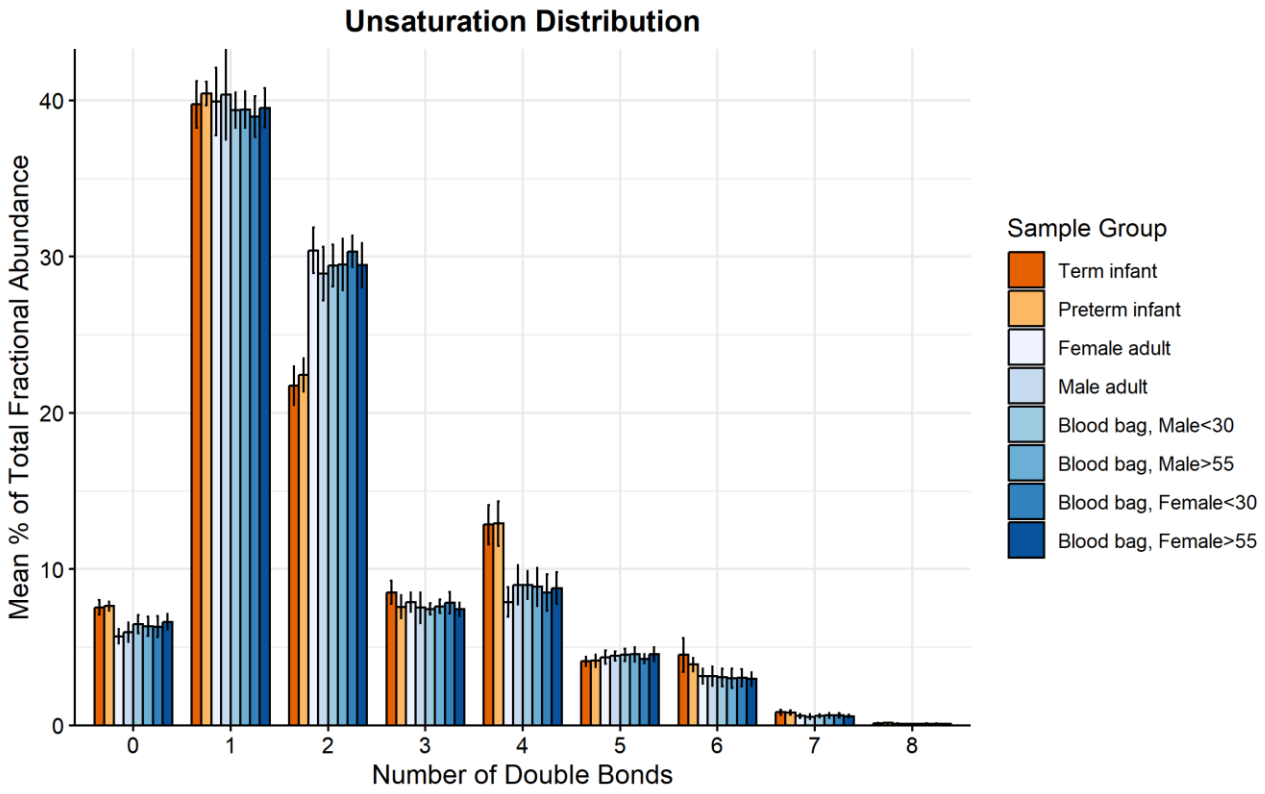

Figure 40: Distribution of unsaturation degree of lipid species in the investigated sample groups

Many major RBC PLs contain one saturated and one unsaturated fatty acyl chain, making lipids with a single DB highly abundant. The dominance of 16:0/18:1-rich PC and monounsaturated sphingolipids in RBC membranes [67] is consistent with the data obtained here.

Neonates have a higher fraction of SFA in their RBC membranes. Classic studies report that newborn RBCs contain about 43% SFAs compared with 38% in adults, consistent with their more rigid and less fluid membranes. This raises the proportion of 0-double-bond species [18] and supports the observed elevation. Newborn RBC PLs also contain much less linoleic acid than adult RBCs, reducing the 2-double-bond fraction and further increasing the relative 0-DB percentage [73]. Preterm infants show distinct SFA elevations. At birth, they have higher levels of stearic acid (18:0) and lignoceric acid (24:0) in RBCs compared with term infants. These increases further contribute to the enrichment of the 0-DB category [74].

Both term and preterm neonates have markedly lower levels of di-unsaturated lipid species in their RBC membranes compared with adults. The main two-double-bond fatty acid is linoleic acid (C18:2, n–6), which is significantly reduced in neonatal RBCs. Classic studies showed that RBC PLs of full-term newborns contained about 3.8% linoleic acid, compared with 11.9% in adults [73]. This trend is consistent with the data obtained. Preterm infants at birth had linoleate levels of about 3.9% of total RBC fatty acids, significantly below the ~9.1% measured in term newborns [74], however, this does not align with the data found in the investigation.

Preterm infants' RBC membranes show a relative enrichment of lipids with four DBs, possibly due to higher incorporation of arachidonic acid (20:4, n–6). Recent profiling at birth reported that preterm neonates' RBCs contained about 15.3% arachidonic acid, compared with 11.3% in term infants. This represents a significant increase in the 4-double-bond lipid fraction in preterm RBCs [74]. The found data confirms this finding from the literature, showing a significantly greater percentage than adult groups.

Lipids with six DBs are mainly DHA-containing species (22:6 n-3). The placenta actively transfers long-chain PUFAs such as DHA and arachidonic acid during late gestation. As a result, term neonates often show relatively high RBC DHA compared with adults and RBC DHA reflects maternal supply. This selective transfer explains the small increase in the six-double-bond fraction observed in newborn samples [76]. The findings are in accordance with the found data, since mean fractional abundance is slightly higher in term than in preterm infants.

Apart from the clear differences observed between term and preterm infant RBCs compared with adults, no major differences were detected within the adult donor groups. Neither sex nor age showed significant effects on overall lipid unsaturation patterns. Male and female donors showed very similar profiles and younger versus older donors also showed no consistent shifts in the distribution of DBs. Importantly, there was no evidence that older female donors shared features resembling the lipid profile of preterm infants. Their RBC membranes did not show enrichment of specific unsaturation categories that might mirror neonatal patterns. This suggests that while neonatal RBCs are distinct due to developmental and metabolic factors, adult donor variation in lipid unsaturation is relatively limited.

3.3.6 Chain length distribution

Distribution of fatty acyl chain length was examined to highlight possible difference between the different cohort groups. The shortest lipid detected was LPC 14:0, while the longest was SM species with 44 carbons in various DB states. To analyse this systematically, the dataset was divided into two ranges. For single-chain lipids (LPC, LPE, LPC O-, LPE O-), the longest detected was LPC 24:0. For double-chain lipids, the shortest detected was PC 26:0. Fractional abundances were calculated and normalized to 100 within each sample for the range 14–24 carbons (Figure 41) and separately for the range 26–44 carbons (Figure 42). This allowed comparison of chain length distributions across groups without mixing single- and double-chain classes.

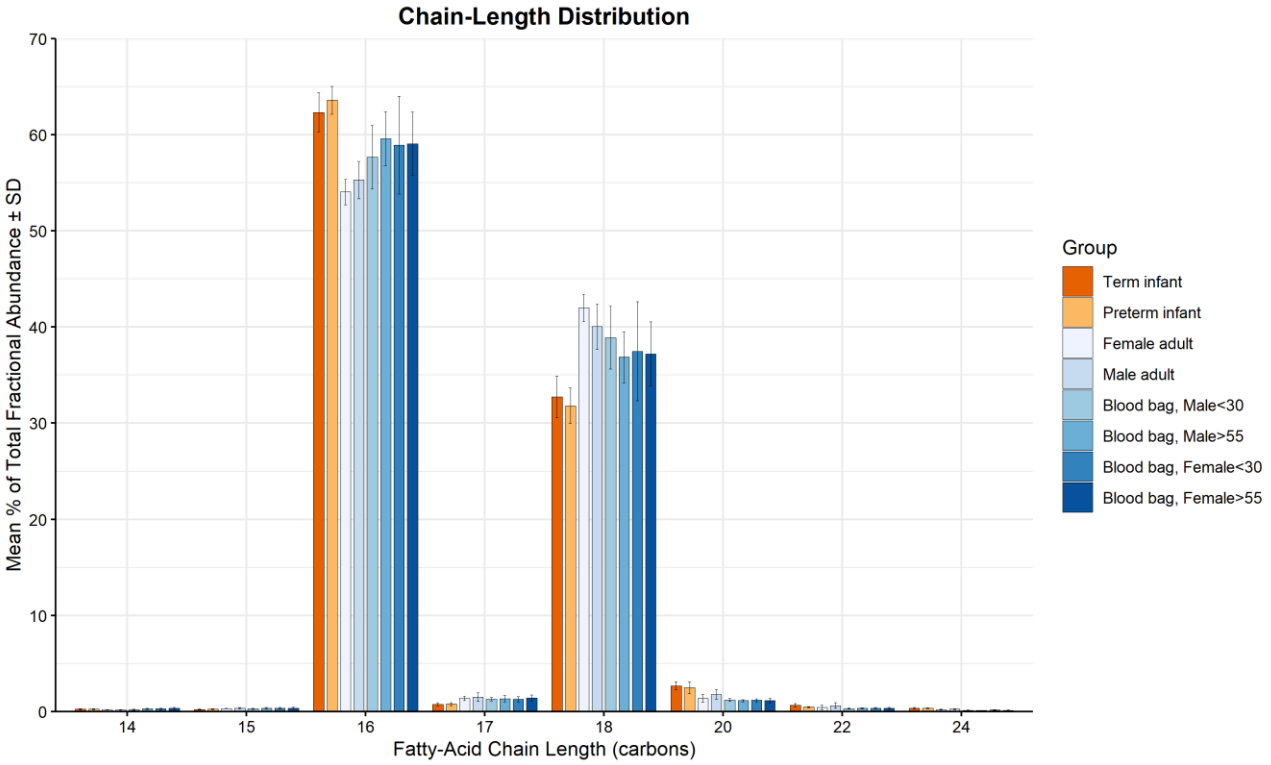

Figure 41: Distribution of chain lengths 14-24 of lipid species in the investigated sample groups

Lipids with 14 and 15 carbons showed no measurable differences between the sample groups, indicating that these chain lengths are consistently represented across all populations. In contrast, lipids with 16 carbons showed a difference. Their mean fractional abundance was elevated in both term and preterm infant samples, while adult groups, including both males and females, showed the lowest levels. This pattern highlights an enrichment of C16-containing lipids in neonatal RBC membranes. The blood bag groups did not differ significantly from each other and remained at a relatively stable baseline, still higher than fresh blood samples, suggesting that age and sex of adult donors do not strongly influence this chain length. Additionally, a slight increase in C20-containing lipids was observed in the neonatal samples compared with adults. This trend was less pronounced than for C16 but still suggests subtle shifts in chain length distribution between infants and adult RBCs.

Children's samples showed a small decrease in fractional abundance at 17 carbons and a significant reduction at 18 carbons. This pattern was consistent in both term and preterm infants. The 18-carbon species, which are abundant in adult RBCs, were significantly underrepresented in neonatal RBCs, suggesting developmental differences in fatty acid incorporation. The reduction at 18 carbons contrasts with the clear enrichment of 16-carbon lipids in infants, indicating a shift toward shorter chain lengths in neonatal RBC membranes. This imbalance may contribute to the distinct structural and biophysical properties of infant RBC membranes compared with those of adults.

Lipids with 30, 32, 38 and 44 carbons showed elevated fractional abundance in both neonatal groups, as shown in Figure 42. In contrast, species with 41 and 43 carbons were significantly reduced in neonates

compared with adults. All other chain lengths showed similar values across groups without notable differences. Importantly, all adult donor groups, regardless of age or sex, showed the same distribution pattern. There was no indication that older adult groups trended toward the lipid profile observed in preterm samples. This suggests that the chain length differences are developmental rather than age-related in adulthood.

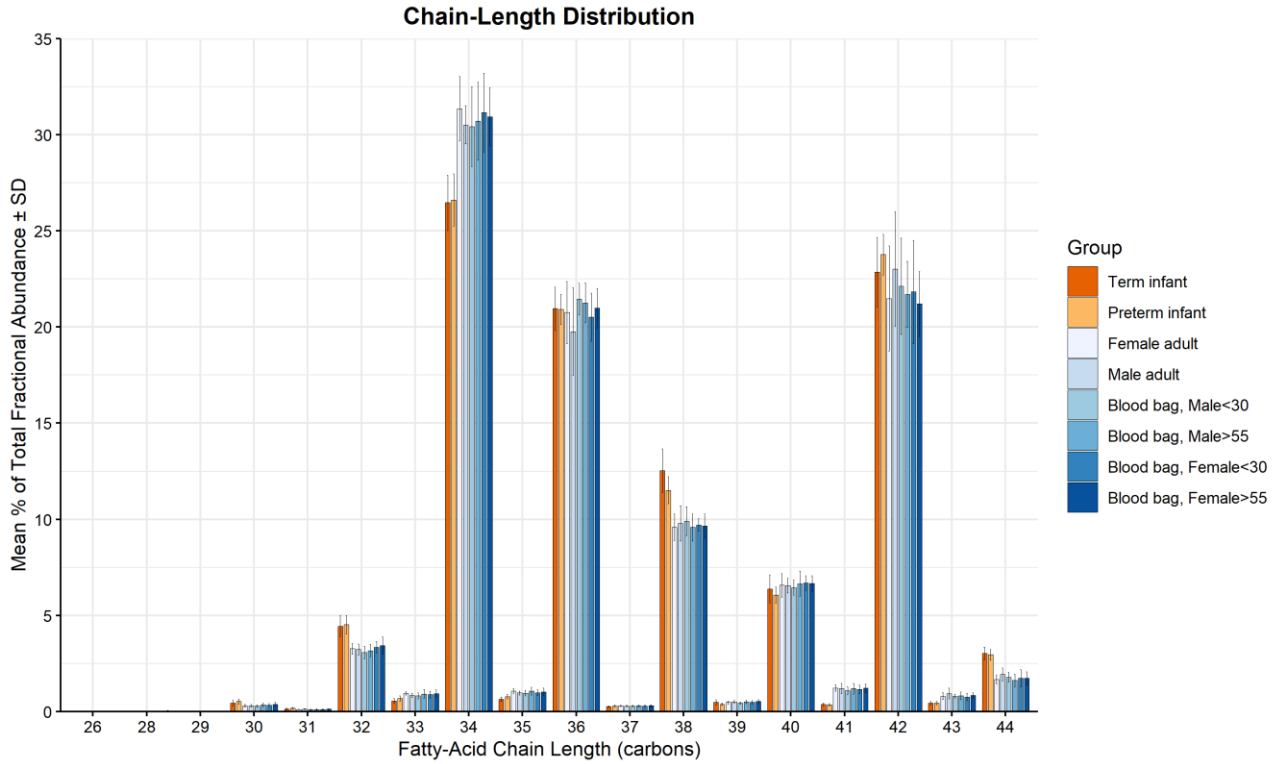

Figure 42: Distribution of chain lengths 26-44 of lipid species in the investigated sample groups

Regardless of donor age or sex, the distribution of total acyl carbons in major RBC lipid classes remains essentially the same. Human RBC membranes contain only a few hundred distinct lipid species, far fewer than the thousands of possible combinations [11]**.** Inter-individual variation is minimal. The RBC membrane lipidome is therefore maintained within a narrow range across the cell's lifespan. As a result, young and elderly, as well as male and female adult donors, show nearly identical total chain-length distributions.

Since odd totals arise only from trace odd-chain fatty acids such as C15:0 or C17:0, derived from diet or metabolism, they make up a very small fraction of RBC membrane lipids, which is in line with the findings [75].

Neonatal RBCs show a higher relative abundance of lipid species with even total carbons such as C30, C32, C38, C40 and C44. Their higher palmitate content promotes shorter even-chain combinations, for example 14:0/16:0 giving 30 or 16:0/16:0 giving 32. At the same time, greater incorporation of long PUFAs such as 20:4, 22:5 and 22:6, often paired with 16:0 or 18:0, increases the prevalence of longer even-chain species [73]. This is consistent with data that neonatal RBCs contain higher fractions of 30, 32, 38 and 44-carbon lipids compared with adults.

3.3.7 SM/PC Ratio

The SM:PC ratio compares SM to PC in RBC membranes for each sample group. The ratio reflects the balance between rigid, cholesterol-associated SM and the more fluidity-promoting PC and is showed in Figure 43, with reported group means and standard deviations, while Table 2 provides the corresponding numerical values for detailed inspection and secondary analyses.

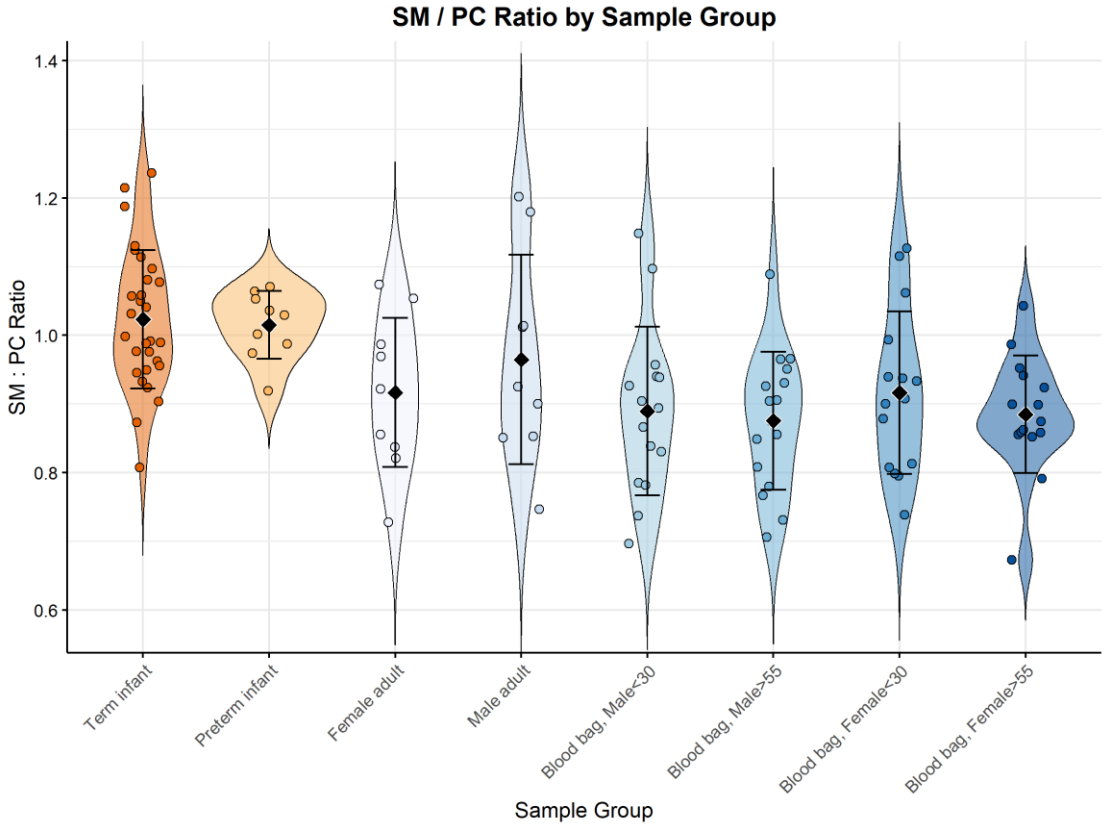

Figure 43: Calculated SM to PC ratio in the investigated sample groups

Table 2: Values for calculated SM to PC ratio in the sample groups

Sample group	SM:PC ratio, mean	SM:PC ratio, SD
Term infant	1.02	0.10
Preterm infant	1.01	0.05
Female adults	0.92	0.11
Male adults	0.96	0.15
Donor: Young men	0.89	0.12
Donor: Elder men	0.88	0.10
Donor: Young women	0.92	0.12
Donor: Elder women	0.88	0.09

The results are consistent with earlier literature reports and with the calculated fractional abundances. Both term and preterm infant groups show higher mean SM to PC ratios compared with adult groups, confirming

that neonatal RBC membranes are relatively enriched in SM. This enrichment reflects a shift toward more ordered and rigid membranes. The consistency of these findings across independent datasets supports the reliability of the observed trend and highlights the biological relevance of the SM to PC ratio as a marker of developmental differences in RBC membrane composition.

Higher SM levels and an increased SM:PC ratio are associated with stronger RBC membranes and reduced hemolysis [25]. This suggests that lipid balance directly influences membrane stability. Infant RBCs, particularly those of preterm neonates, show several consistent differences from adults. They contain more cholesterol, which further stiffens the bilayer. Their SM:PC ratio is elevated, shifting the membrane toward a more ordered state. They also have lower levels of plasmalogens, reducing antioxidant protection and show distinct fatty acid profiles, including lower linoleate and DHA and higher arachidonic acid. Together, these features create membranes that are less fluid, more oxidation-prone and shorter-lived than adult RBCs.

4 Conclusion

This thesis investigated the RBC lipid profile across eight groups using two techniques, shotgun lipidomics and RP-HPLC-MS. The objective was to determine how RBC membrane lipid composition varies between human populations, with a focus on donors of different sex and age compared to neonatal RBCs from term and preterm infants. The aim was to assess whether these differences could explain why blood from elder female donors is linked to improved outcomes in preterm infants.

Only a small subset of lipid species differs between infants and adults. No adult or donor subgroup showed a distinct lipid signature for blood bags from elder females. In every PCA, term and preterm infants formed clear clusters apart from fresh blood and donor groups. This consistent overlap indicates that lipid composition in adult RBCs is individually variable, independent by sex or age or blood storage. The differences observed in neonates are unique to early development rather than adult donor characteristics. When analysing unsaturation and chain length distribution, results showed either clustering between preterm and term infants or an even lipid class or species distribution across all cohort groups, as confirmed by statistical analyses.

Even though no unique lipid profile was identified for older female donors, clear differences emerged between adults and infants. The neonatal samples, especially cord blood, showed consistent patterns that set them apart from adults. These included shifts in saturation, chain length distribution and specific lipid class abundances. Such differences highlight the distinct lipid composition of neonatal RBC membranes. While adults, regardless of sex or age, clustered closely together, both preterm and term infants consistently formed separate groups. This demonstrates that neonatal RBCs carry characteristic lipid signatures, which are preserved in cord blood and reflect developmental biology.

The data suggest that older female donors do not share a unique lipid pattern compared to lipid patterns from other donor or fresh blood groups. Their RBC membrane lipids are not linked to the reported survival benefit after transfusion. The effect may depend on factors outside this study, including membrane proteins, glycans, glycolipids, small metabolites and circulating plasma components.

Beyond compatibility, the results also indicate that lipid distribution remains consistent across adults and is not significantly altered by processing blood into storage bags. This consistency across adult groups underscores that the observed neonatal–adult differences are intrinsic to developmental biology rather than donor age, sex, or blood storage. Not all female donors will have the same lipid profile. A subset of older women could carry a specific pattern that our analysis did not detect. The cohort was limited in size and the scope was restricted to membrane lipids. Important information may be missing. Future work should expand the cohort, include longitudinal sampling and integrate proteomics, glycomics, metabolomics and functional assays. This broader view could reveal donor features that better explain clinical outcomes in neonatals.

5 Bibliography

(1) Bellach, L.; Eigenschink, M.; Hassanein, A.; Savran, D.; Salzer, U.; Müllner, E. W.; Repa, A.; Klebermass-Schrehof, K.; Wisgrill, L.; Giordano, V.; Berger, A. Packed Red Blood Cell Transfusion in Preterm Infants. *The Lancet Haematology* **2022**, *9* (8), e615–e626. https://doi.org/10.1016/S2352-3026(22)00207-1.

(2) Patel, R. M.; Lukemire, J.; Shenvi, N.; Arthur, C.; Stowell, S. R.; Sola-Visner, M.; Easley, K.; Roback, J. D.; Guo, Y.; Josephson, C. D. Association of Blood Donor Sex and Age With Outcomes in Very Low-Birth-Weight Infants Receiving Blood Transfusion. *JAMA Network Open* **2021**, *4* (9), e2123942–e2123942. https://doi.org/10.1001/JAMANETWORKOPEN.2021.23942.

(3) Murphy, T.; Chawla, A.; Tucker, R.; Vohr, B. Impact of Blood Donor Sex on Transfusion-Related Outcomes in Preterm Infants. *The Journal of Pediatrics* **2018**, *201*, 215–220. https://doi.org/10.1016/j.jpeds.2018.04.023.

(4) D'Alessandro, A.; Fu, X.; Kanias, T.; Reisz, J. A.; Culp-Hill, R.; Guo, Y.; Gladwin, M. T.; Page, G.; Kleinman, S.; Lanteri, M.; Stone, M.; Busch, M. P.; Zimring, J. C. Donor Sex, Age and Ethnicity Impact Stored Red Blood Cell Antioxidant Metabolism through Mechanisms in Part Explained by Glucose 6-Phosphate Dehydrogenase Levels and Activity. *Haematologica* **2021**, *106* (5), 1290–1302. https://doi.org/10.3324/HAEMATOL.2020.246603.

(5) Yang, K.; Han, X. Lipidomics: Techniques, Applications, and Outcomes Related to Biomedical Sciences. *Trends in Biochemical Sciences* **2016**, *41* (11), 954–969. https://doi.org/10.1016/j.tibs.2016.08.010.

(6) Reid, M. E.; Westhoff, C. M. Membrane Blood Group Antigens and Antibodies. In *Blood Banking and Transfusion Medicine: Basic Principles and Practice: Second Edition*; Elsevier, 2006; pp 53–68. https://doi.org/10.1016/B978-0-443-06981-9.50010-7.

(7) Cory, S. Phosphatidylserine Hide-and-Seek. *Proc. Natl. Acad. Sci. U.S.A.* **2018**, *115* (48), 12092–12094. https://doi.org/10.1073/pnas.1817485115.

(8) Pellegrino, C.; Stone, E. F.; Valentini, C. G.; Teofili, L. Fetal Red Blood Cells: A Comprehensive Review of Biological Properties and Implications for Neonatal Transfusion. *Cells* **2024**, *13* (22), 1843. https://doi.org/10.3390/cells13221843.

(9) Ballas, S. K.; Krasnow, S. H. Structure of Erythrocyte Membrane and Its Transport Functions. *Ann Clin Lab Sci* **1980**, *10* (3), 209–219.

(10) Heckers, H.; Platt, D. Red Cell Membrane Lipids and Aging. In *Blood Cells, Rheology, and Aging*; Platt, D., Ed.; Springer Berlin Heidelberg: Berlin, Heidelberg, 1988; pp 16–28. https://doi.org/10.1007/978-3-642-71790-1_3.

(11) Bernecker, C.; Köfeler, H.; Pabst, G.; Trötzmüller, M.; Kolb, D.; Strohmayer, K.; Trajanoski, S.; Holzapfel, G. A.; Schlenke, P.; Dorn, I. Cholesterol Deficiency Causes Impaired Osmotic Stability of Cultured Red Blood Cells. *Front. Physiol.* **2019**, *10*, 1529. https://doi.org/10.3389/fphys.2019.01529.

(12) Sagawa, S.; Shiraki, K. Changes of Osmotic Fragility of Red Blood Cells Due to Repletion or Depletion of Cholesterol in Human and Rat Red Cells in Vitro. *Journal of Nutritional Science and Vitaminology, J Nutr Sci Vitaminol* **1980**, *26* (2), 161–169. https://doi.org/10.3177/jnsv.26.161.

(13) Neerhout, R. G. Erythrocyte Lipids in the Neonate. *Pediatr Res* **1968**, *2* (3), 172–178. https://doi.org/10.1203/00006450-196805000-00003.

(14) Neerhout, R. C. Erythrocyte Lipids in Childhood. *Pediatr Res* **1972**, *6* (9), 736–741. https://doi.org/10.1203/00006450-197209000-00007.

(15) Piazze Garnica, J. J.; Pierucci, F.; Vozzi, G.; Cosmi, E. V.; Anceschi, M. M. The Cholesterol to Phospholipids Ratio (C/PL) of the Erythrocyte Membrane in Normotensive, Hypertensive Pregnant and in Cord Blood as Assessed by a Simple Enzymatic Method. *Scandinavian Journal of Clinical and Laboratory Investigation* **1994**, *54* (8), 631–635. https://doi.org/10.3109/00365519409087543.

(16) Linderkamp, O.; Nash, G.; Wu, P.; Meiselman, H. Deformability and Intrinsic Material Properties of Neonatal Red Blood Cells. *Blood* **1986**, *67* (5), 1244–1250. https://doi.org/10.1182/blood.V67.5.1244.1244.

(17) Matovcik, L. M.; Chiu, D.; Lubin, B.; Mentzer, W. C.; Lane, P. A.; Mohandas, N.; Schrier, S. L. The Aging Process of Human Neonatal Erythrocytes. *Pediatr Res* **1986**, *20* (11), 1091–1096. https://doi.org/10.1203/00006450-198611000-00006.

(18) Crespo, L. M.; Bifano, E. M.; Freedman, J. C. Membrane Lipid Fluidity and Filterability of Red Blood Cells from Adults and Newborns. *Pediatr Res* **1988**, *24* (4), 433–437. https://doi.org/10.1203/00006450-198810000-00003.
(19) Braverman, N. E.; Moser, A. B. Functions of Plasmalogen Lipids in Health and Disease. *Biochimica et Biophysica Acta (BBA) - Molecular Basis of Disease* **2012**, *1822* (9), 1442–1452. https://doi.org/10.1016/j.bbadis.2012.05.008.
(20) Labadaridis, I.; Moraitou, M.; Theodoraki, M.; Triantafyllidis, G.; Sarafidou, J.; Michelakakis, H. Plasmalogen Levels in Full-term Neonates. *Acta Paediatrica* **2009**, *98* (4), 640–642. https://doi.org/10.1111/j.1651-2227.2008.01205.x.
(21) Karadayi, R.; Pallot, C.; Cabaret, S.; Mazzocco, J.; Gabrielle, P.-H.; Semama, D. S.; Chantegret, C.; Ternoy, N.; Martin, D.; Donier, A.; Gregoire, S.; Creuzot-Garcher, C. P.; Bron, A. M.; Bretillon, L.; Berdeaux, O.; Acar, N. Modification of Erythrocyte Membrane Phospholipid Composition in Preterm Newborns with Retinopathy of Prematurity: The omegaROP Study. *Front. Cell Dev. Biol.* **2022**, *10*, 921691. https://doi.org/10.3389/fcell.2022.921691.
(22) Van 'T Erve, T. J.; Wagner, B. A.; Martin, S. M.; Knudson, C. M.; Blendowski, R.; Keaton, M.; Holt, T.; Hess, J. R.; Buettner, G. R.; Ryckman, K. K.; Darbro, B. W.; Murray, J. C.; Raife, T. J. The Heritability of Hemolysis in Stored Human Red Blood Cells. *Transfusion* **2015**, *55* (6), 1178–1185. https://doi.org/10.1111/trf.12992.
(23) Szczesny-Malysiak, E.; Mohaissen, T.; Bulat, K.; Kaczmarska, M.; Wajda, A.; Marzec, K. M. Sex-Dependent Membranopathy in Stored Human Red Blood Cells. *Haematologica* **2021**, *106* (10), 2779–2782. https://doi.org/10.3324/HAEMATOL.2021.278895.
(24) Kanias, T.; Lanteri, M. C.; Page, G. P.; Guo, Y.; Endres, S. M.; Stone, M.; Keating, S.; Mast, A. E.; Cable, R. G.; Triulzi, D. J.; Kiss, J. E.; Murphy, E. L.; Kleinman, S.; Busch, M. P.; Gladwin, M. T. Ethnicity, Sex, and Age Are Determinants of Red Blood Cell Storage and Stress Hemolysis: Results of the REDS-III RBC-Omics Study. *Blood Advances* **2017**, *1* (15), 1132–1141. https://doi.org/10.1182/bloodadvances.2017004820.
(25) Melzak, K. A.; Muth, M.; Kirschhöfer, F.; Brenner-Weiss, G.; Bieback, K. Lipid Ratios as a Marker for Red Blood Cell Storage Quality and as a Possible Explanation for Donor Gender Differences in Storage Quality. *Vox Sanguinis* **2020**, *115* (8), 655–663. https://doi.org/10.1111/vox.12924.
(26) Crawford, T. M.; Andersen, C. C.; Stark, M. J. Red Blood Cell Donor Sex Associated Effects on Morbidity and Mortality in the Extremely Preterm Newborn. *Children* **2022**, *9* (12), 1980. https://doi.org/10.3390/children9121980.
(27) D'Alessandro, A.; Kriebardis, A. G.; Rinalducci, S.; Antonelou, M. H.; Hansen, K. C.; Papassideri, I. S.; Zolla, L. An Update on Red Blood Cell Storage Lesions, as Gleaned through Biochemistry and Omics Technologies. *Transfusion* **2015**, *55* (1), 205–219. https://doi.org/10.1111/TRF.12804.
(28) Laurén, E.; Tigistu-Sahle, F.; Valkonen, S.; Westberg, M.; Valkeajärvi, A.; Eronen, J.; Siljander, P.; Pettilä, V.; Käkelä, R.; Laitinen, S.; Kerkelä, E. Phospholipid Composition of Packed Red Blood Cells and That of Extracellular Vesicles Show a High Resemblance and Stability during Storage. *Biochimica et Biophysica Acta (BBA) - Molecular and Cell Biology of Lipids* **2018**, *1863* (1), 1–8. https://doi.org/10.1016/j.bbalip.2017.09.012.
(29) Doctor, A.; Spinella, P. Effect of Processing and Storage on Red Blood Cell Function In Vivo. *Seminars in Perinatology* **2012**, *36* (4), 248–259. https://doi.org/10.1053/j.semperi.2012.04.005.
(30) Silliman, C. C.; Moore, E. E.; Kelher, M. R.; Khan, S. Y.; Gellar, L.; Elzi, D. J. Identification of Lipids That Accumulate during the Routine Storage of Prestorage Leukoreduced Red Blood Cells and Cause Acute Lung Injury. *Transfusion* **2011**, *51* (12), 2549–2554. https://doi.org/10.1111/j.1537-2995.2011.03186.x.
(31) Kim, C. Y.; Johnson, H.; Peltier, S.; Spitalnik, S. L.; Hod, E. A.; Francis, R. O.; Hudson, K. E.; Stone, E. F.; Gordy, D. E.; Fu, X.; Zimring, J. C.; Amireault, P.; Buehler, P. W.; Wilson, R. B.; D'Alessandro, A.; Shchepinov, M. S.; Thomas, T. Deuterated Linoleic Acid Attenuates the RBC Storage Lesion in a Mouse Model of Poor RBC Storage. *Front. Physiol.* **2022**, *13*, 868578. https://doi.org/10.3389/fphys.2022.868578.
(32) Cloos, A.-S.; Ghodsi, M.; Stommen, A.; Vanderroost, J.; Dauguet, N.; Pollet, H.; D'Auria, L.; Mignolet, E.; Larondelle, Y.; Terrasi, R.; Muccioli, G. G.; Van Der Smissen, P.; Tyteca, D. Interplay Between

Plasma Membrane Lipid Alteration, Oxidative Stress and Calcium-Based Mechanism for Extracellular Vesicle Biogenesis From Erythrocytes During Blood Storage. *Front. Physiol.* **2020**, *11*, 712. https://doi.org/10.3389/fphys.2020.00712.

(33) Himbert, S.; Qadri, S. M.; Sheffield, W. P.; Schubert, P.; D'Alessandro, A.; Rheinstädter, M. C. Blood Bank Storage of Red Blood Cells Increases RBC Cytoplasmic Membrane Order and Bending Rigidity. *PLoS ONE* **2021**, *16* (11), e0259267. https://doi.org/10.1371/journal.pone.0259267.

(34) Maślanka, K.; Smoleńska-Sym, G.; Michur, H.; Wróbel, A.; Lachert, E.; Brojer, E. Lysophosphatidylcholines: Bioactive Lipids Generated During Storage of Blood Components. *Arch. Immunol. Ther. Exp.* **2012**, *60* (1), 55–60. https://doi.org/10.1007/s00005-011-0154-x.

(35) Cunningham, K. E.; Okolo, F. C.; Baker, R.; Mollen, K. P.; Good, M. Red Blood Cell Transfusion in Premature Infants Leads to Worse Necrotizing Enterocolitis Outcomes. *Journal of Surgical Research* **2017**, *213*, 158–165. https://doi.org/10.1016/j.jss.2017.02.029.

(36) Schwaiger, M.; Schoeny, H.; Abiead, Y. E.; Hermann, G.; Rampler, E.; Koellensperger, G. Merging Metabolomics and Lipidomics into One Analytical Run. *Analyst* **2018**, *144* (1), 220–229. https://doi.org/10.1039/C8AN01219A.

(37) Lísa, M.; Holčapek, M. High-Throughput and Comprehensive Lipidomic Analysis Using Ultrahigh-Performance Supercritical Fluid Chromatography–Mass Spectrometry. *Anal. Chem.* **2015**, *87* (14), 7187–7195. https://doi.org/10.1021/acs.analchem.5b01054.

(38) Triebl, A.; Trötzmüller, M.; Hartler, J.; Stojakovic, T.; Köfeler, H. C. Lipidomics by Ultrahigh Performance Liquid Chromatography-High Resolution Mass Spectrometry and Its Application to Complex Biological Samples. *Journal of Chromatography B* **2017**, *1053*, 72–80. https://doi.org/10.1016/j.jchromb.2017.03.027.

(39) Schwudke, D.; Liebisch, G.; Herzog, R.; Schmitz, G.; Shevchenko, A. Shotgun Lipidomics by Tandem Mass Spectrometry under Data-Dependent Acquisition Control. In *Methods in Enzymology*; Elsevier, 2007; Vol. 433, pp 175–191. https://doi.org/10.1016/S0076-6879(07)33010-3.

(40) Ovčačíková, M.; Lísa, M.; Cífková, E.; Holčapek, M. Retention Behavior of Lipids in Reversed-Phase Ultrahigh-Performance Liquid Chromatography–Electrospray Ionization Mass Spectrometry. *Journal of Chromatography A* **2016**, *1450*, 76–85. https://doi.org/10.1016/j.chroma.2016.04.082.

(41) Liebisch, G. *The Role of LC–MS in Lipidomics | LCGC International*. https://www.chromatographyonline.com/view/role-lc-ms-lipidomics (accessed 2025-10-02).

(42) Burla, B.; Arita, M.; Arita, M.; Bendt, A. K.; Cazenave-Gassiot, A.; Dennis, E. A.; Ekroos, K.; Han, X.; Ikeda, K.; Liebisch, G.; Lin, M. K.; Loh, T. P.; Meikle, P. J.; Orešič, M.; Quehenberger, O.; Shevchenko, A.; Torta, F.; Wakelam, M. J. O.; Wheelock, C. E.; Wenk, M. R. MS-Based Lipidomics of Human Blood Plasma: A Community-Initiated Position Paper to Develop Accepted Guidelines. *Journal of Lipid Research* **2018**, *59* (10), 2001–2017. https://doi.org/10.1194/JLR.S087163.

(43) Lange, M.; Ni, Z.; Criscuolo, A.; Fedorova, M. Liquid Chromatography Techniques in Lipidomics Research. *Chromatographia* **2019**, *82* (1), 77–100. https://doi.org/10.1007/s10337-018-3656-4.

(44) Rund, K. M.; Carpanedo, L.; Lauterbach, R.; Wermund, T.; West, A. L.; Wende, L. M.; Calder, P. C.; Schebb, N. H. LC-ESI-HRMS — Lipidomics of Phospholipids: Characterization of Extraction, Chromatography and Detection Parameters. *Anal Bioanal Chem* **2024**, *416* (4), 925–944. https://doi.org/10.1007/s00216-023-05080-0.

(45) Brügger, B.; Erben, G.; Sandhoff, R.; Wieland, F. T.; Lehmann, W. D. Quantitative Analysis of Biological Membrane Lipids at the Low Picomole Level by Nano-Electrospray Ionization Tandem Mass Spectrometry. *Proc. Natl. Acad. Sci. U.S.A.* **1997**, *94* (6), 2339–2344. https://doi.org/10.1073/pnas.94.6.2339.

(46) Liigand, P.; Kaupmees, K.; Haav, K.; Liigand, J.; Leito, I.; Girod, M.; Antoine, R.; Kruve, A. Think Negative: Finding the Best Electrospray Ionization/MS Mode for Your Analyte. *Anal. Chem.* **2017**, *89* (11), 5665–5668. https://doi.org/10.1021/acs.analchem.7b00096.

(47) White, J. B.; Trim, P. J.; Salagaras, T.; Long, A.; Psaltis, P. J.; Verjans, J. W.; Snel, M. F. Equivalent Carbon Number and Interclass Retention Time Conversion Enhance Lipid Identification in Untargeted Clinical Lipidomics. *Analytical Chemistry* **2022**, *94* (8), 3476–3484. https://doi.org/10.1021/ACS.ANALCHEM.1C03770/SUPPL_FILE/AC1C03770_SI_002.XLSX.

(48) Smith, M.; Jungalwala, F. B. Reversed-Phase High Performance Liquid Chromatography of Phosphatidylcholine: A Simple Method for Determining Relative Hydrophobic Interaction of Various Molecular Species. *Journal of Lipid Research* **1981**, *22* (4), 697–704. https://doi.org/10.1016/S0022-2275(20)37381-8.
(49) Wishart, D.; Guo, A.; Oler, E.; et al. *Human Metabolome Database: Database Statistics*. https://hmdb.ca/statistics (accessed 2025-12-21).
(50) *Isomeric Overlap – lipidomicstandards.org*. https://lipidomicstandards.org/isomeric-overlap/ (accessed 2025-09-02).
(51) Kyle, J. E.; Zhang, X.; Weitz, K. K.; Monroe, M. E.; Ibrahim, Y. M.; Moore, R. J.; Cha, J.; Sun, X.; Lovelace, E. S.; Wagoner, J.; Polyak, S. J.; Metz, T. O.; Dey, S. K.; Smith, R. D.; Burnum-Johnson, K. E.; Baker, E. S. Uncovering Biologically Significant Lipid Isomers with Liquid Chromatography, Ion Mobility Spectrometry and Mass Spectrometry. *Analyst* **2016**, *141* (5), 1649–1659. https://doi.org/10.1039/C5AN02062J.
(52) Hu, Q.; Noll, R. J.; Li, H.; Makarov, A.; Hardman, M.; Graham Cooks, R. The Orbitrap: A New Mass Spectrometer. *J. Mass Spectrom.* **2005**, *40* (4), 430–443. https://doi.org/10.1002/jms.856.
(53) Bromirski, M. *What Makes Orbitrap Mass Spectrometry the First Choice for Routine and Research Mass Spec?*. AnalyteGuru. https://www.thermofisher.com/blog/analyteguru/what-makes-orbitrap-mass-spectrometry-the-first-choice-for-both/ (accessed 2025-07-03).
(54) Kalli, A.; Smith, G. T.; Sweredoski, M. J.; Hess, S. Evaluation and Optimization of Mass Spectrometric Settings during Data-Dependent Acquisition Mode: Focus on LTQ-Orbitrap Mass Analyzers. *J. Proteome Res.* **2013**, *12* (7), 3071–3086. https://doi.org/10.1021/pr3011588.
(55) Valmori, M.; Marie, V.; Fenaille, F.; Colsch, B.; Touboul, D. Recent Methodological Developments in Data-Dependent Analysis and Data-Independent Analysis Workflows for Exhaustive Lipidome Coverage. *Front. Anal. Sci.* **2023**, *3*, 1118742. https://doi.org/10.3389/frans.2023.1118742.
(56) Honda, A.; Yamashita, K.; Miyazaki, H.; Shirai, M.; Ikegami, T.; Xu, G.; Numazawa, M.; Hara, T.; Matsuzaki, Y. Highly Sensitive Analysis of Sterol Profiles in Human Serum by LC-ESI-MS/MS. *Journal of Lipid Research* **2008**, *49* (9), 2063–2073. https://doi.org/10.1194/jlr.D800017-JLR200.
(57) Timperio, A. M.; Mirasole, C.; D'Alessandro, A.; Zolla, L. Red Blood Cell Lipidomics Analysis through HPLC-ESI-qTOF: Application to Red Blood Cell Storage. *JIOMICS* **2013**, *3* (1), 11–24. https://doi.org/10.5584/jiomics.v3i1.123.
(58) Vasku, G.; Peltier, C.; He, Z.; Thuret, G.; Gain, P.; Gabrielle, P.-H.; Acar, N.; Berdeaux, O. Comprehensive Mass Spectrometry Lipidomics of Human Biofluids and Ocular Tissues. *Journal of Lipid Research* **2023**, *64* (3), 100343. https://doi.org/10.1016/j.jlr.2023.100343.
(59) Kaufmann, A. Selecting the Best Q Exactive Orbitrap Mass Spectrometer Scan Mode for Your Application.
(60) Schwudke, D.; Schuhmann, K.; Herzog, R.; Bornstein, S. R.; Shevchenko, A. Shotgun Lipidomics on High Resolution Mass Spectrometers. *Cold Spring Harbor Perspectives in Biology* **2011**, *3* (9), a004614–a004614. https://doi.org/10.1101/cshperspect.a004614.
(61) Zhang, S.; Van Pelt, C. K.; Henion, J. D. Automated Chip-based Nanoelectrospray-mass Spectrometry for Rapid Identification of Proteins Separated by Two-dimensional Gel Electrophoresis. *Electrophoresis* **2003**, *24* (21), 3620–3632. https://doi.org/10.1002/elps.200305585.
(62) Wilm, M. Principles of Electrospray Ionization. *Molecular & Cellular Proteomics* **2011**, *10* (7), M111.009407. https://doi.org/10.1074/mcp.M111.009407.
(63) Henion, J. The Reality of Lab-on-a-Chip Technology for the Mass Spectrometry Laboratory. **2009**, *27*, 900–915.
(64) Han, X.; Gross, R. W. Shotgun Lipidomics: Multidimensional MS Analysis of Cellular Lipidomes. *Expert Review of Proteomics* **2005**, *2* (2), 253–264. https://doi.org/10.1586/14789450.2.2.253.
(65) Herzog, R.; Schuhmann, K.; Schwudke, D.; Sampaio, J. L.; Bornstein, S. R.; Schroeder, M.; Shevchenko, A. LipidXplorer: A Software for Consensual Cross-Platform Lipidomics. *PLoS ONE* **2012**, *7* (1), e29851. https://doi.org/10.1371/journal.pone.0029851.
(66) Leidl, K.; Liebisch, G.; Richter, D.; Schmitz, G. Mass Spectrometric Analysis of Lipid Species of Human Circulating Blood Cells. *Biochimica et Biophysica Acta (BBA) - Molecular and Cell Biology of Lipids* **2008**, *1781* (10), 655–664. https://doi.org/10.1016/j.bbalip.2008.07.008.

(67) Vahedi, A.; Bigdelou, P.; Farnoud, A. M. Quantitative Analysis of Red Blood Cell Membrane Phospholipids and Modulation of Cell-Macrophage Interactions Using Cyclodextrins. *Sci Rep* **2020**, *10* (1), 15111. https://doi.org/10.1038/s41598-020-72176-3.
(68) Carquin, M.; Pollet, H.; Veiga-da-Cunha, M.; Cominelli, A.; Van Der Smissen, P.; N'kuli, F.; Emonard, H.; Henriet, P.; Mizuno, H.; Courtoy, P. J.; Tyteca, D. Endogenous Sphingomyelin Segregates into Submicrometric Domains in the Living Erythrocyte Membrane. *Journal of Lipid Research* **2014**, *55* (7), 1331–1342. https://doi.org/10.1194/jlr.M048538.
(69) Hürter, P.; Schröter, W.; Schedel, I.; Gercken, G. PHOSPHOLIPIDS OF RED CELLS AND BLOOD PLASMA IN ADULTS, NEWBORN INFANTS, AND PATIENTS WITH RH ERYTHROBLASTOSIS. *Pediatrics* **1970**, *46* (2), 259–266. https://doi.org/10.1542/peds.46.2.259.
(70) Vlaar, A. P. J.; Kulik, W.; Nieuwland, R.; Peters, C. P.; Tool, A. T. J.; Van Bruggen, R.; Juffermans, N. P.; De Korte, D. Accumulation of Bioactive Lipids during Storage of Blood Products Is Not Cell but Plasma Derived and Temperature Dependent. *Transfusion* **2011**, *51* (11), 2358–2366. https://doi.org/10.1111/j.1537-2995.2011.03177.x.
(71) Natarajan, A.; Christopher, R. Age and Gender-Specific Reference Intervals for a Panel of Lysophosphatidylcholines Estimated by Tandem Mass Spectrometry in Dried Blood Spots. *Practical Laboratory Medicine* **2023**, *33*, e00305. https://doi.org/10.1016/j.plabm.2022.e00305.
(72) Takatera, A.; Takeuchi, A.; Saiki, K.; Morioka, I.; Yokoyama, N.; Matsuo, M. Blood Lysophosphatidylcholine (LPC) Levels and Characteristic Molecular Species in Neonates: Prolonged Low Blood LPC Levels in Very Low Birth Weight Infants. *Pediatr Res* **2007**, *62* (4), 477–482. https://doi.org/10.1203/PDR.0b013e31814625ca.
(73) Gercken, G.; Tiling, T.; Brockmann, U.; Schröter, W. Fatty Acid Composition of Phospholipids in Erythrocytes of Adults, Normal Newborn Infants, and Neonates with Rh Erythroblastosis. *Pediatr Res* **1972**, *6* (5), 487–494. https://doi.org/10.1203/00006450-197205000-00002.
(74) Castillo Salinas, F.; Montaner Ramón, A.; Castillo Ferrer, F.-J.; Domingo-Carnice, A.; Cordobilla, B.; Domingo, J. C. Erythrocyte Membrane Docosahexaenoic Acid (DHA) and Lipid Profile in Preterm Infants at Birth and Over the First Month of Life: A Comparative Study with Infants at Term. *Nutrients* **2022**, *14* (23), 4956. https://doi.org/10.3390/nu14234956.
(75) Wendel, U. Abnormality of Odd-Numbered Long-Chain Fatty Acids in Erythrocyte Membrane Lipids from Patients with Disorders of Propionate Metabolism. *Pediatr Res* **1989**, *25* (2), 147–150. https://doi.org/10.1203/00006450-198902000-00014.
(76) Aparicio, E.; Martín-Grau, C.; Hernández-Martinez, C.; Voltas, N.; Canals, J.; Arija, V. Changes in Fatty Acid Levels (Saturated, Monounsaturated and Polyunsaturated) during Pregnancy. *BMC Pregnancy Childbirth* **2021**, *21* (1), 778. https://doi.org/10.1186/s12884-021-04251-0.
(77) Pasini, E. M.; Kirkegaard, M.; Mortensen, P.; Lutz, H. U.; Thomas, A. W.; Mann, M. In-Depth Analysis of the Membrane and Cytosolic Proteome of Red Blood Cells. *Blood* **2006**, *108* (3), 791–801. https://doi.org/10.1182/blood-2005-11-007799.
(78) Bryk, A. H.; Wiśniewski, J. R. Quantitative Analysis of Human Red Blood Cell Proteome. *J. Proteome Res.* **2017**, *16* (8), 2752–2761. https://doi.org/10.1021/acs.jproteome.7b00025.
(79) Jiang, F.; Liu, Q.; Li, Q.; Zhang, S.; Qu, X.; Zhu, J.; Zhong, G.; Huang, M. Signal Drift in Liquid Chromatography Tandem Mass Spectrometry and Its Internal Standard Calibration Strategy for Quantitative Analysis. *Anal. Chem.* **2020**, *92* (11), 7690–7698. https://doi.org/10.1021/acs.analchem.0c00633.

6 List of Aids Used

Used AI model	Aim of usage	Affected part of thesis
OpenAI ChatGPT 4.5	Creation of R scripts for the data visualization and figure creation	Figures 10-12, 19-33, 40-43
OpenAI ChatGPT 4.5	Improvement of the writing style and performing grammar checks	Subchapters 1.1 – 1.2 and 1.4 – 1.9
OpenAI ChatGPT 4o	Creation of a mindmap for the papers and articles referenced in the thesis	Chapter 1

7 Appendix

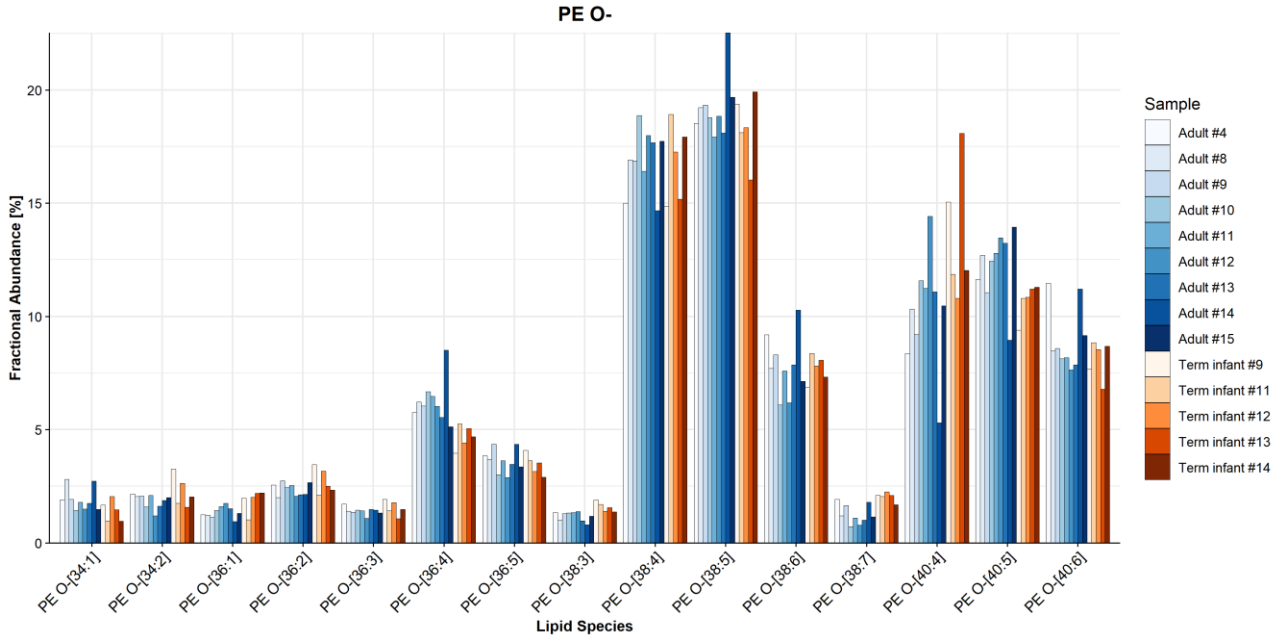

Figure A 1: Top 15 PE O- species by fractional abundance and their distribution in fresh blood samples from adults and term infants, shotgun technique

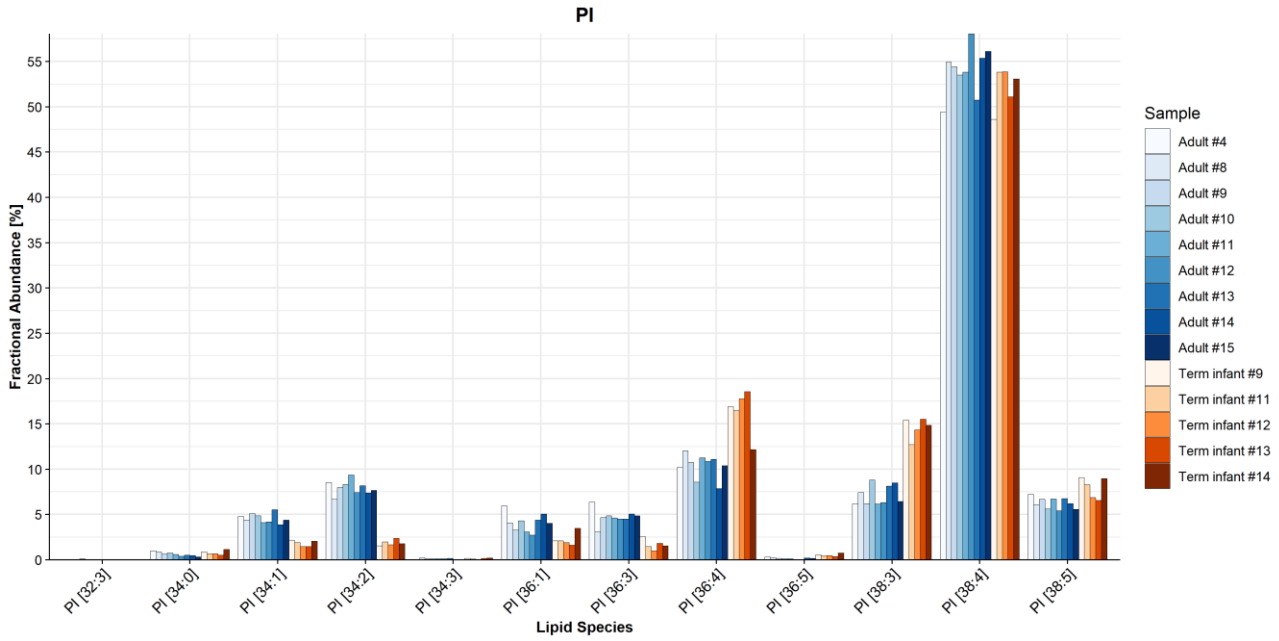

Figure A 2: PI species by fractional abundance and their distribution in fresh blood samples from adults and term infants, shotgun technique

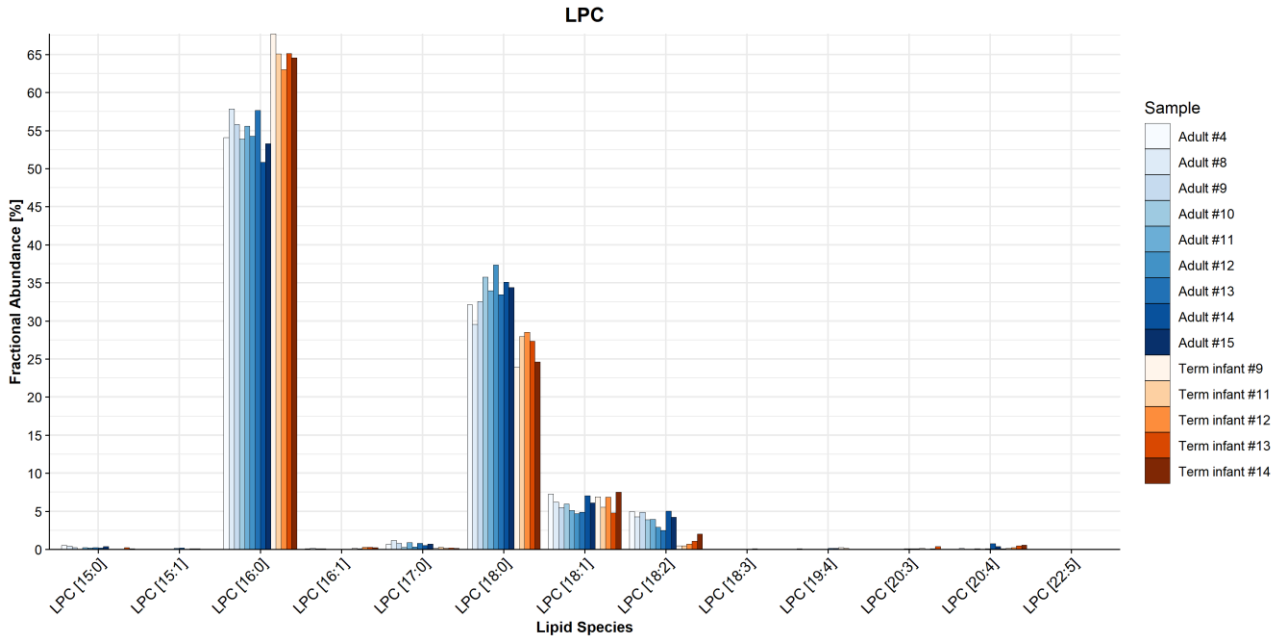

Figure A 3: LPC species by fractional abundance and their distribution in fresh blood samples from adults and term infants, shotgun technique

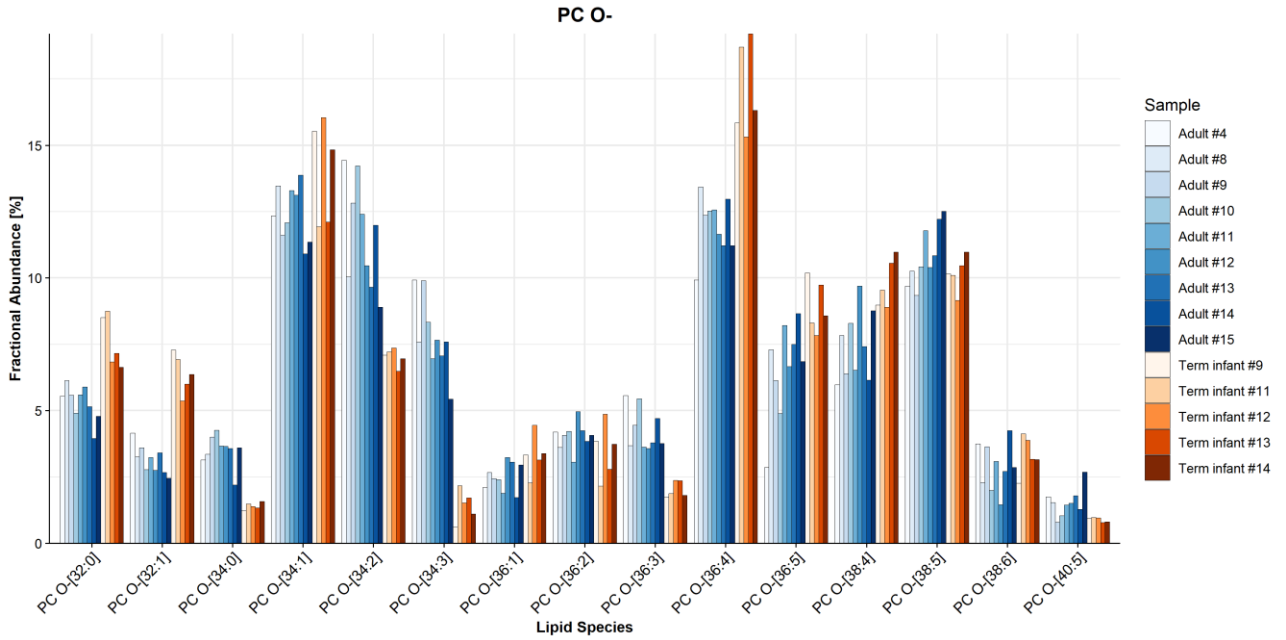

Figure A 4: Top 15 PC O- species by fractional abundance and their distribution in fresh blood samples from adults and term infants, shotgun technique

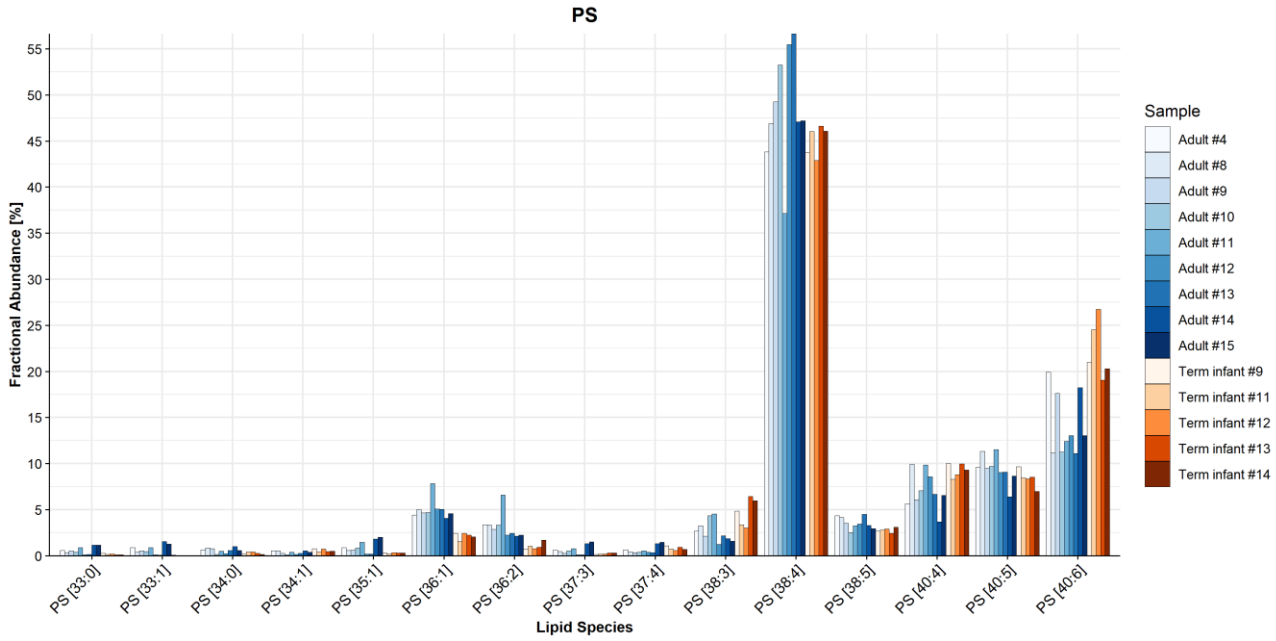

Figure A 5: Top 15 PS species by fractional abundance and their distribution in fresh blood samples from adults and term infants, shotgun technique

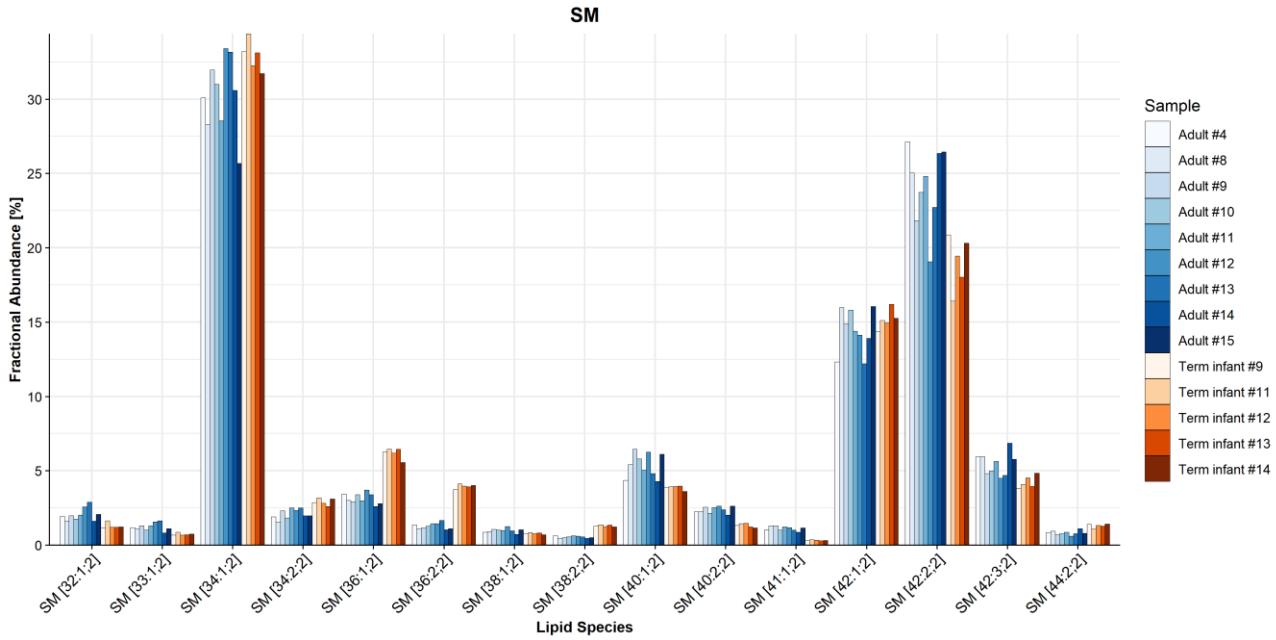

Figure A 6: Top 15 SM species by fractional abundance and their distribution in fresh blood samples from adults and term infants, shotgun technique